

For Reference

NOT TO BE TAKEN FROM THIS ROOM

For Reference

NOT TO BE TAKEN FROM THIS ROOM

Ex libris
UNIVERSITATIS
ALBERTAENSIS





Digitized by the Internet Archive
in 2019 with funding from
University of Alberta Libraries

<https://archive.org/details/Clowes1966>

Thesis
1966(F)
31

THE UNIVERSITY OF ALBERTA

DEEP CRUSTAL SEISMIC REFLECTIONS
AT NEAR-VERTICAL INCIDENCE

by

RONALD MARTIN CLOWES

A THESIS

SUBMITTED TO THE FACULTY OF GRADUATE STUDIES
IN PARTIAL FULFILLMENT OF THE REQUIREMENTS FOR THE DEGREE
OF MASTER OF SCIENCE

DEPARTMENT OF PHYSICS

EDMONTON, ALBERTA

MAY, 1966

UNIVERSITY OF ALBERTA
FACULTY OF GRADUATE STUDIES

The undersigned certify that they have read,
and recommend to the Faculty of Graduate Studies for
acceptance, a thesis entitled DEEP CRUSTAL SEISMIC
REFLECTIONS AT NEAR-VERTICAL INCIDENCE, submitted by
Ronald Martin Clowes, in partial fulfillment of the
requirements for the degree of Master of Science.

ABSTRACT

Near-vertical incidence deep reflecting events from within the earth's crust have been recorded on seismograms along three different lines in southern Alberta. Predesigned systems of geophone and hole patterns have been synthesized into an effective filter for long-period surface waves while vertical- and horizontal-component geophones established their vertical incidence character.

The data were recorded on FM magnetic tape recorders with a wide dynamic range and the results have been digitized. By application of digital processing techniques, the signal-to-noise ratio has been enhanced. Power spectra calculations indicate that the reflected wavelets have energy contained in the range 5 to 15 cps.

A synthetic seismogram program has been developed. Three important results have been obtained from its application: (1) multiple reflections are severely attenuated within 1.5 seconds after a primary event; (2) any transition layer yielding a deep reflection must be less than 1 km. in extent; (3) the Conrad velocity discontinuity is a transition over less than 0.5 km.

A strong reflection at 11.6 seconds representing the Conrad discontinuity has been continuously correlated over 30 km., enabling average vertical velocity and depth values to be calculated. Other reflections are evident on some seismograms suggesting that the deeper crust may be more complex than can be resolved by refraction methods. In addition, evidence is presented which suggests a high angle fault deep within the crust of the earth.

It is hoped that this thesis will demonstrate the applicability of the seismic reflection technique for deep crustal research.

ACKNOWLEDGEMENTS

With sincere appreciation, I wish to thank Dr. E. R. Kanasewich who initially proposed the project to me. His counsel, work and encouragement have been indispensable throughout the entire programme.

Dr. G. L. Cumming was closely involved with all phases of the project. Discussions with him often provided new ideas to be considered.

Mr. M. D. Burke supervised the technical aspect of the operation. His patience in making an excellent digital conversion of the analog tapes is appreciated.

Mr. L. W. Jackson spent many hours converting the data on paper punch tape to punch cards. His development of a number of essential computer programs expedited the analyses immeasurably.

Messrs. Stanley Allen and Charles McCloughan, the recording truck operators, are to be commended for the quality of the seismograms which they made. In addition, Mr. McCloughan did an exceptionally fine job in making the gravity survey.

A special vote of thanks is extended to the many other persons who assisted in the field operation.

Tenneco Oil and Minerals, Limited and Amerada Petroleum Corporation provided near-surface reflection seismograms from the area. Their cooperation in supplying these is gratefully acknowledged.

Century Geophysical Corporation of Canada furnished the drilling rigs and technical personnel necessary for the emplacement and detonation of the explosives.

I wish to especially thank the Defence Research Board's Suffield Experimental Station for providing accommodation for the field personnel and the sites for the Suffield profile.

During the course of his research, the author was supported by a Graduate Teaching Assistantship from the Department of Physics, University of Alberta.

This project was sponsored by the National Research Council of Canada; the Defence Research Board of Canada; and the Advanced Research Projects Agency, Project Vela Uniform.

TABLE OF CONTENTS

	<u>Page</u>
<u>Abstract</u>	iii
<u>Acknowledgements</u>	v
<u>List of Illustrations</u>	ix
<u>Chapter 1. Introduction</u>	1
1.1 The Crust	1
1.2 Seismic Methods	3
1.3 The Project	5
1.4 Prior Work	9
<u>Chapter 2. Equipment, Location and Techniques</u>	14
2.1 Instrumentation	14
2.11 Amplifier and recording system	14
2.12 Geophones	17
2.2 Location	17
2.3 Refraction Summary and Geological Cross-section	23
2.4 Geophone-hole Patterns	23
<u>Chapter 3. The Digitized Records</u>	32
3.1 Method of Digitization	32
3.2 Analyses of the Digitized Records	35
3.21 Signal enhancement techniques	35
3.22 Power spectra analyses	44

<u>Chapter 4. Synthetic Seismograms</u>	57
4.1 The Synthetic Seismogram Computer Program	57
4.2 The Mohorovičić Discontinuity as a Transition Zone	63
4.3 The Synthetic Seismogram from Acoustic Log Data	65
<u>Chapter 5. Interpretation of the Analog Records</u>	73
5.1 Suffield and Lake Newell Data	73
5.2 The Velocity Determination along the Lomond Profile	77
5.3 Interpretation of the Lomond Seismograms	86
<u>Conclusions</u>	96
<u>Bibliography</u>	101
<u>Appendix 1.</u> Geophone-hole Patterns	103
<u>Appendix 2.</u> Fourier Transform and Power Spectra Analyses	114
<u>Appendix 3.</u> Listings of Computer Programs	127

LIST OF ILLUSTRATIONS

<u>Figure</u>		<u>Page</u>
2.1	Arrangement of equipment in the recording truck.	15
2.2	Seismometer characteristics	18
2.3	Profile locations in southern Alberta	21
2.4	Summary of refraction data in southern Alberta	24
2.5	Geological cross-section for southern Alberta	25
2.6	Amplitude responses of geophone and hole patterns; hole spacing is 30.5 m.	29
2.7	Amplitude responses of geophone and hole patterns; hole spacing is 61 m.	30
3.1	Block diagram of procedure for analog to digital conversion	33
3.2	Filter response as a function of real conversion frequency	34
3.3	Traces representative of the normalization and stacking of digitized data	39
3.4	Crosscorrelation coefficients of representative digitized traces	40
3.5	Some results of 600% compositing and Gaussian stacking	43
3.6	Record section including Conrad reflector (from Gaussian stack)	46
3.7	Fourier transform amplitudes for traces 1 to 3 of figure 3.6	47
3.8	Fourier transform amplitudes for traces 4 to 7 of figure 3.6	48
3.9	Autopower spectra for 1 second interval preceding time interval of figure 3.6 (traces 1 to 3)	50

<u>Figure</u>		<u>Page</u>
3.10	Autopower spectra for 1 second interval preceding time interval of figure 3.6 (traces 4 to 7)	51
3.11	Autopower spectra for traces 1 to 3 of figure 3.6	52
3.12	Autopower spectra for traces 4 to 7 of figure 3.6	53
3.13	Autopower spectra for 3 traces; time interval of 9.5 to 15.5 seconds	56
4.1	Data from Berryman et al (1958)	60
4.2	The equivalent data of figure 4.1 computed by the author	61
4.3	Reflections from a transition layer	64
4.4	Examples of anticipated simple multiple reflections	67
4.5	Input pulse and its Fourier transform; reflection coefficient of crustal model	69
4.6	The synthetic seismogram	70
4.7	Field recording and selected portions of the synthetic seismogram	72
5.1	Field record from the Suffield profile	74
5.2	Field records from the Lake Newell profile	76
5.3	Lomond profile reflection data (1964) between 4 and 11 seconds after the shot instant	78
5.4	Lomond profile reflection data (1964) between 11 and 16 seconds after the shot instant	79
5.5	Lomond profile seismograms (1964) for time interval 10 to 12.8 seconds	81
5.6	IBM 1407 line printer output of six 600% composited traces	83

<u>Figure</u>		<u>Page</u>
5.7	X^2 versus T^2 diagram of the Conrad reflection for all available data along the Lomond profile	85
5.8	Seismogram at vertical incidence from position 0 on Lomond profile	87
5.9	Record sections from three different shots along the Lomond profile	89
5.10	Geometry of the postulated fault with respect to seismic ray paths	90
5.11	Lomond profile seismogram (1965) between 9 and 16 seconds after the shot instant	92
5.12	Bouguer gravity anomaly map for southern Alberta	94
A1.1	Amplitude response of geophone-hole pattern: 4 holes, 30.5 m. spacing; 8 seismometers, 18 m. spacing	110
A1.2	Amplitude response of geophone-hole pattern: 5 holes, 30.5 m. spacing; 16 seismometers; spread length 134 m.	111
A1.3	Amplitude response of geophone-hole pattern: 4 holes, 30.5 m. spacing; 16 seismometers; spread length 122 m.	112
A1.4	Amplitude response of geophone-hole pattern: 4 holes, 30.5 m. spacing; 16 seismometers; spread length 73 m.	113

CHAPTER 1.

INTRODUCTION

1.1 The Crust

Knowledge of deep structure within the crust of the earth would greatly enhance our understanding of its historical evolution. With such knowledge, it might even be possible to predict the occurrence of some earthquakes and so minimize the destruction they cause. The seismic reflection method of geophysical research is particularly suited for yielding structural information, as evidenced by its widespread use in petroleum exploration. However, its use in exploring deep crustal structure has been limited by technological difficulties, but these are now being overcome. This thesis examines various methods by which reflected energy may be enhanced over different types of disturbing noise and gives details about crustal properties obtained from this reflection study. Over the years, a great deal of effort has been expended in examining crustal properties by other means; refracted body waves, surface waves, potential field methods and geochemical observations. With so much interest focussed on the earth's crust, it seems appropriate to present a brief discussion of its salient features.

Usage of the term 'crust' to describe the outer layers of the earth is a relic from ancient beliefs in which it was thought the earth was a thin spherical shell enclosing a hot liquid. However, while retaining the term, modern usage has generally redefined it as being that part of the earth above the Mohorovičić (M) seismic velocity discontinuity (Steinhart and Meyer, 1961). In 1909, A. Mohorovičić discovered this seismic discontinuity from an analysis of earthquake waves and evidence since then supports its universality, giving depths averaging about 40 km. under continents and 10 km. under oceans. Although seismic results continually verify its existence, the nature of the M discontinuity is as yet undetermined. MacDonald and Ness (1960) have proposed, as a consequence of phase transition theory, that it may be represented by a gradual transition in velocity and density from basaltic material in the crust to eclogitic material in the upper mantle. Their work indicates that this transition zone exists over a distance of several kilometers. In contrast to this viewpoint, Nakamura and Howell (1964) have suggested, as a result of analysis of refraction arrivals, that the M discontinuity may be represented by a relatively sharp transition extending over less than half a kilometer. The observation of reflections from the M would enable the formulation of a more precise theory, be it either of the above possibilities, a combination of the two or the proposal of

something quite different. Within the crust itself, there is certainly some form of layering. The near-surface sedimentary system of layers forms a relatively thin upper region, but until 1925 little other information was known. In that year the German seismologist, V. Conrad, discovered evidence for a discontinuity at an intermediate depth within the crust. Seismic events from this discontinuity are frequently obtained in continental regions, but definite proof has not been obtained that it is a world-wide continental phenomenon. In general, the Conrad discontinuity is interpreted as a boundary between an upper 'granitic' zone and a lower 'basic' zone within the crust, the nature of separation being unknown. It should also be pointed out that on seismic records, events from the Conrad refractor very seldom appear as first arrivals so that identification is dependent upon the quality of the data and subject to ambiguous interpretation. However, if reflections could be obtained from such a discontinuity the ambiguity would be removed and it may be possible to determine whether there exists a widespread continental velocity discontinuity within the crust. Inherent in these data would be information about the nature of such a discontinuity.

1.2 Seismic Methods

Mention has been given to the discovery of the M discontinuity by A. Mohorovičić from an analysis of earthquake

waves. The recording of the earth motion as a result of earthquakes and the subsequent analysis of the records provided the first seismic methods for ascertaining properties and characteristics of the earth. For years this was the only seismic method, but the unreliability in determining the origin times, poor knowledge of the source mechanism plus many other problems reduced the significance of the results. Steinhart and Meyer (1961), pp. 3-5, point out the shortcomings inherent in experimental techniques with earthquake seismograms. With these difficulties the natural trend was toward the use of controlled explosions for studying crustal and sub-crustal earth properties. Thus were born refraction and reflection seismology, although the initial interest for crustal studies lay with the former technique. Long range refraction surveys were begun in the 1950's in various areas and contributed valuable information to our knowledge of the crust. However, because the energy recorded is from critical refraction along various layers, the technique cannot identify low velocity layers and any such layers contribute to errors in calculated apparent vertical velocities. As well, the calculation of the depth to any refracting layer necessitates an assumption concerning the variation of velocity with depth (Tuve et al, 1954). Some of these difficulties may be overcome with use of the seismic reflection method, a technique whereby energy propagating downwards in a near-vertical direction is partially

reflected from velocity discontinuities of sufficient magnitude. In addition to inherent traits of greater precision and resolution, the method allows the detection of discontinuous low-velocity layers and a means of ascertaining the average velocity to any reflecting interface (Green, 1938). It should be emphasized at this point that the 'sharpness' of any discontinuity deduced by reflection work is a function of the wavelength involved; hence the unit of measurement may vary. The reflection technique has been of invaluable use in petroleum exploration, but it is only recently that attempts have been made to ascertain characteristics of the crust utilizing this method.

1.3 The Project

It has been noted that the recording of near-vertical incidence seismic reflections from deep within the crust would be of tremendous assistance in the determination of the existence and of the nature of any crustal layering. With this thought in mind, in the summer of 1964 a seismic reflection program was begun by the Geophysics section of the Department of Physics under the direction of Drs. E. R. Kanasewich and G. L. Cumming.

The field operation and equipment was controlled by certain criteria which were necessary to establish the presence of primary reflected energy.

(1) Since such energy must arrive at near-vertical incidence, the direction of earth movement should be substantiated with the use of both vertical- and horizontal-component seismometers.

(2) As previously mentioned, the reflection technique enables the calculation of average velocities. Thus enough data should be obtained (preferably about a common depth point) in order that average velocities may be obtained from reflecting layers. In order to do this, the quality of the data must be sufficiently adequate that correlation from one record to another is unambiguous. Because of the presence of horizontally travelling energy, this generally requires the use of multiple holes and geophone patterns (Section 2.4).

(3) Multiply-reflected events may be prevalent at any time on a seismogram; for this reason, all events should be regarded as multiples unless it is possible to remove any ambiguity.

(4) Amplitudes of the reflected events as a function of distance should be smooth and consistent and possess some correlation (or valid reasons for non-correlation) with theoretical amplitudes. It should be noted that near-surface velocity irregularities, shot environment, and positioning of the seismometer (on soft earth or hard rock) will greatly influence the amplitude on actual recordings.

(5) Reflected events which are established as being from some velocity discontinuity within the crust should be obtained at different recording and shooting sites within some region, providing there are no near-surface noise problems obliterating all events.

(6) Because higher frequency wave forms are attenuated more rapidly than lower frequency ones, it would be expected that the frequency content of any deep reflections would be considerably lower than those obtained from the sedimentary layers. This criteria thus dictated the use of low-frequency geophones.

The experiment was begun during the summer of 1964 in a region in southern Alberta, the specific location chosen having previously been used during the recording of a long reversed refraction profile (Cumming et al, 1962). By recording a reflection profile over part of the refraction profile, it was hoped that the reflected events could be correlated with suggested structure from refraction work, while at the same time yielding more precise information about the nature of the structure. In addition to a continuation of the 1964 profile, work in the summer of 1965 included the recording of profiles at two different locations. Inherent in the entire experiment is the basic and corequisite problem of developing a technique which could record deep crustal

reflections continually and reliably. It is felt that such a technique, while still subject to much improvement, has been developed.

In conjunction with the actual field data, a major part of the author's work has concerned itself with the deduction, construction and employment of analysis techniques to extract useful information from the recorded seismograms, or provide theoretical data which may be compared to or applied to the empirical data. To this end computer programs have been written and the most important ones have been documented in the appendices.

Since it is now believed the reflection technique will provide valuable information, future plans are being made for the continuation of the program. This includes an active field program for part of the summer of 1966, possibly extending into 1967 for completion. More time and attention, however, will be directed toward gleaning all available information from present and future data, a problem which will involve extensive data analysis techniques and theoretical model studies. By means of projects such as the University's reflection program, it is hoped that the seismic reflection method will become a proven and accepted technique for detailing deep crustal structure.

1.4 Prior Work

Over the years, many instances of deep crustal reflections have been reported, but many of these were recorded during the course of some routine seismic investigation and no ancillary equipment or techniques were used to ascertain that they were primary reflections. The first report of reflections from the deep crust seems to be that of Junger (1951). By keeping the camera running to 10 seconds, reflections were observed in the time ranges of 7.0 to 8.5 seconds. Junger effectively argues, on the strength of repeatable results and identical reflections for one shot from two perpendicular spreads, that the energy must be arriving from some reflecting layers inside the basement. Although the results do not indicate a horizontally continuous velocity transition, he assumes a velocity distribution and suggests the range of depths for the layers to be 18 to 21 km. and notes that these depths are in the range quoted for the granitic layer.

This initial publication seemed to enliven research and subsequently papers were published in many countries. In Germany, Dohr (1957) was one of the first to publish records including late arrivals. His work is monumental primarily for the number of records with deep reflection-type events he has included. With so much data, he employed a statistical

approach to the interpretation, showing that while any one reflecting event was not continuous, on a statistical basis there existed some form of layering. The depths corresponding to his reflections, assuming some velocity distribution, range from a shallow layer 8 to 8.5 km. deep to the deepest at 30 to 31 km. In a summary on crustal structure in western Germany, the German Research Group for Exploration Seismology (1964) notes other areas in which deep reflections have been recorded and includes a bibliography of the main researchers. In line with Dohr's work, there were many records available for analysis and a statistical approach was again the basis for interpretation, since no single reflection event could be correlated continuously over more than two kilometers. The results were similar to those of Dohr: layering existed in a statistical sense. The German researchers argue that their events are true reflections, but these arguments would certainly be enhanced had they definitely proven the events were due to primary energy, and that the wave-fronts associated with the reflection arrived at normal incidence.

Elsewhere in Europe, Bath and Tryggvason (1962) have reported on the first seismic investigations of deeper crustal structure in Fennoscandia. This was a direct attempt to record deep near-vertical reflections but the results

were certainly not conclusive. The authors state that the arrivals are weak, of erratic occurrence and their recognition is based on phase correlation, while admitting that some of the assumed reflections could be spurious signals. Nevertheless, they expected such problems and only identify their events as 'possible reflections'. Assuming horizontal layers, and a velocity distribution their results suggest a depth of 19 km. to the Conrad discontinuity and a depth of 33 to 34 km. to the M.

During the 1950's, researchers in the U.S.S.R. undertook a detailed program of seismic investigations of the earth's crust. In 1960-1961, Soviet researchers initiated an experimental program to record deep reflected waves. Subsequently, Belousov et al (1962) reported on the results. The groups involved analysed much data from previous seismic work (primarily supercritically reflected and refracted waves) and adduced an optimum recording system. This involved the grouping of receivers and shot holes to enhance desired signals; figure 5 of their paper emphasizes the effectiveness of their system. The recordings show apparent reflections at times as late as 18 secs. and greater. In addition they could phase correlate reflected waves along their 120 km. profile over distances varying from 2-3 to 8-10 km. Geophysicists in the Soviet Union have recorded many deep reflecting events but their results would be more useful if they indicated those

events which could be due to multiply-reflected energy, as distinct from primary energy. However, their work exemplifies the amount of information which can be obtained from an organized deep reflection program.

In North America, various attempts have been made to record near-vertical incidence reflections. Subsequent to Junger's report, Shor (1955) presented two records purported to have deep reflections, but these were of poor quality and the possibility of multiply-reflected events could not be eliminated. In addition, on other records in the same area no reflections could be found because of high reverberation levels. Narans et al (1961) claim to have obtained reflections from two sites in northern Utah. Unfortunately, their records were of poor quality, requiring a statistical approach for interpretation, and they could not exclude the possibility of multiple reflections. Two times from events they chose, when combined with velocity data from prior refraction work, gave depths corresponding to earlier results from that work. Robertson (1963) exhibited a record section, obtained by extending the record time in routine petroleum exploration to about six seconds, in which there was a continuous deep-reflecting event in the basement complex. The reflections correspond to depths much less than those reported for the Conrad and M discontinuities from refraction data. Over the 29 km. of the profile in southwestern Alberta, the reflecting

layer shows considerable dip, increasing in depth from 7.5 km. to 14 km. Robertson effectively argues that the reflections are true near-vertical ones, but he only speculates on possible interpretations. More recently Dix (1965) has reported on reflection studies of the crust. He has included locations in which cross-records were shot to exclude the possibility of interpretation of shallow energy from a side reflector or scatterer as primary reflected energy. His records exhibit many possible reflecting horizons, with a strong sequence of pulses centering around 8.0 secs., corresponding to a depth of 25 km., the crustal depth for the region of his survey. Finally, Kanasewich and Cumming (1965) have given some initial results from the 1964 data of the present project.

CHAPTER 2.

EQUIPMENT, LOCATION AND TECHNIQUES

2.1 Instrumentation

For recording purposes, two identical sets of equipment were arranged in two panel trucks. This equipment consisted of power supplies, low frequency amplifiers, filter networks, a recording oscillograph, an analog magnetic tape recorder and a chronometer, WWV receiver and standard broadcast receiver for timing purposes. In figure 2.1 a block diagram shows the arrangement of the apparatus. A geophysical contractor was hired for the drilling of shot holes, their loading and detonation, but the shot instant was recorded in a suitably equipped university vehicle.

2.11 Amplifier and Recording System

Texas Instruments VLF-2 refraction amplifiers were used throughout the operations. Minor modifications were made to the output circuit to provide the necessary signal amplitude for the FM analog tape recorder. For rejection of 60 cps signals induced by power lines, a line balancing switch is provided with each amplifier. In addition to this switch, useful features of the instrument included two input plugs, a line test switch to check that proper connections were made with the main cable, individual step attenuators (6 db steps), and a 24 db per octave, 6 position high-cut

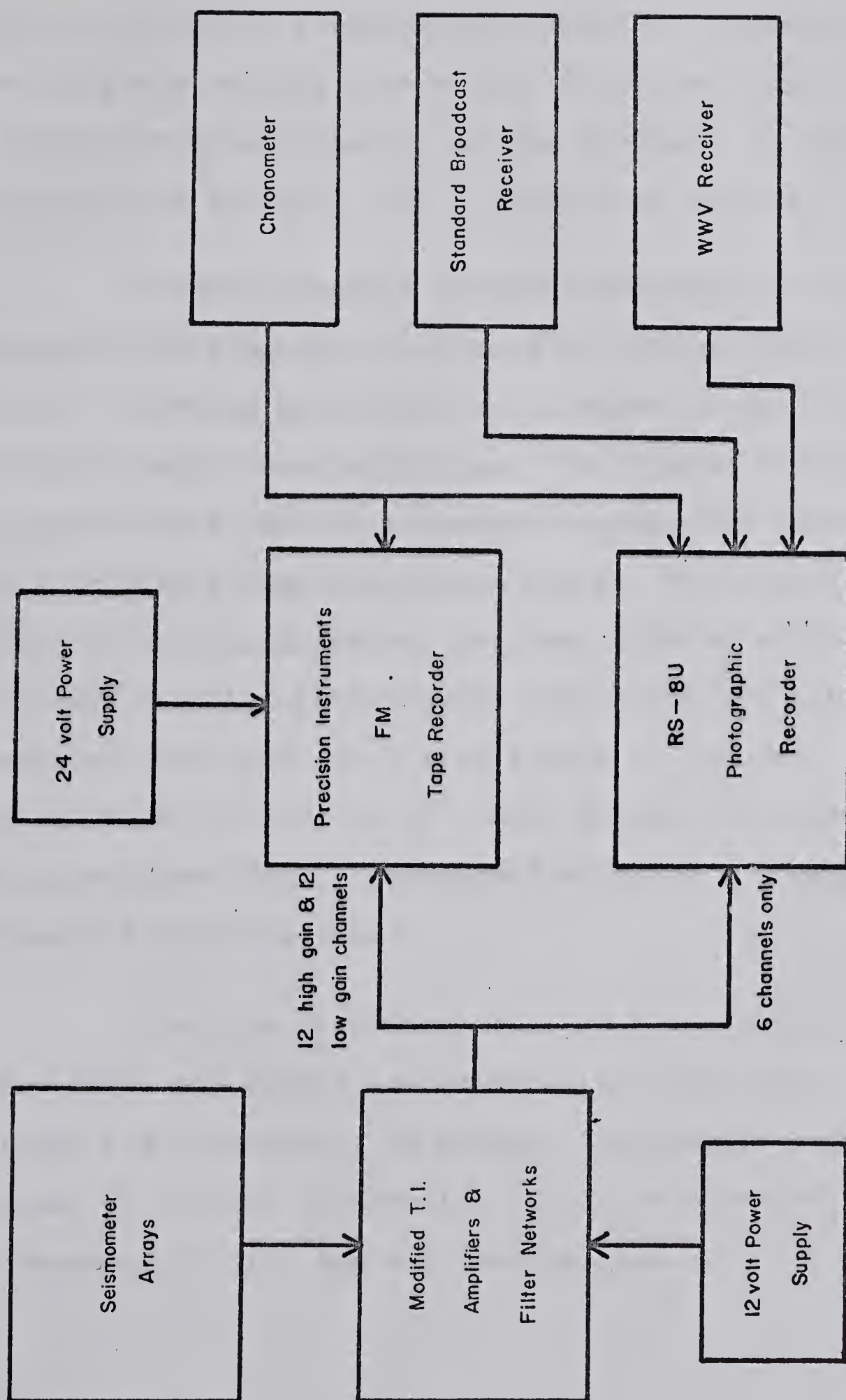


FIGURE 2.1

Arrangement of equipment in the recording truck.

filter with cutoff frequencies adjustable between 8 and 48 cps. Recording was usually done with a filter setting of 24 cps. A further important feature of the equipment is dual outputs--high gain and low gain with a deflection ratio of 4 to 1.

The photographic recorder employed, an RS-8U recording oscillograph, comprised an optical system, timing system, recording galvanometers, a paper transport system and photographic developing box. The timing lines are obtained from a 100 cps transistor supply and a synchronous motor driving a drum containing slits. For recording purposes, thirty galvanometers are available of which twelve were used for high gain traces, twelve for low gain and the remainder were used for timing traces or ignored. The recording was made on roles of 8" x 200' seismic photographic paper. The paper speed was 5" per second allowing a timing precision of about ± 0.002 seconds.

The tape recorders utilized were Precision Instruments PS207 and PS207A instrumentation tape decks. These allowed six channels of FM seismic information plus one channel of AM time information (from the chronometer) to be recorded on 1/2" magnetic analog tape.

2.12 Geophones

Signals from six of the recording channels were obtained from geophone arrays (Section 2.4) consisting of Electro-Tech EVS-4 seismic detectors. The main characteristics and a sensitivity versus frequency plot of this seismometer is given in figure 2.2a. Also used to record earth motion were three Hall-Sears HS-10 detectors. Figure 2.2b shows the principal characteristics of these geophones. In some instances, signals were recorded on Texas Instruments S-36 seismometers. These geophones are the ones employed for the University's refraction experiments. The main specifications for the S-36 are given in figure 2.2c.

2.2 Location

The near-vertical incidence reflection program is being carried out in a region in southern Alberta near the town of Brooks. The main reflection profile, called the Lomond profile, is located on a twenty-mile line extending west from the NEC Sec. 24, Twp. 17, Rge. 18, W4M to the NWC Sec. 19, Twp. 17, Rge. 20, W4M. As mentioned before, this location was chosen because it had previously been used for part of a reversed refraction profile (Cumming et al, 1962) and it was a location known to be relatively free of power lines. All the reflection data from the summer of 1964 plus

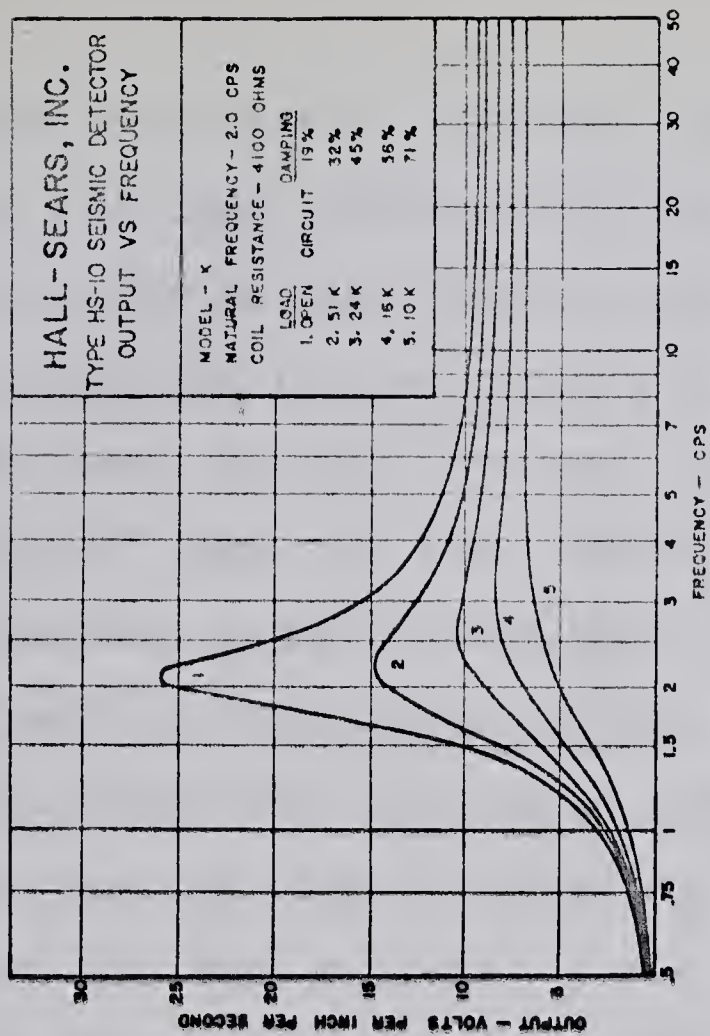
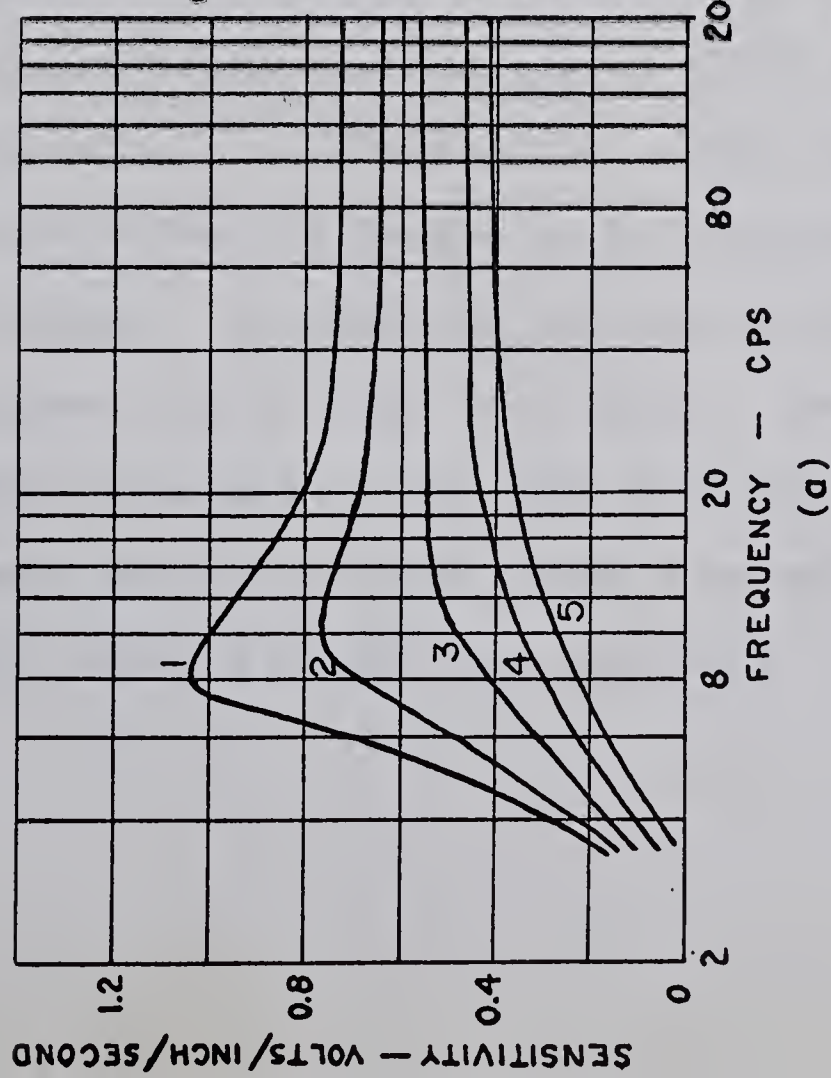
EVS 4

NATURAL
FREQUENCY
7.5 CPS

COIL RESISTANCE
215 OHMS

LOAD DAMPING

1. OPEN	.36
2. 2000	.50
3. 700	0.7
4. 400	0.9
5. 300	1.0



HALL-SEARS, INC.

TYPE HS-10 SEISMIC DETECTOR
OUTPUT VS FREQUENCY

MODEL - K

NATURAL FREQUENCY - 2.0 CPS

COIL RESISTANCE - 4100 OHMS

LOAD CIRCUIT DAMPING

1. OPEN		19%
2. 51 K		32%
3. 24 K		45%
4. 16 K		58%
5. 10 K		71%

TI S-36

NATURAL FREQUENCY - 2 CPS

COIL RESISTANCE - 4K OHMS

LOAD

DAMPING

1. INFINITE	0
2. 15 K	.311
3. 6 K	.500
4. 2.6 K	.707
5. 444	1.00

OUTPUT - VOLTS/INCH/SEC.

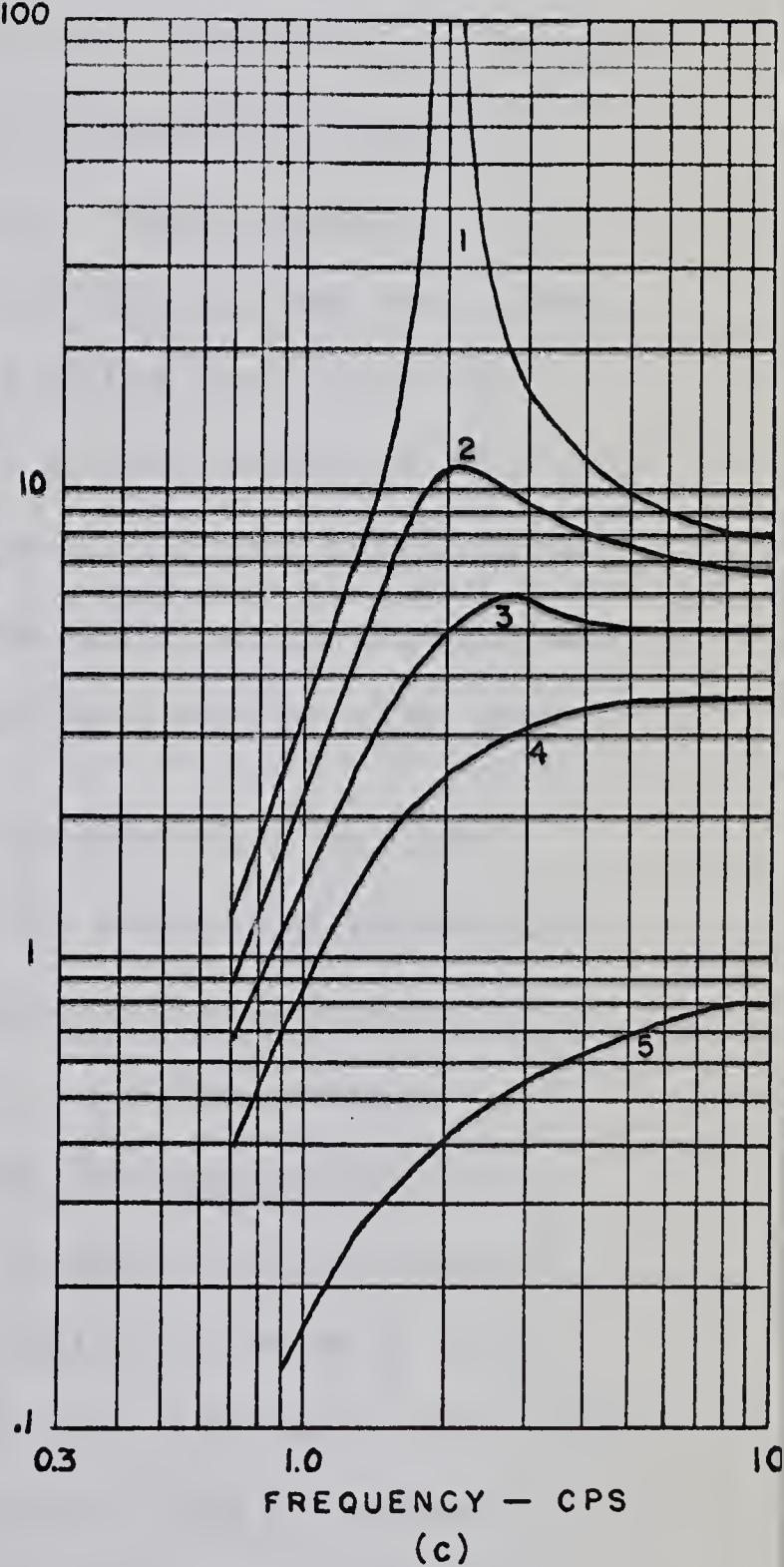


FIGURE 2.2

SEISMOMETER CHARACTERISTICS

some from that of 1965 were obtained along this line. As well in 1965, further data were acquired from a short profile just west of Lake Newell, Alberta (Newell profile). This profile was located along a line extending west from NEC Sec. 22, Twp. 17, Rge. 15, W4M to the NEC Sec. 22, Twp. 17, Rge. 16, W4M. Records were also obtained from several locations along an east-west line on the Defence Research Board's Suffield Experimental Station. Specifically, recordings were made along lines extending 4 miles east from NEC Sec. 33, Twp. 17, Rge. 9, W4M; 4 miles east from NEC Sec. 33, Twp. 17, Rge. 7, W4M and 4 miles east from NEC Sec. 31, Twp. 17, Rge. 5, W4M. Figure 2.3 shows the general area in which reflection work is being done and the positions of the profiles including the designations of the mile positions.

The arrangement of holes and detectors for the Lomond profile was an adaptation of the expanding reflection spread technique (Musgrave, 1962) with center point at position 0 on the profile. This was to enable average velocities and depths to be calculated for any reflecting horizon. In 1964 the centers of the detector arrays were spaced 293 m. (960 ft.) apart. Two duplicate sets of data were obtained as for each position of the detectors, two shots were recorded, there being a separation of 293 m. between the centers of the hole patterns. The duplication of data

FIGURE 2.3

Figure 2.3 shows the seismic reflection profile locations. Also included in the figure are some well locations from which data were obtained to compute the geological cross-section. Listed by number these wells are:

2. Cal-Standard Parkland 4-12, 4-12-15-27 W4M, 1955
3. Grt. Plains Pageant 10-21, 10-21-18-21 W4M, 1962
4. Tenneco Eyremore 10-15, 10-15-18-19 W4M, 1963
5. Cree Scurry Lomond 7-17, 7-17-16-18 W4M, 1960
6. Imperial-Calstan Lake Newell 5-1, 5-1-17-W4M, 1960
7. Calstan C. P. R. Princess No. 1, 13-22-20-12 W4M, 1941
8. Richfield Shell Rapid Narrows 11-20, 11-20-16-4 W4M, 1957

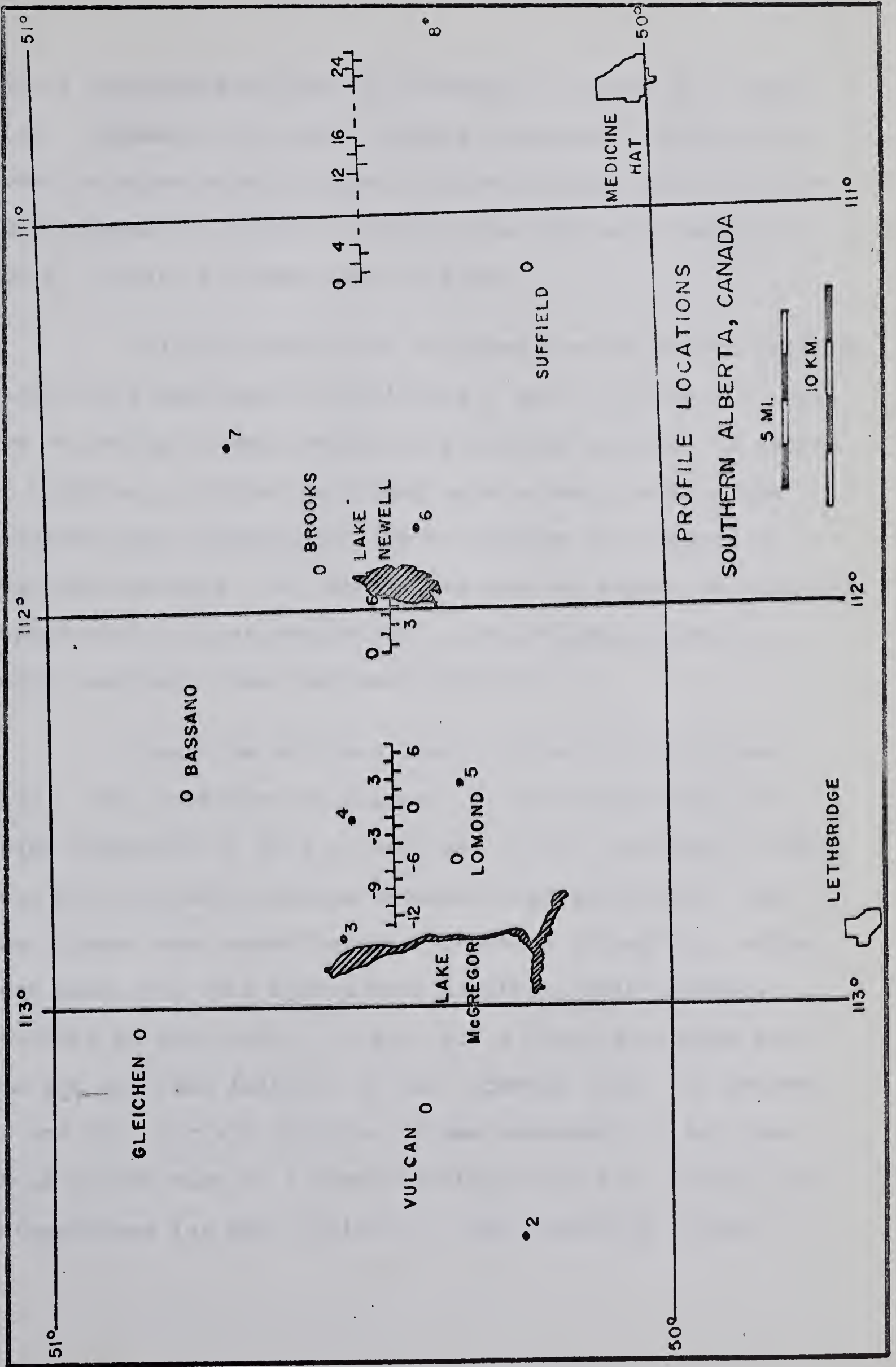


FIGURE 2.3

was to facilitate mixing and stacking of traces at a later time. Because of the good results obtained in 1964 and in order to cover more distance at an equivalent cost, for the 1965 program the center-to-center spacings were doubled to 586 m., except for some special shots.

Only two shots were recorded for the Newell profile, these being detonated at positions 0 and 6 (figure 2.3) with the recording trucks located at positions 1 and 5. A spread of 1.609 km. (1 mile) to either side of each vehicle was utilized with a spacing of 586 m. between the centers of geophone patterns. No attempt was made to employ an expanding spread as the first desire was to record reflections in a region separate from the Lomond profile.

Along the Suffield line a number of shots were made. With reference to figure 2.3, patterned shots of 4 holes separated by 30.5 m. were set off at locations 0 and 4 into four one-mile spreads between these positions. Then the spreads were moved between locations 12 and 16; shots were made into this spread with identical hole patterns centered at positions 0, 4 and 16. A final patterned shot was set off from position 24 into spreads laid out between 22 and 26. For all profiles it was necessary to lay down about 25,000 feet of interconnecting cable and install 212 seismometers for each position of the recording trucks.

2.3 Refraction Summary and Geological Cross-section

The Geophysics laboratory, University of Alberta has previously recorded seismic refraction arrivals across southern Alberta and Saskatchewan (Cumming et al, 1962 and Maureau, 1964). A summary of the data obtained from these studies is illustrated by figure 2.4. The small insert shows the location of the profile.

A geological cross-section of the area has been computed from formation tops obtained from available well log data. This information is presented in figures 2.3 and 2.5. Digitized acoustic logs from the Pageant 10-21 and Eyremore 10-15 wells were used to compute the upper two average vertical velocities. The first value, 3.2 km./sec., applies from the surface to the top of the Mississippian; the second, 5.8 km./sec., from the top of the Mississippian to the top of the Nisku formation in the upper Devonian. The two basement velocities have been transferred from the refraction summary.

2.4 Geophone-hole Patterns

The primary information desired was recorded on arrays of EVS-4 seismometers in conjunction with hole patterns, the combined system being an effective filter of long period surface waves. Six channels of information per

CRUSTAL MODEL FOR SOUTHERN ALBERTA (BASED ON REFRACTION STUDIES)

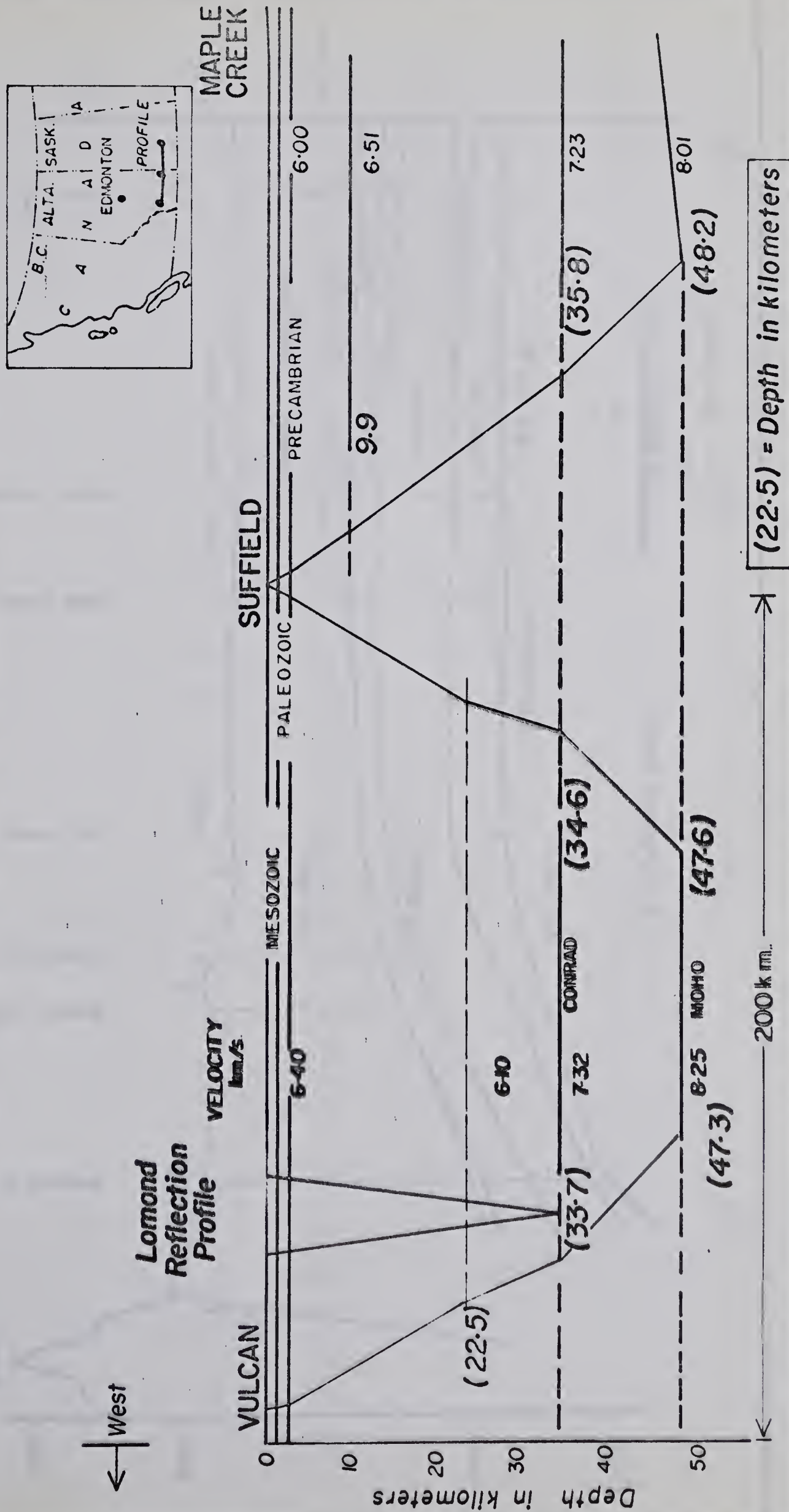


FIGURE 2.4

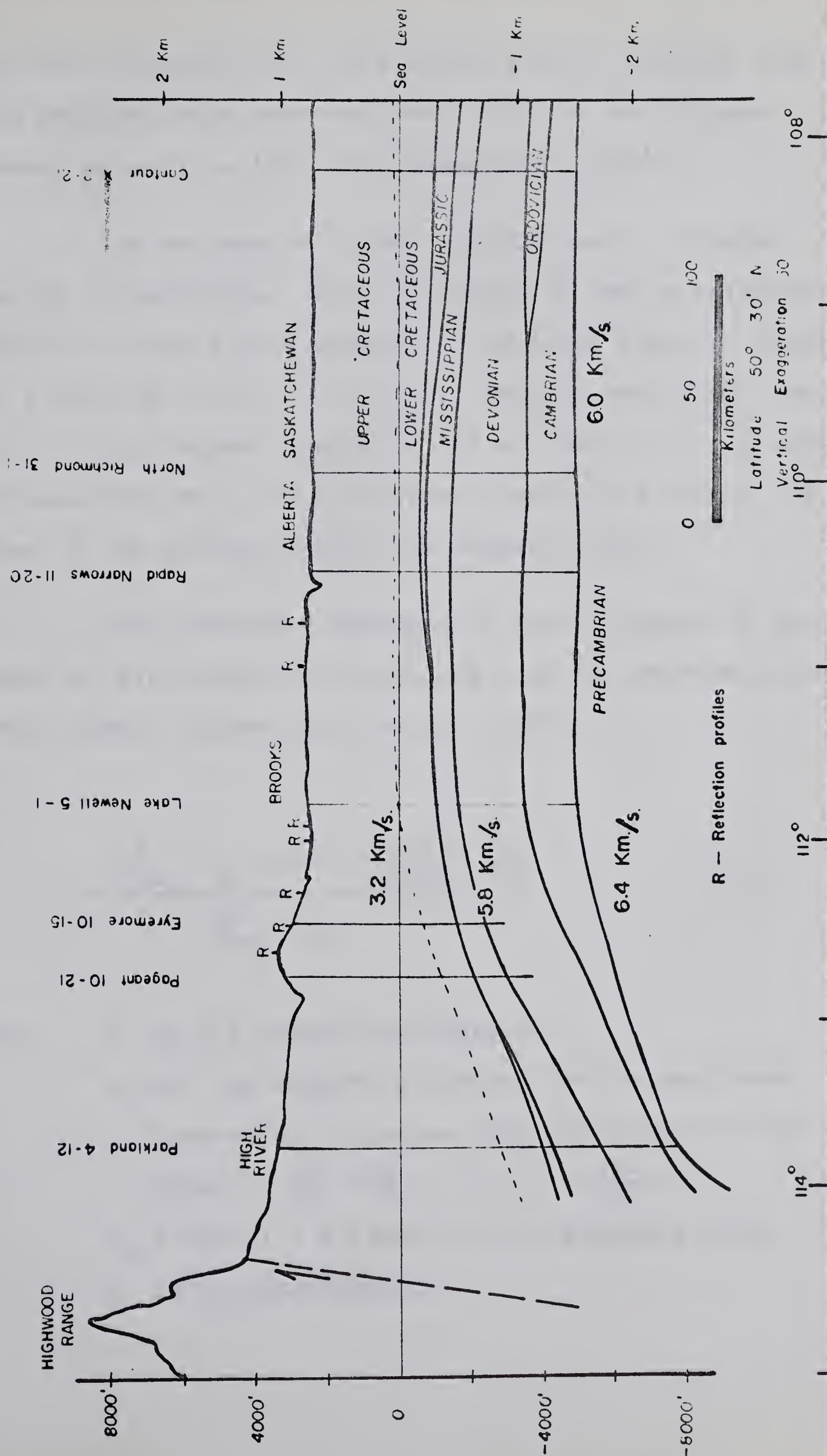


FIGURE 2.5 GEOLOGICAL CROSS-SECTION FOR SOUTHERN ALBERTA

truck were obtained with this system and the signals from these geophone-hole patterns were fed into the FM tape recorder as well as into the photographic system.

The seismometer array utilized was a 'tapered' array of 16 geophones. This consisted of twelve seismometers being laid along a line symmetric about the take-out location, with a spacing of 12.2 m. (40 ft.) between detectors, resulting in a total spread length of 134 m. (440 ft.). An additional 4 seismometers with the same spacing were laid out at the center of the system to give the tapered array.

The normalized response of such a system of geophones (an even number of locations) can be computed using antenna theory (after Savit et al, 1958):

$$G = \frac{\sum_{k=1}^m a_k \cos \left[\pi \left(\frac{2k-1}{2m-1} \right) \frac{D_G}{\lambda} \right]}{\sum_{k=1}^m a_k} \quad (2.1)$$

where G is the normalized response

a_k are the weighting factors for $2m$ geophones

located at distances from the center of the

array of $\pm \frac{d}{2}$, $\pm \frac{3d}{2}$, . . . , $\pm \frac{2k-1}{2} d$, . . . , $\pm \frac{2m-1}{2} d$

$D_G = (2m-1) d \equiv$ length of the geophone array

λ is the wavelength.

For the case discussed, then, $a_1=a_2=a_3=a_4=a_5=a_6=1$;
 $D_G = (12-1)40 = 440$ feet. Included in figure 2.6 is a plot of (2.1) for the designated parameter values.

The hole patterns employed were quite simple, principally for the sake of economy. In 1964 all arrayed shots except the first two were made with a pattern of 4 holes, separated by 61 m. (200 ft.) and symmetric about a central axis, each hole normally being loaded with 50 lbs. of explosive charge. The initial arrayed shots were made with separation distances of 30.5 m. However, in 1965, an attempt was made to record all shots with a hole pattern of 4 holes separated by 30.5 m. This was a result of a computer program being written which could produce many response curves, enabling the best filtering system to be chosen.

The normalized response for an even number of holes is given by an equation identical in form to (2.1).

$$H = \frac{\sum_{j=1}^n b_j \cos \left[\pi \left(\frac{2j-1}{2n-1} \right) \frac{D_H}{\lambda} \right]}{\sum_{j=1}^n b_j} \quad (2.2)$$

where H is the normalized response
 b_j are the weighting factors (relative charge size)
 for $2n$ holes located at distances from the

center of the pattern of $\pm \frac{1}{2}d'$, $\pm \frac{3}{2}d'$, ..., $\pm \frac{2j-1}{2}d'$, ..., $\pm \frac{2n-1}{2}d'$

$D_H = (2n-1) d' \equiv \text{length of the hole pattern.}$

Figure 2.6 includes the hole response for the system of 4 holes, spaced 30.5 m. apart. The total response of the hole-geophone combination when all holes and geophones are lying along the same line is given by the products of the two amplitudes. This curve is also given in figure 2.6. Figure 2.7 gives essentially the same information as the previous one except the hole response is for 4 holes located 61 m. apart. In addition, it includes the response curve of an infinite number of geophones on a line over the distance of 134 m. for comparison purposes. It will be noted from figure 2.6 that the combined response is an effective filter for attenuation of arrivals with an apparent wavelength less than 270 m., while figure 2.7 indicates an effective filter for apparent wavelengths less than 400 m. Previous mention has been given for the choice of two different hole pattern lengths. Appendix 1 includes a derivation of the responses for odd numbers of holes or geophones, and some additional response curves.

FIGURE 2.6. Amplitude responses of geophone and hole patterns; hole spacing is 30.5 m.

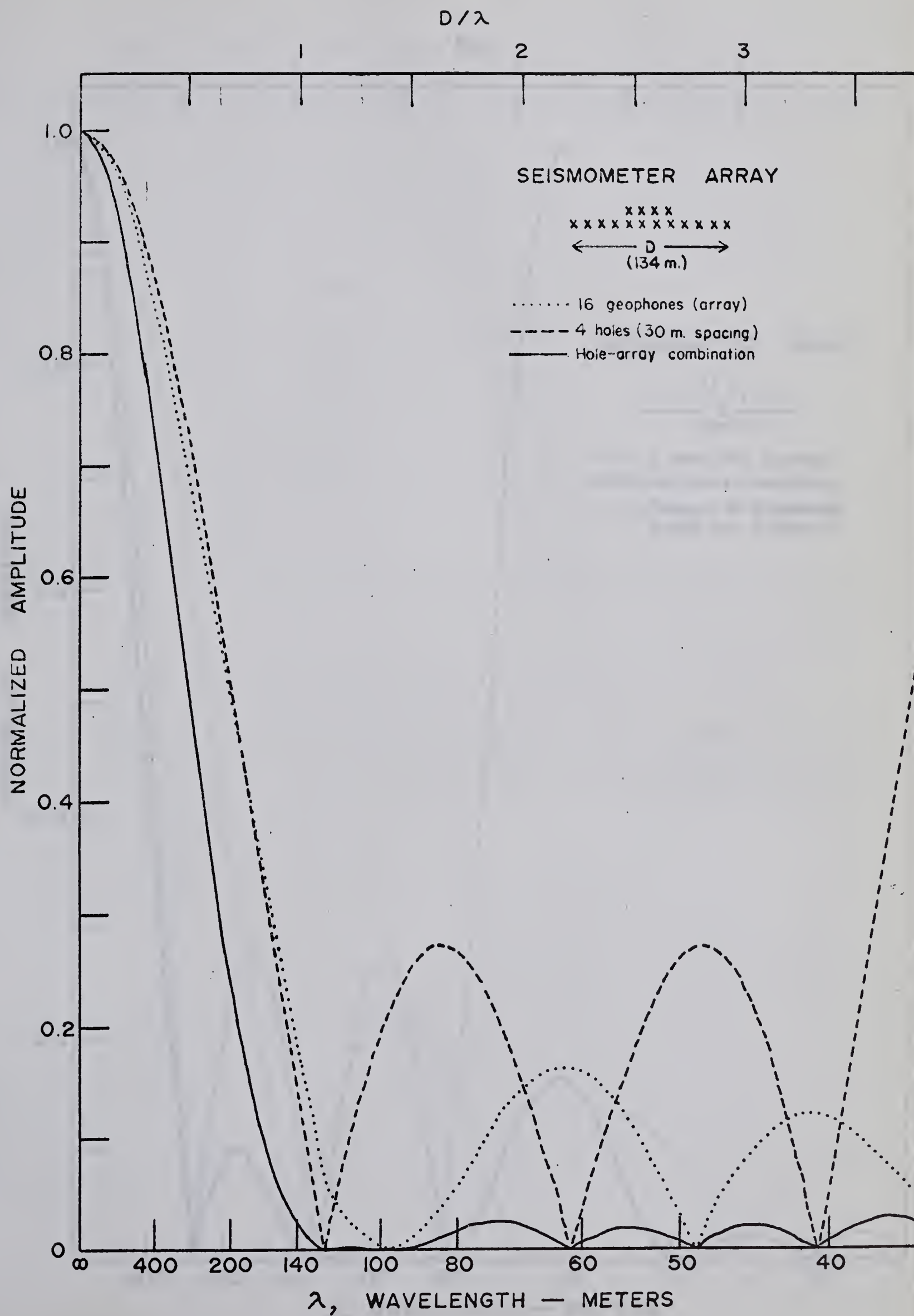
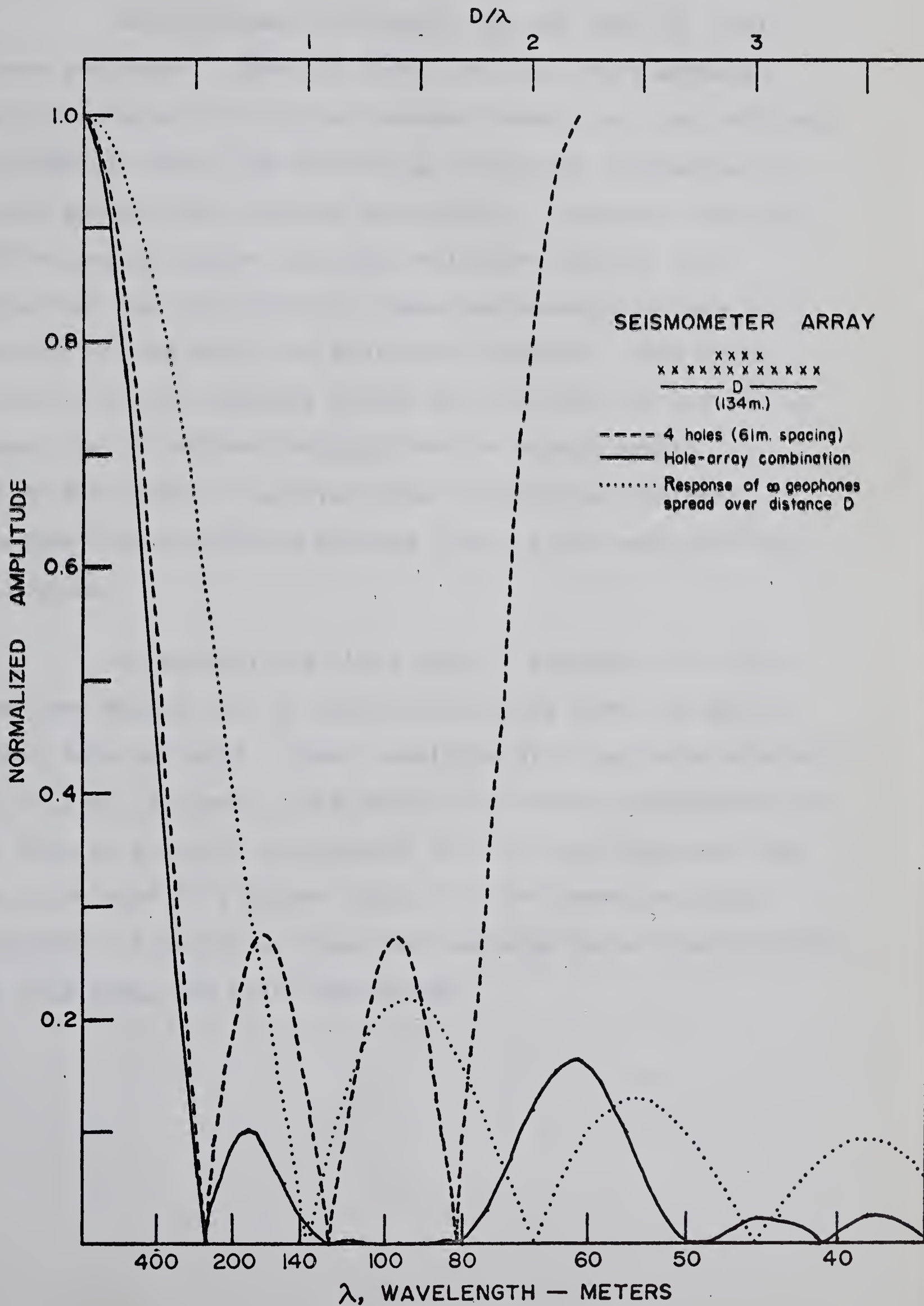


FIGURE 2.7. Amplitude responses of geophone and hole patterns; hole spacing is 61 m.



As previously mentioned, use was made of Hall-Sears geophones. Three of these per truck were arranged at one location with three take-out leads such that vertical, horizontal radial and horizontal transverse components of earth motion were recorded separately. Component recording of the ground motion for deep reflection work is very important for the output of these geophones indicates the direction from which the energy has arrived. Thus while traces from the geophone arrays may indicate the arrival at some time of coherent energy over the spread length (a 'reflection'), the directional cluster may indicate whether this energy has arrived from a truly near-vertical direction.

In general the third type of geophone, the S-36, was used singly, but in certain instances linear arrays of these were employed. These consisted of 8 geophones separated by 18.3 m. (60 feet). The noise attenuation characteristics of such an array in conjunction with the hole patterns can be calculated in a manner similar to the previous arrays. Appendix 1 includes a normalized response curve characteristic of this array and hole combination.

CHAPTER 3.

THE DIGITIZED RECORDS

3.1 Method of Digitization

Conversion to digital form of the analog FM magnetic tape, recorded along the Lomond profile in 1964, was performed by the technical staff in our geophysics laboratory. Figure 3.1 is a block diagram of the procedure followed. The conversion apparatus was originally designed for the digitization of magnetotelluric data for which the tape drive speed was much less. This necessitated that the original tape drive speed for the seismic data of about 30 inches per second be reduced by a factor of sixteen before conversion. The optimum conversion rate for synchronization with the paper tape punch was 13.6 conversions per second, machine time. In effect, this meant 217.6 conversions per second for the seismic data, yielding a digitizing interval in real time of 4.59 milliseconds.

The individual channel which was to be converted to digital form was selected and its starting time controlled by the box labelled "clock and control". The filters were specially designed to prevent aliasing of power from frequencies greater than half the conversion frequency. Built into the filter system was an amplitude modification factor

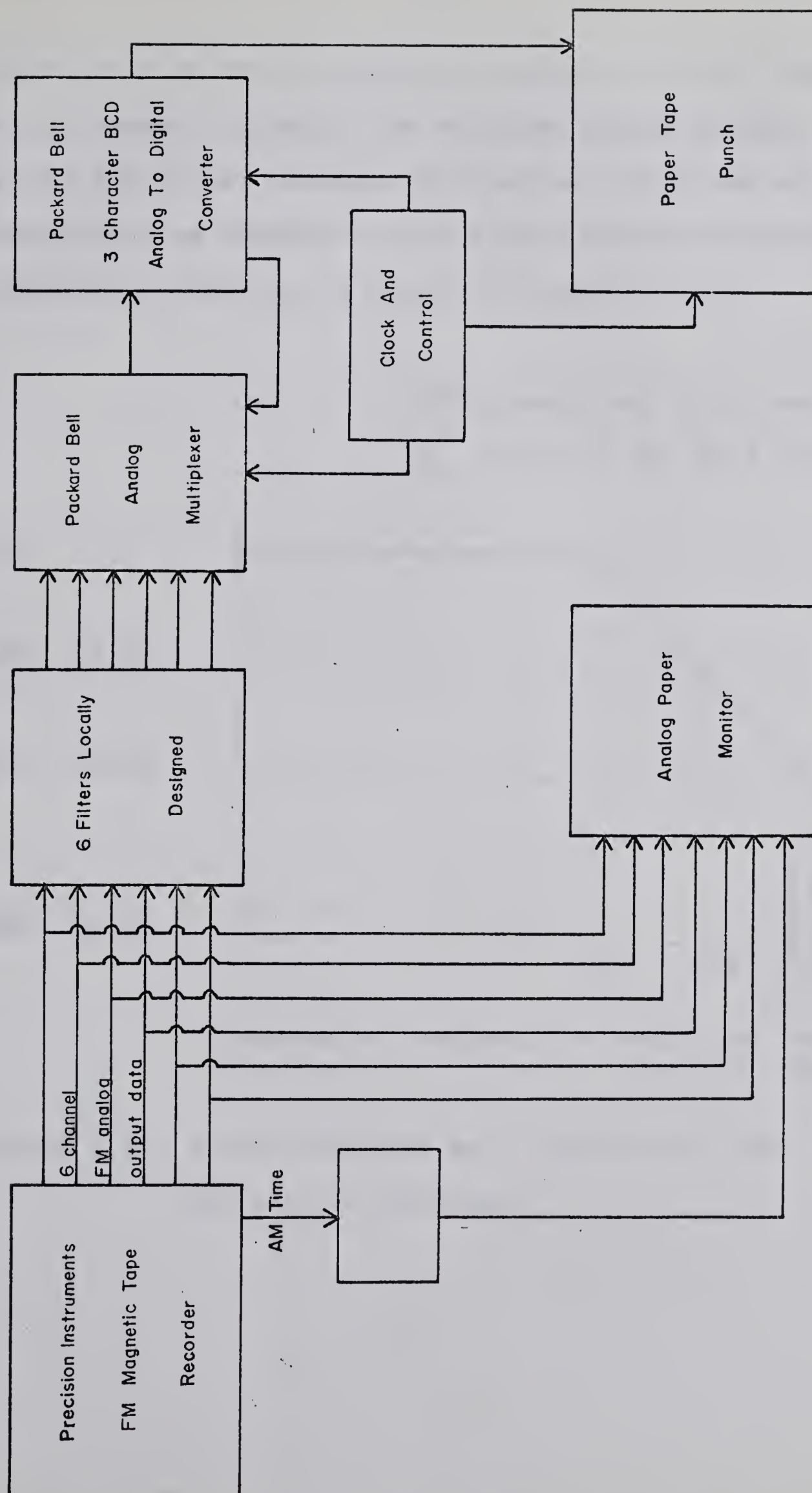


FIGURE 3.1

Procedure For Analog To Digital Conversion

which could be set at +10 db., 0 db., or -10 db. depending on the dynamic range of the recorded analog signal. Figure 3.2 is the filter response plotted as a function of real frequencies as opposed to the actual machine conversion frequencies which are a factor of sixteen less.

AMF \equiv Amplitude modification factor

$f_c = 217.6$, the data conversion freq.

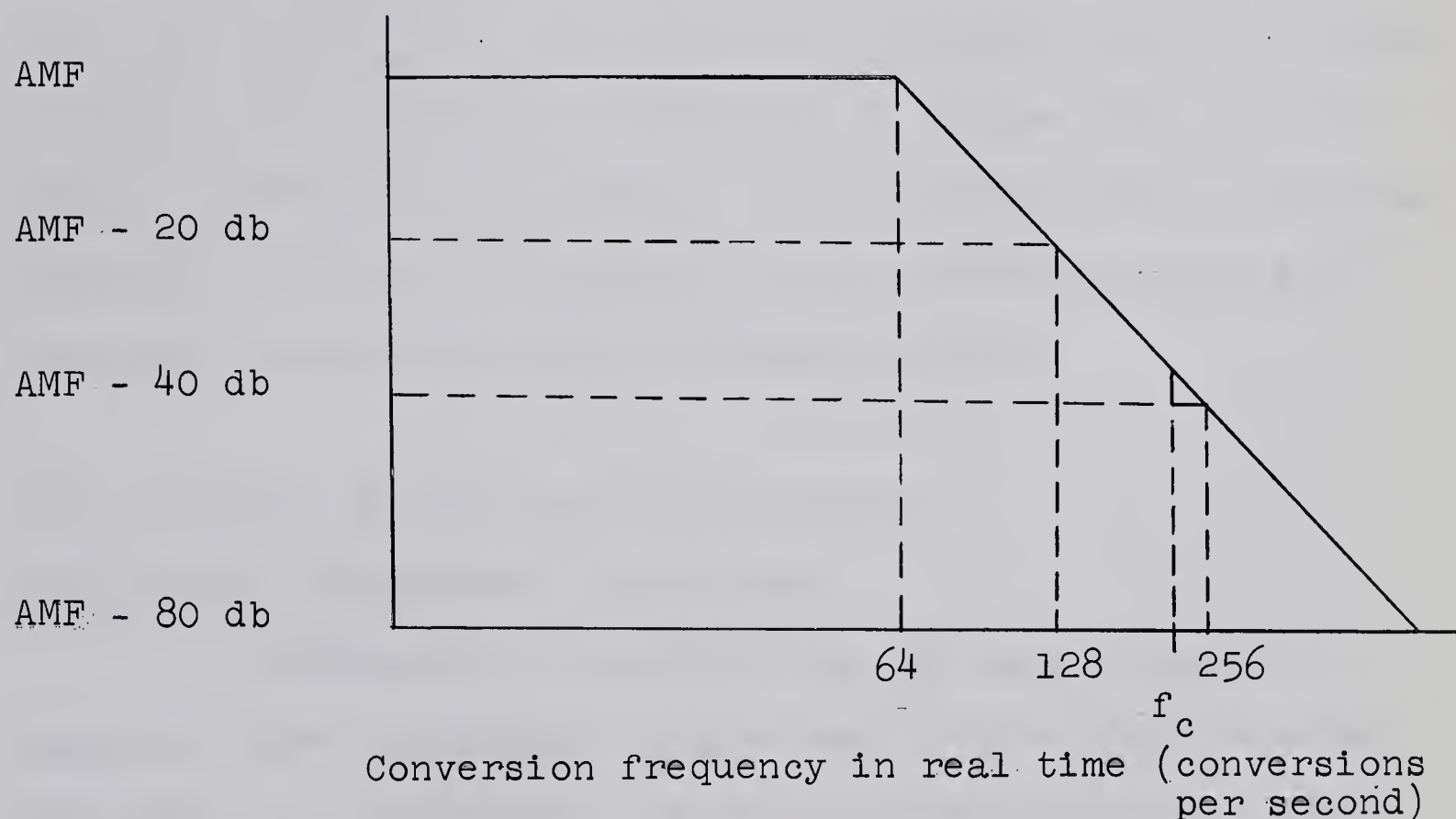


FIGURE 3.2. Filter response as a function of real conversion frequency.

Signals with frequencies greater than f_c may be aliased into lower frequencies but they are attenuated by 40 db (a factor of 100) or more. It should be repeated that prior to recording on tape, the seismic signals above 24 cps were attenuated at a rate of 24 db per octave.

Once all channels had been converted to digital form on paper punch tape, the data were transferred to punch cards and subsequently put onto digital magnetic tape. Since this manipulation of data could be a possible source of error, a listing was carefully scrutinized to ensure that all data were in their proper sequence. In the future, such a tedious procedure will not be necessary as the converted data will be placed directly on digital magnetic tape.

3.2 Analysis of the Digitized Records

3.21 Signal enhancement techniques.

Subsequent to transferring the data to digital magnetic tape, a computer program was written which enabled the data to be plotted on the IBM 1403 line printer. This was a quick method of plotting, enabling a visual picture of all the digitized data to be obtained and compared to the photographic records. Thus a correspondence was set up in which each digital point for each trace could be related to a time, accurate to within 5 milliseconds, on the photographic record.

The initial step in the analysis of the 96 digitized traces was the normalization of amplitudes and removal of the normal move-out. For the former, a relatively simple procedure was decided upon: one representative trace was chosen and over the region of a strong reflection at 11.6 seconds (Conrad event), the amplitudes of all other traces were normalized to that of the representative one. This process also included the removal of any D.C. average prevalent over the part of the record used for normalizing. Specifically, a half second interval on either side of the Conrad event was chosen; the mean of the values in this total interval and the sum of the absolute value of the deviations from the mean was computed for the standard trace; the same quantities were computed for all remaining traces; the normalized values were obtained by subtracting the mean value of each trace from every point in that trace, and multiplying the result by the ratio of the sum of the deviations for the standard trace to that for the trace under consideration. It should also be pointed out that while the total record length of the original traces varied, the output of the normalization program was 96 traces of equal length. Mathematically this procedure can be explained as

$$N_i = (G_i - \bar{G}) \frac{\sum_j |G_j^{\text{std}} - \bar{G}^{\text{std}}|}{\sum_j |G_j - \bar{G}|} \quad (3.1)$$

where N_i is the normalized digital value
 G_i is the unnormalized value
 j refers to a sum over the 1 second interval
 $\bar{}$ refers to an average value over the interval
and the 'std' superscript refers to the standard trace.

For removal of normal move-out, the digital value corresponding to the bottom of the 'picked' trough for the Conrad event was labelled as zero point on each trace. Effectively, this meant that the times of events representing reflections from the Conrad discontinuity were set at the reflection time (11.571 secs.) of the representative trace and established with zero moveout. Any events at different times thus had the move-out of the Conrad reflection removed, so compensation for the normal move-out was not ideal. In fact a calculation, assuming direct ray paths and utilizing known refraction data, showed that the difference in normal move-out between a reflector at the depth of the Conrad (34 km.) and one at the depth of the M discontinuity (47 km.) for a horizontal distance from the shot point of 12 km. was approximately 45 msec. This horizontal distance corresponded

to the maximum shot-to-detector distance for the 1964 data. In effect then, for record times greater than that of the Conrad reflector an excess amount of time has been removed to compensate for normal move-out, while for record times less, an insufficient amount of time has been removed. In the future, the removal of normal move-out will be accomplished by a factor which is a function of recording time and horizontal distance from the shot point. Since this would involve a more complex computer program, it was deemed expedient for the present to proceed with the system described. Figure 3.3 includes two traces which have been normalized, together with a small part of the traces to the same scale before normalization.

As a check on the zero points chosen, neighboring traces were run through a crosscorrelation computer program to see that the best correlation was indeed at zero lag. The computer program is similar to the autocorrelation part of a program to be discussed shortly. Four representative crosscorrelation coefficients are plotted in figure 3.4 as a function of point lag. In conjunction with the remaining coefficients, they indicate that the proper zero points were chosen.

It has been previously noted that reflections for any position of the geophone spreads were recorded from two

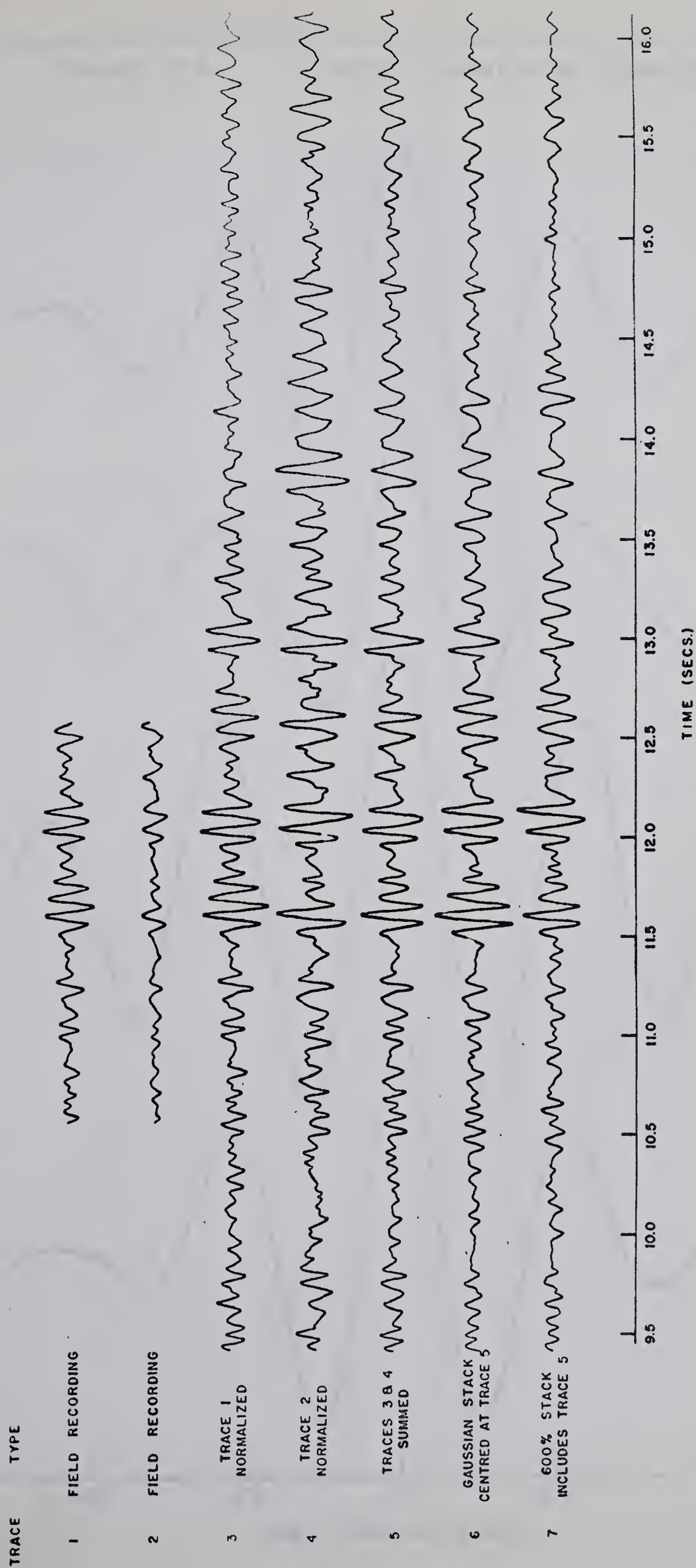
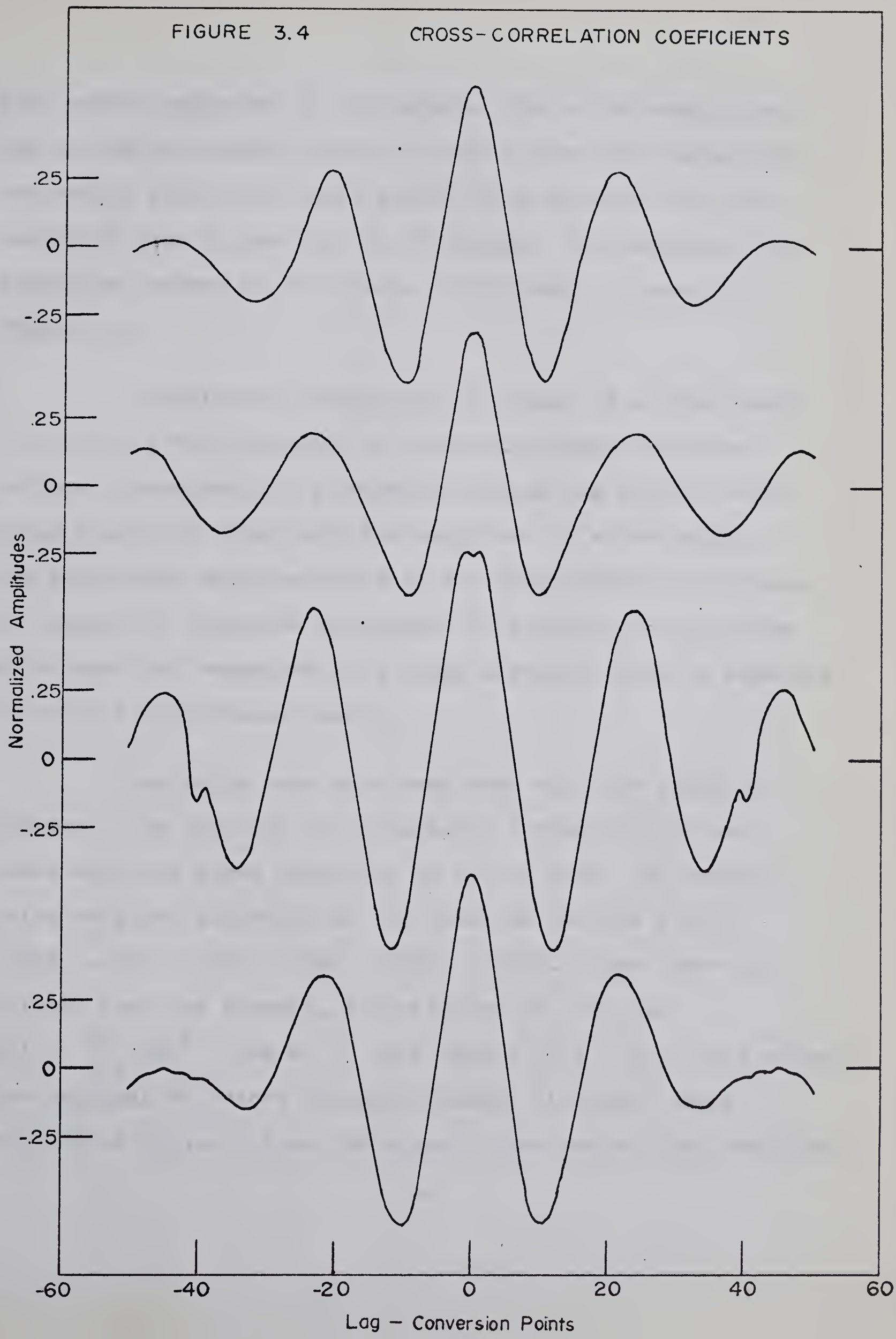


FIGURE 3.3. Traces representative of the normalization and stacking of digitized data.



shot points separated by 293 meters. Hence the next process was to add equivalent values on each of the two traces which had nearly identical travel paths, thus reducing the total amount of data by one half to 48 traces. The result of this summation process on two traces is included in trace 5, figure 3.3.

Stacking or compositing of traces is a relatively direct and effective means of increasing signal-to-noise ratios. Consequently, a computer program was written which would stack one trace with its neighbors to either side, the amplitudes being weighted by any desired factor. Because of changes in character and amount of step-out, only traces which were not separated by a large distance could be expected to yield a significant result.

Two major runs have been made with the stacking program. One involved the successive compositing of one trace with its three neighbors to either side, the traces being weighted according to the Gaussian factors (.0156, .0938, .2344, .3125, .2344, .0938, .0156). These were calculated from the binomial distribution of the type $B(j) = {}^6C_j \left(\frac{1}{2}\right)^6$, where j runs from 0 to 6. With this process the original 48 traces yielded 48 newly filtered traces. Trace 6 of figure 3.3 was obtained in the manner just described.

The second major run involved the direct compositing of six traces, each of these the sum of two traces from nearby shot points, to yield just one trace (see trace 7, figure 3.3). With this procedure, all the field data may be compressed into eight traces representing, in general, successively increasing detector-to-shot point distances.

Reproduced in figure 3.5 are five different traces; the first three are a result of 600% compositing while the final two are a product of the Gaussian stacking. It will be noted from the diagrams that the stacking procedure has significantly lowered the 'noise' amplitude, while retaining the original strength of any reflected signals. Evident on these records is a lack of coherent energy before the train of waves beginning near 11.5 seconds, but considerable energy appears to be present later. The possibility of multiple reflections is clearly indicated in figure 3.5 by the duplicated time interval between prominent events. Unfortunately, the stacking procedure has not notably enhanced the signal amplitude of any event reflecting from the M discontinuity. However, arrows have been placed in the figure around 15.0 secs. depicting coherent energy which could possibly be reflected from M, as such a time for the reflection is to be expected from refraction data. That the pick is highly questionable is undoubtedly true and future work both in the

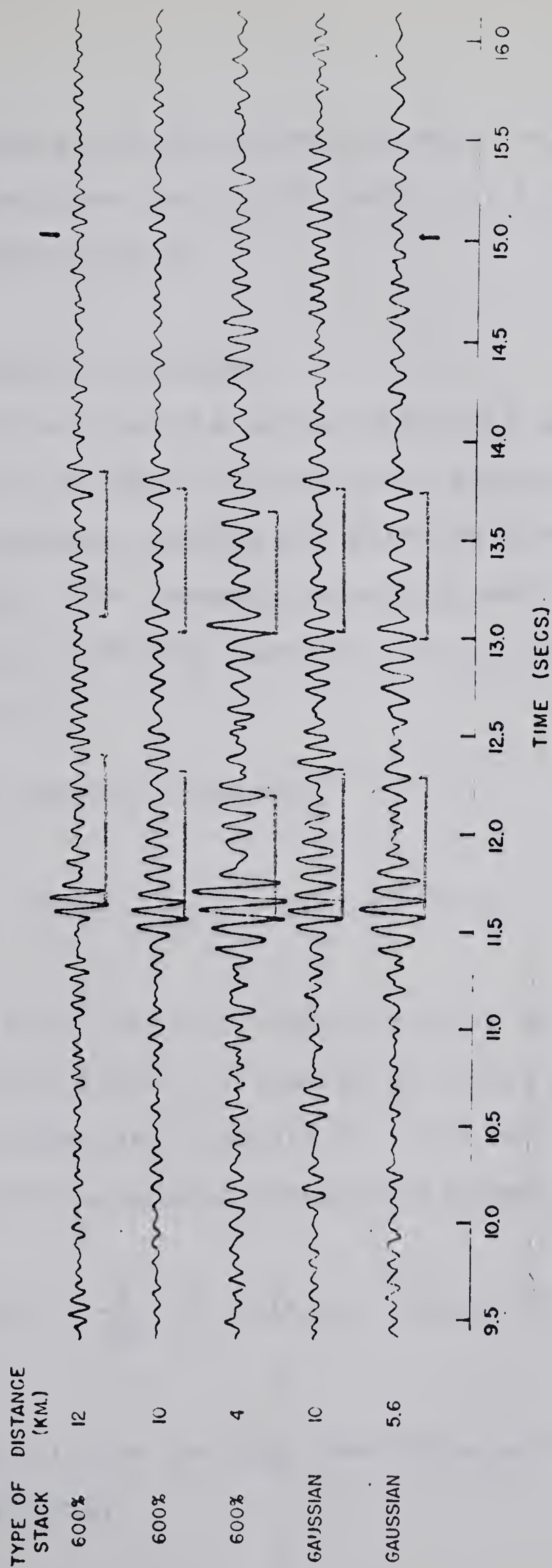


FIGURE 3.5. Some results of 600% compositing and Gaussian stacking.

recording of data and its processing will include as one of its prime objectives the identification of a good reflection from the M discontinuity.

3.22 Power spectra analyses

Further analysis of the digitized data involved the calculation of Fourier transforms, autocorrelation coefficients and autopower spectra for selected portions of the available data. The necessary equations were programmed for the University's IBM 7040 computer and all calculations were performed on it.

The Fourier transform,

$$F(\omega) = \frac{1}{2\pi} \int_{-\infty}^{+\infty} f(t) e^{-i\omega t} dt \quad (3.2)$$

was resolved into real and imaginary parts with the integration being based on a linear interpolation between digital data points (H.S. Howe, see Appendix 2). The real part of the transform, for programming purposes, is then given by

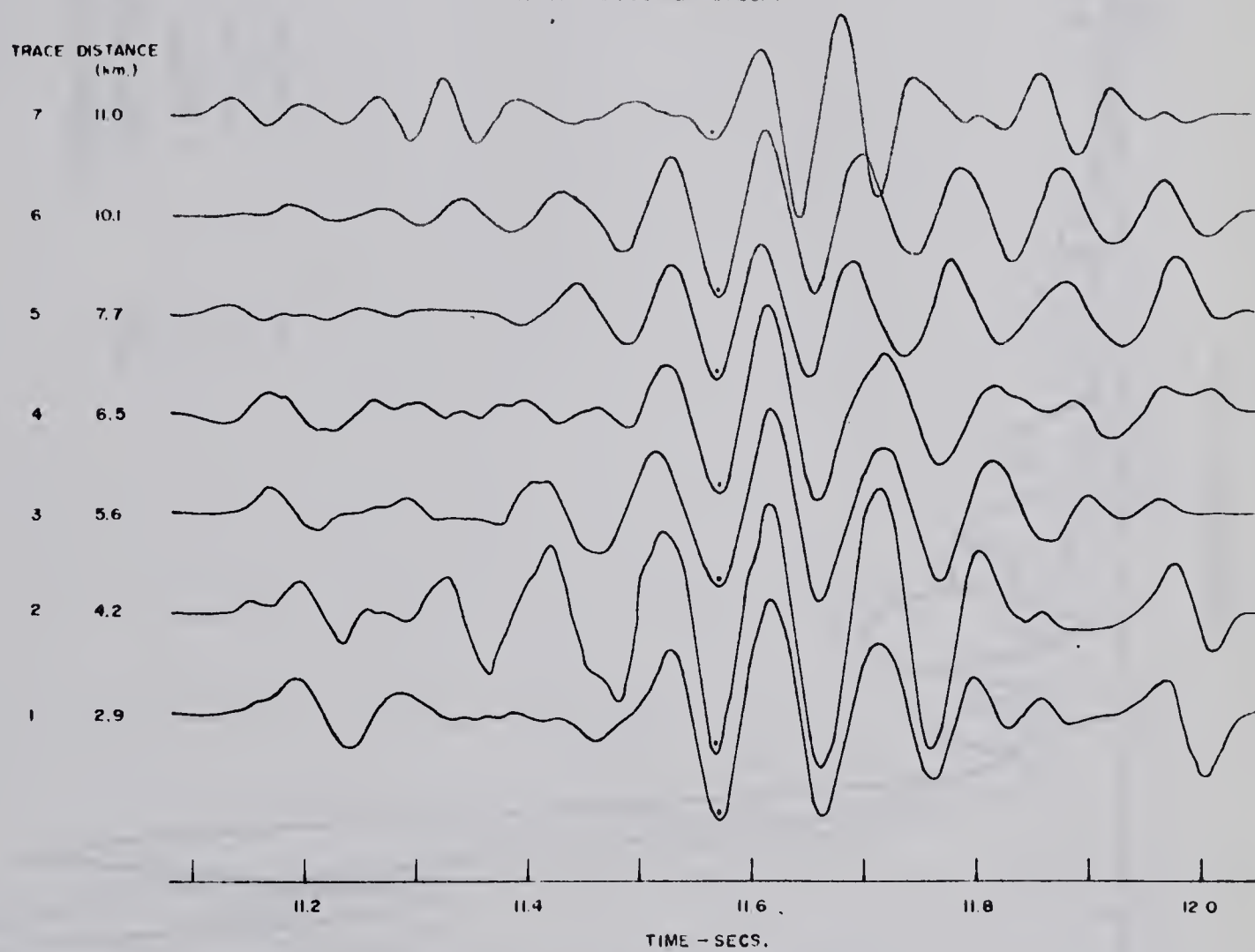
$$\text{Re } [G(\omega)] = \frac{1}{\omega^2 \tau} \sum_i [G(t_{i+1}) - G(t_i)] [\cos \omega t_{i+1} - \cos \omega t_i] \quad (3.3)$$

where the $G(t_i)$ are the digitized data points and τ is the digitizing interval.

For computing Fourier transforms, an interval representing one half second to either side of the reflection at about 11.6 seconds was chosen. Seven different traces from the Gaussian stacked data were analysed, these representing varying horizontal distances of the detectors from the shot point. Figure 3.6 is a plot of the data used for the various computations while the following graphs, figures 3.7 and 3.8 give the moduli of the Fourier transforms of these traces. Most noticeable on these figures is the strong amplitude peak in the vicinity of 10 cps. Since the square of the Fourier amplitude is representative of energy, it is evident that most of the energy in the traces is concentrated within a narrow band of frequencies extending from about 8 to 13 cps. This is presumably due to the strong reflected signal while the low amplitude side peaks are probably due to energy from undesired noise. There is a trend for the moduli to peak at higher frequencies with increasing distance from the shot, a point which will be mentioned shortly.

Power spectral calculations were made following the method of Blackman and Tukey (1958), (see Appendix 2). The digitizing interval of $\tau = .00459$ secs. gives a Nyquist frequency (f_N) for the data of about 108 cps. Let N be the number of points involved in a computation, L be a correlation lag index and J be a frequency index for the equally

FIGURE 36
Record Section Including Conrad Reflector
(from Gaussian stack)



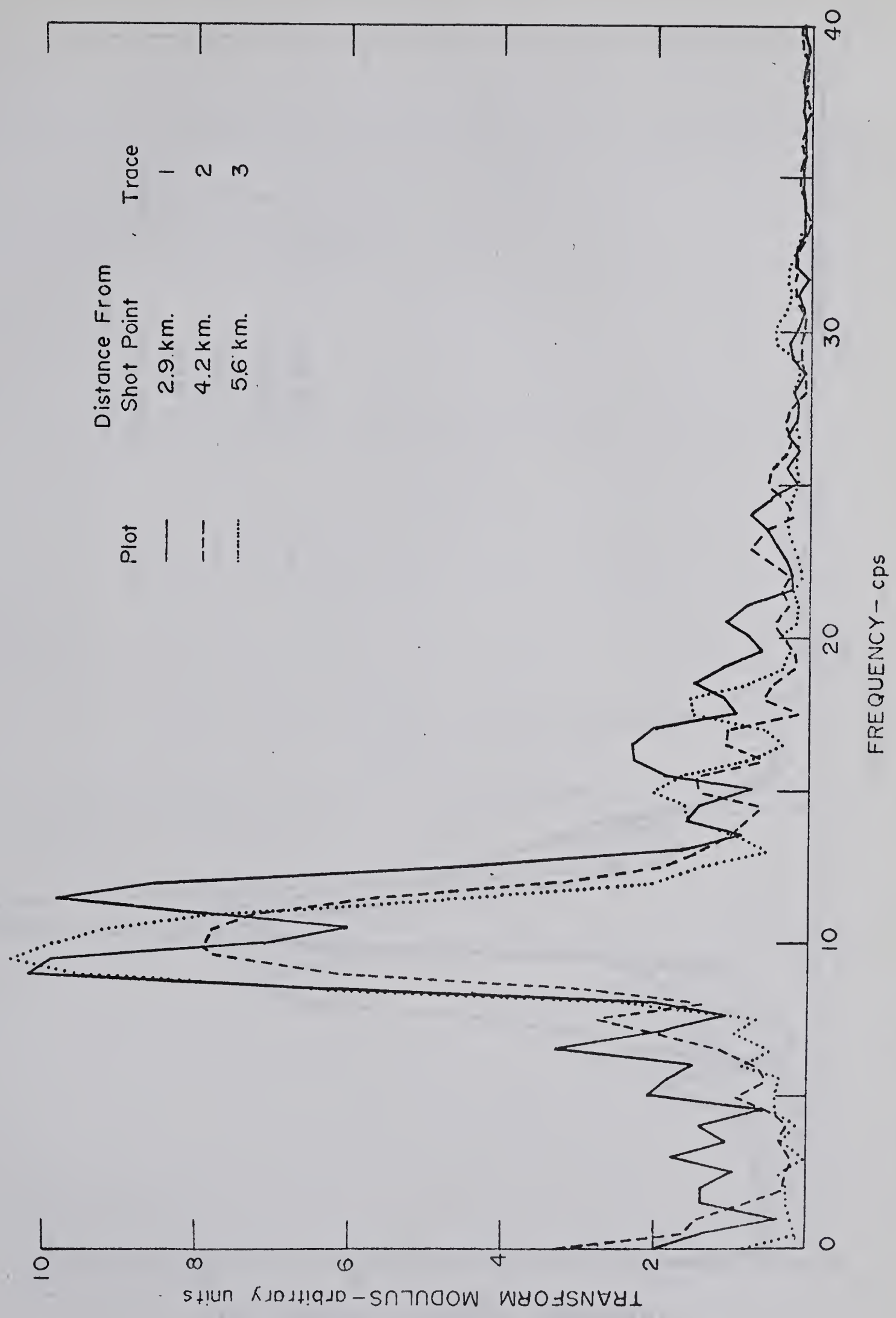


FIGURE 3.7 Fourier transform amplitudes for traces 1 to 3 of figure 3.6.

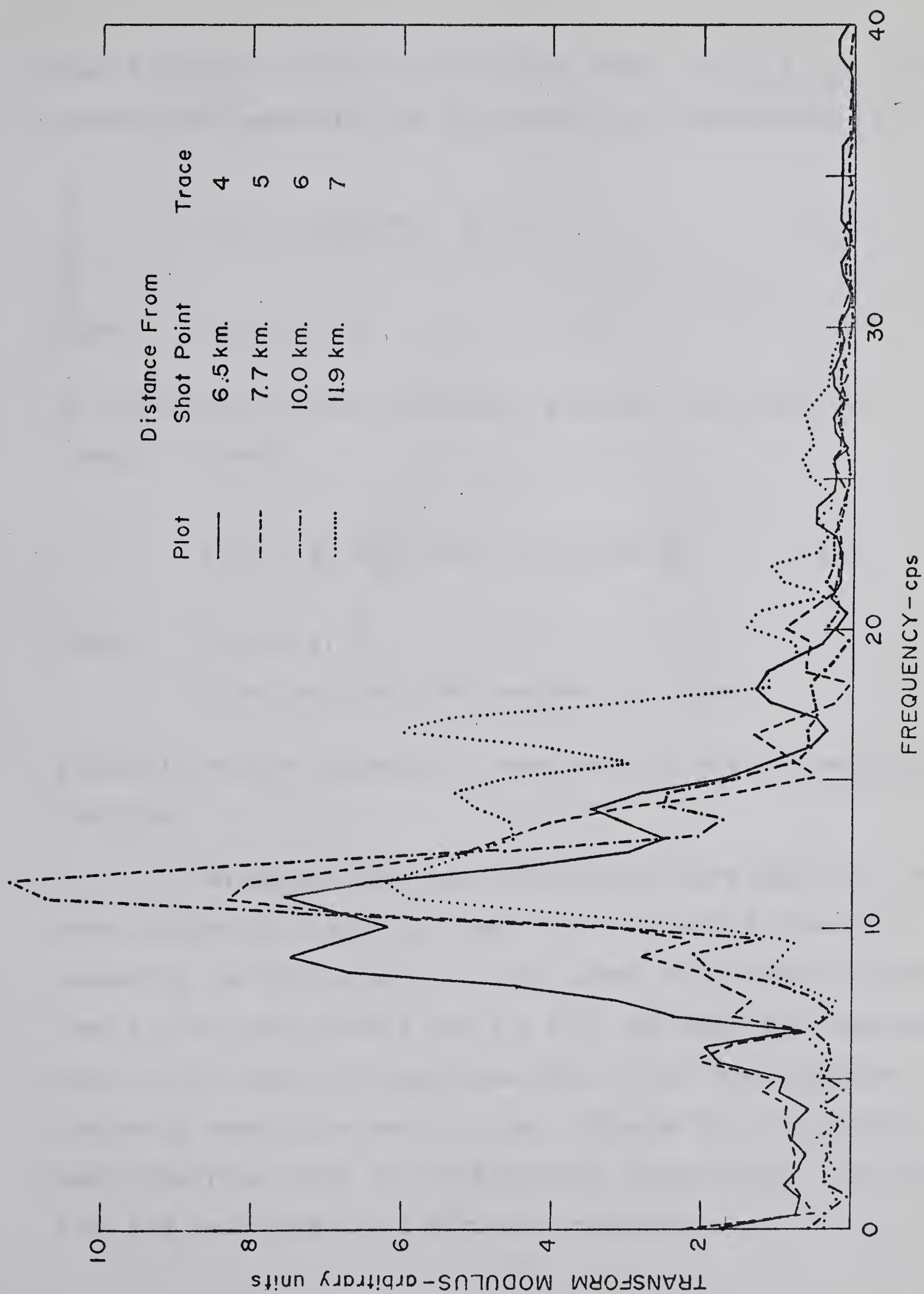


FIGURE 3.8 Fourier transform amplitudes for traces 4 to 7 of figure 3.6.

spaced spectral calculations in the range $0 \leq f \leq f_N$. The formula for computing the autocorrelation coefficient is

$$C(L) = \frac{1}{N-L} \sum_{i=1}^{N-L} G_i G_{i+L} \quad (3.4)$$

where $L = 0, 1, 2, \dots, (N-1)$.

For calculation of the autopower spectra, the following formula is used:

$$P(J) = 2\tau \sum_{L=0}^{N-1} W(L) C(L) \cos \frac{\pi L J}{M} \quad (3.5)$$

where $J = 0, 1, 2, \dots, M$

M is the specified maximum J value.

A Daniell window (Appendix 2) was used for $W(L)$, a weighting function.

Autopower spectral calculations were made for the seven traces of figure 3.6 and for a one second interval preceding the data shown. In all cases, the number of points used in the calculations was $N = 216$, the constant characteristic of the Daniell window was $N/M = 3$ and the effective frequency resolution was 1.5 cps. Figures 3.9 to 3.12 are semi-logarithm plots of the frequency versus power. No correction has been made for instrument response.

FIGURE 3.9

Autopower Spectra for 1 Second Interval Preceding Time Interval of Figure 3.6.

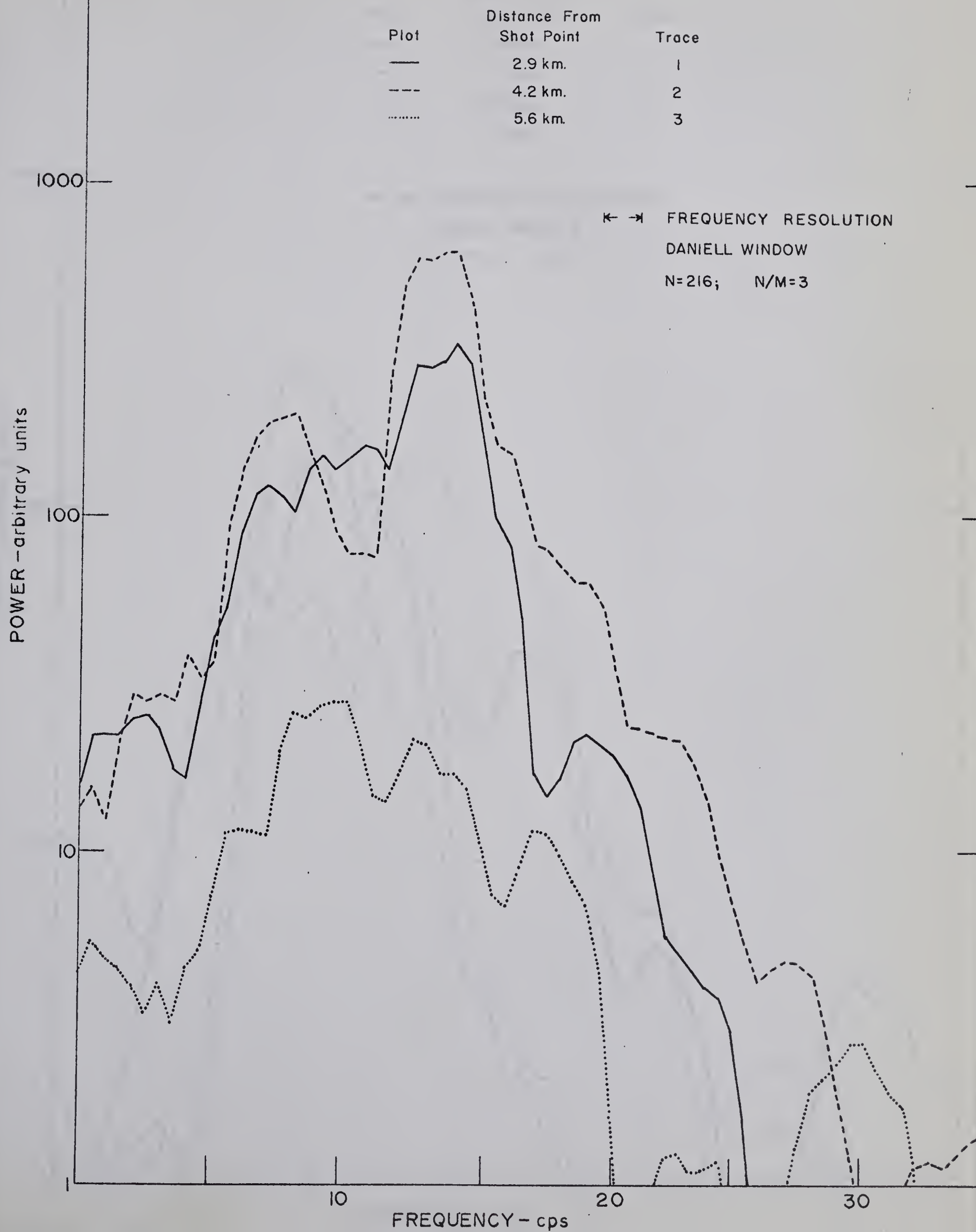


FIGURE 3.10

Autopower Spectra for 1 Second Interval Preceding Time Interval of Figure 3.6.

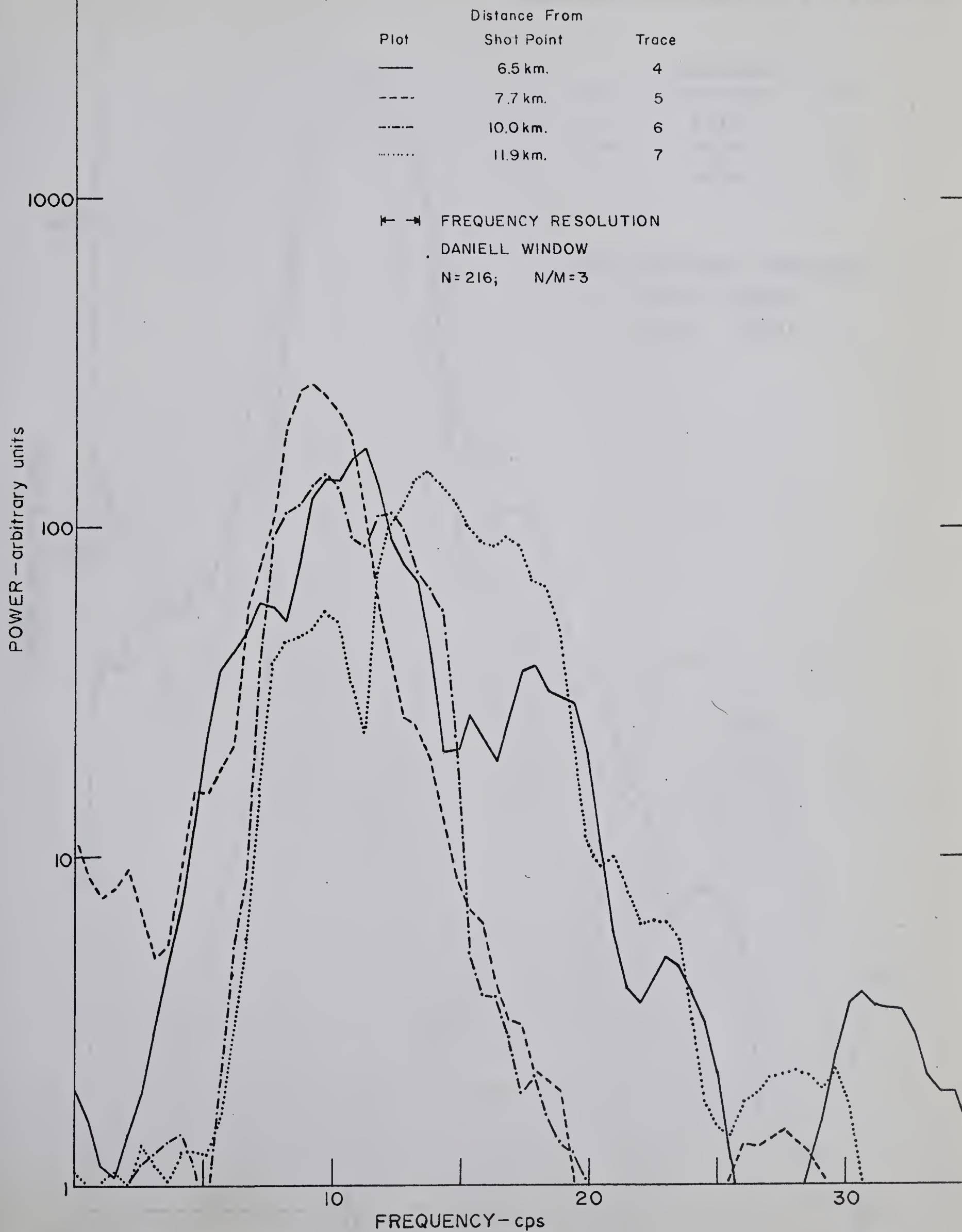


FIGURE 3.11

Power Spectra for Traces 1 to 3 of Figure 3.6.

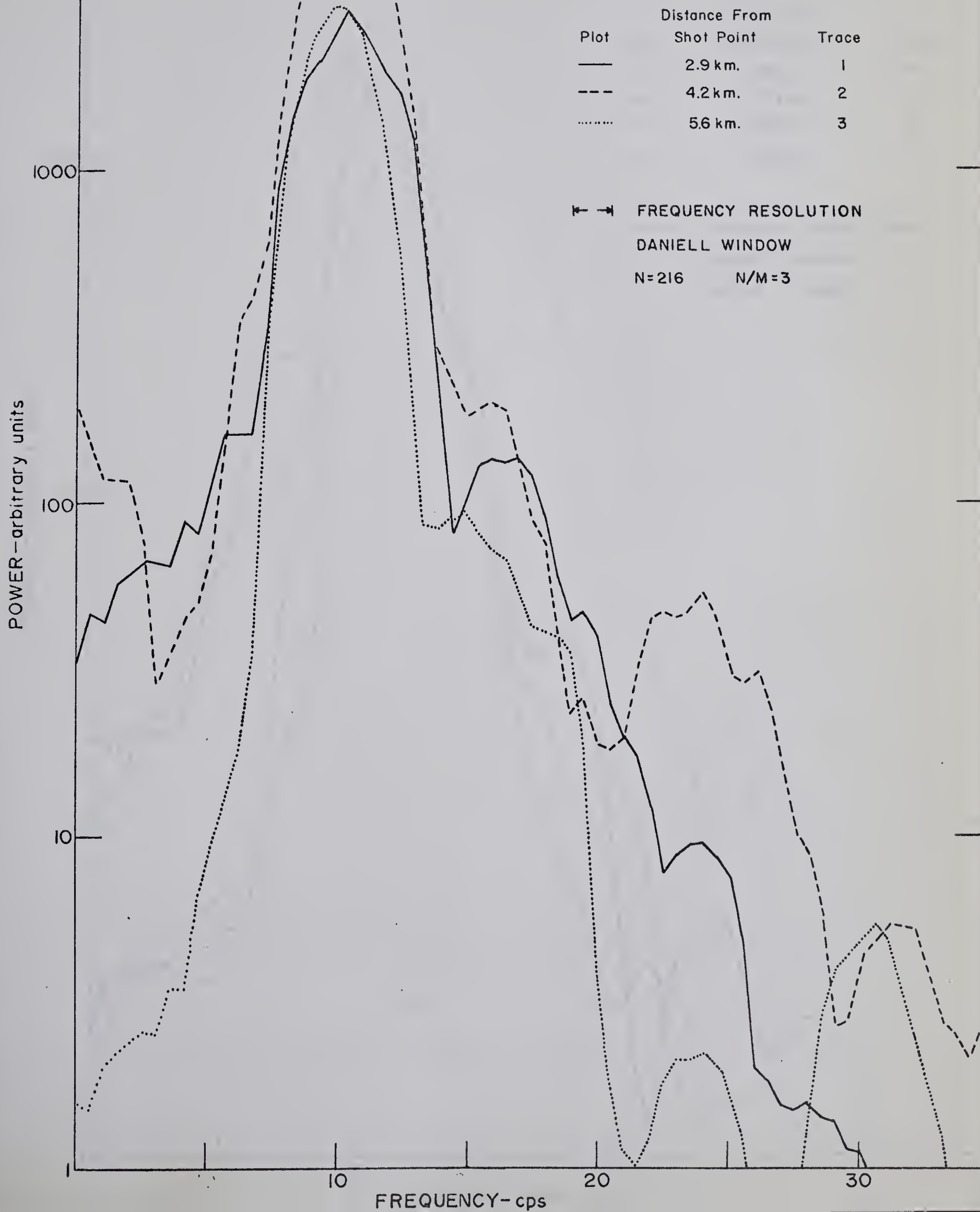
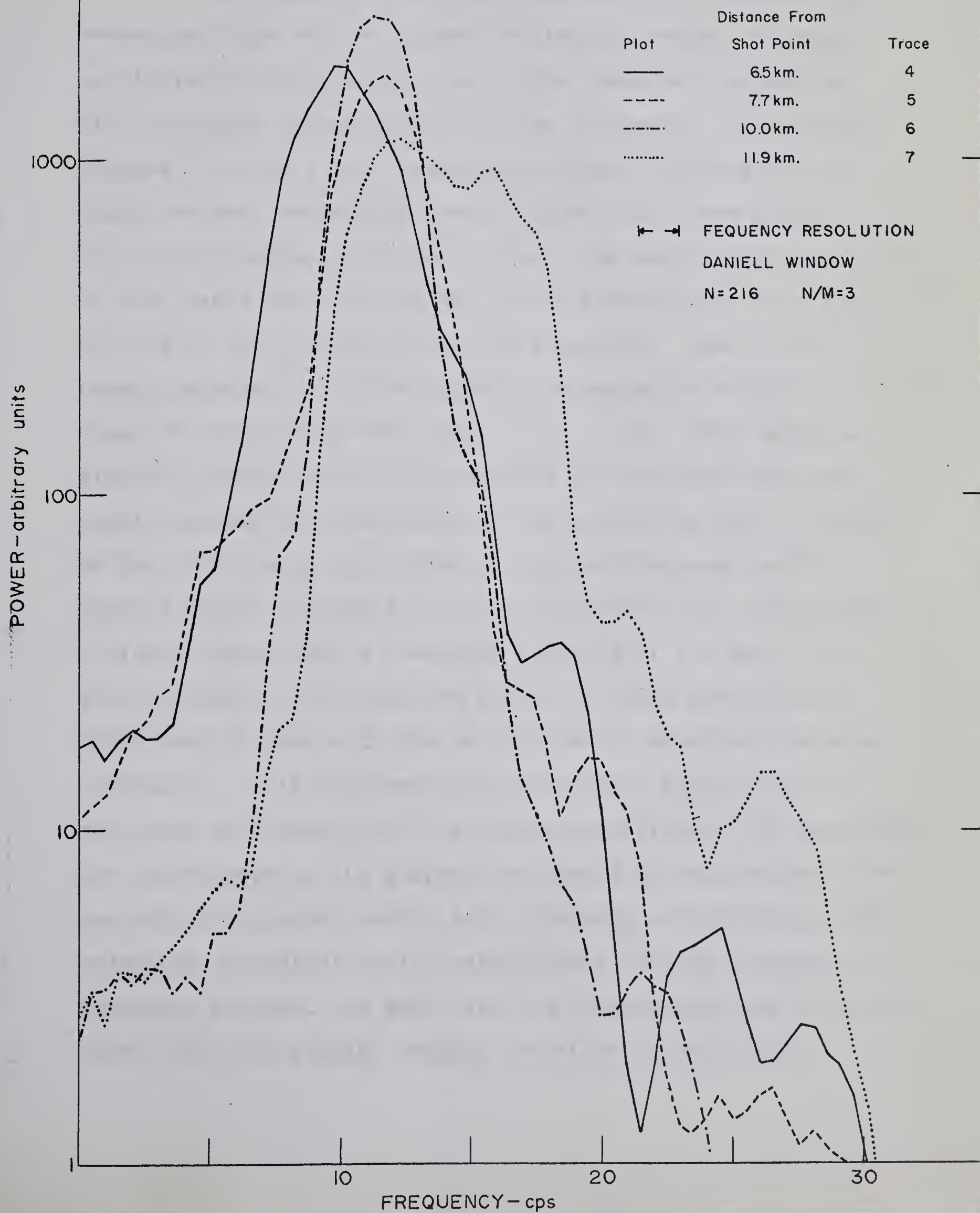


FIGURE 3.12

Power Spectra for Traces 4 to 7 of Figure 3.6



The graphs of the first two figures, representing record sections with no evident reflecting event, indicate considerable energy over quite a wide range of frequencies with no maxima characteristic of one frequency. In contrast, figures 3.11 and 3.12, representing record sections with a highly evident reflecting event (figure 3.6), show graphs with strong maxima at around 11 cps. The energy depicted by such peaks must thus be due to the introduction onto the records of the reflection near 11.6 seconds. Most of the energy represented by the peaks is concentrated within a range of frequencies from about 7 to 17 cps. This range is slightly greater than that indicated by the transforms primarily because the resolution of the spectra is only 1.5 cps, so that the energy calculated at any one frequency as the Daniell window is passed over the autocorrelation coefficient includes energy over a frequency interval of 1.5 cps. As also denoted by the transform plots, the peak power shifts from about 10 cps to 12 cps as the shot-to-detector distance increased. It is believed that this trend is due mainly to shot-hole environment and the surface location of the geophones. The correctness of the supposition should be resolved with the analysis of more and varied data. Because of stability, and rejection of statistically insignificant changes through an averaging process, the power spectra computations are to be preferred over the simpler Fourier transform calculations.

An important task of the power spectra program was to give an indication of the range of frequencies over which all signals are received. Thus the autopower spectrum was computed for traces 5 to 7 of figure 3.3, the time interval being from 9.4 to 15.9 seconds. With $N = 1440$ points and a characteristic constant for the Daniell window of $N/M = 10$, resulting in a frequency resolution of 0.7 cps, the calculations were made. Figure 3.13 is a plot of the resultant spectra.

Since the graphs represent different stacking techniques including the same trace, a few comments can be made concerning the results of stacking. Both methods involving a number of traces reduced the amplitudes on either side of the large energy peaks. The Gaussian stack reduced the low frequency peak most and increased slightly the power of the center peak to that of the two adjacent peaks in the large energy region. Reduction of the amplitudes at higher frequencies for both methods was about the same.

The most important point from the spectra is the suggestion that band-pass filtering with a band width from 5 to 15 cps would reduce the magnitude of the side bands which are thought to represent undesirable surface waves or wind noise. Following this suggestion, future plans for analysis include digital filtering of the data prior to any other major processing techniques.

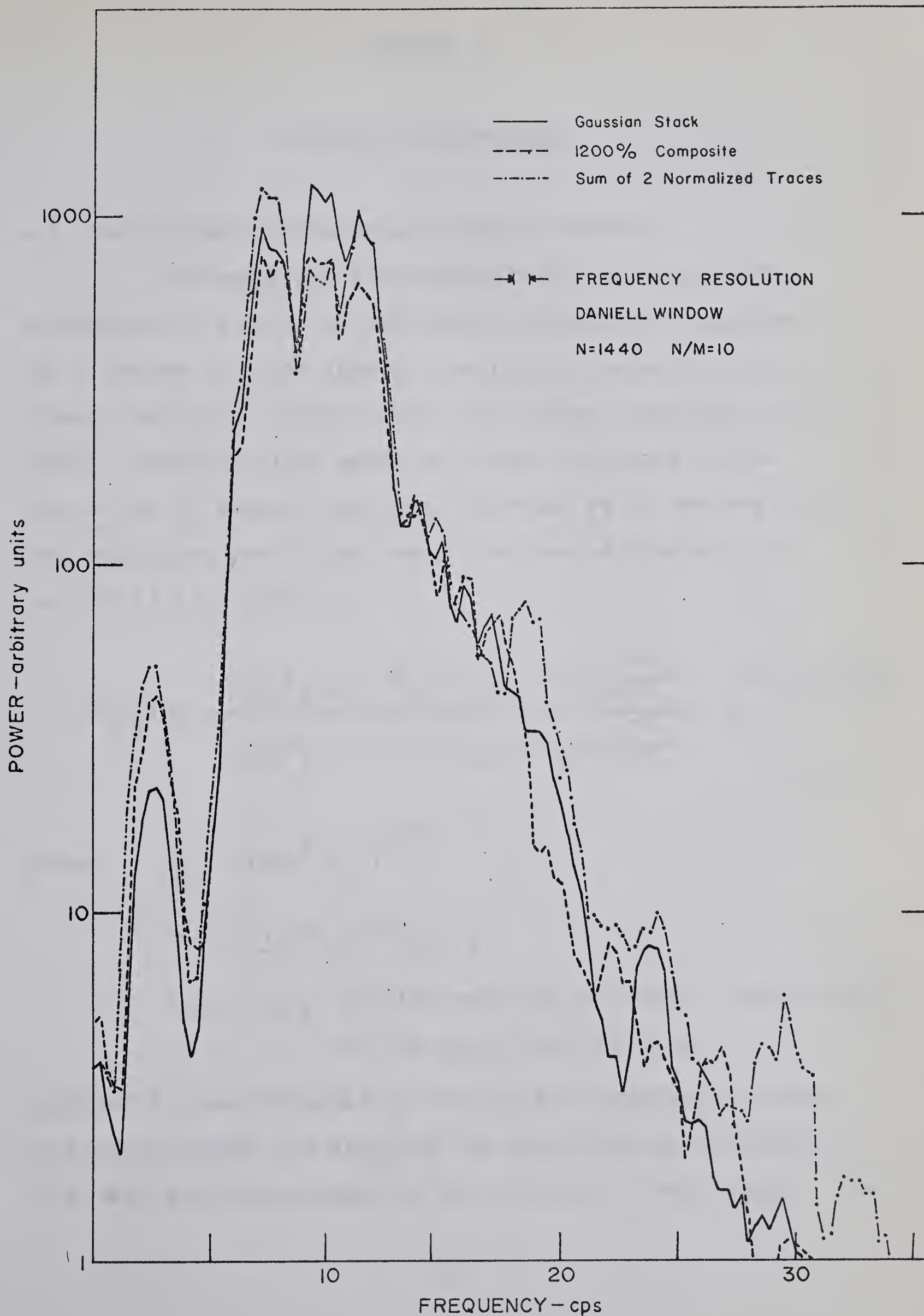


FIGURE 3.13 Autopower Spectra for 3 Traces;
 Time Interval of 9.5 to 15.5 Seconds

CHAPTER 4.

SYNTHETIC SEISMOGRAMS

4.1 The Synthetic Seismogram Computer Program

The basis for the computation of the synthetic seismogram is a means of calculating reflection responses for a system of plane layers in which the velocity is a linear function of depth within each layer (Berryman et al, 1958). Assuming plane waves at normal incidence to the layers and no density contrast, Berryman et al deduced that the reflection coefficient as a function of frequency, ω , for the $(j-1)$ th layer is

$$R_{j-1}(\omega) = \frac{b_{j-1}\beta_{j-1} + (b_j - b_{j-1}) - b_j\beta_j\left(\frac{1-R_j}{1+R_j}\right)}{b_{j-1}\beta_{j-1} - (b_j - b_{j-1}) + b_j\beta_j\left(\frac{1-R_j}{1+R_j}\right)} e^{-\beta_{j-1} \ln \frac{v_j}{v_{j-1}}} \quad (4.1)$$

where $\beta_j = [1 - 4\omega^2/b_j^2]^{1/2}$

$$b_j = (v_{j+1} - v_j)/(z_{j+1} - z_j)$$

v_{j+1} , z_{j+1} are the velocity and depth, respectively, at the end of the j th zone.

Equation 4.1 was obtained by solving the equation of motion in elastic solids and applying the conditions of continuity of stress and displacement at the boundary of each layer. The

N^{th} or last layer is unlimited and its reflection coefficient, R_N , is zero. In the first layer, R_0 represents the ratio between the reflected wave and incident wave amplitudes and consequently is the transfer function of the entire layer system to waves at normal incidence.

The value of R_0 is computed from 4.1 by an iterative procedure beginning with R_{N-1} ($R_N=0$), and so gives the reflection coefficient for plane waves of normal stress. For displacement the calculated value is multiplied by -1. Since R_{j-1} is indeterminate if either b_j or b_{j-1} is zero, the equation may be solved for this special case or more simply for computer processing, one can set the velocity gradient, b_j , equal to a very small value such as 0.001. The latter was done in the author's program.

In addition to having the reflection response of a layered system as a function of frequency, it is necessary to have some form of an input to the system before a synthetic seismogram can be generated. A Ricker wavelet (Ricker, 1953) has often been used as a close approximation to a seismic pulse. Examples of its use are given by Jones and Morrison (1954) and by Berryman et al. The form of the Ricker wavelet used by the latter consists of the sum of the fifth and sixth derivatives of the error function, $\phi(x)$:

$$G(x) = - [\phi^5(x) + \phi^6(x)] \quad (4.2)$$

where

$$\phi^n(x) = \frac{d^n}{dx^n} \left[\frac{1}{\sqrt{2\pi}} e^{-x^2/2} \right] \quad (4.3)$$

and $x = t/T$, t representing time and T a parameter characteristic of the period of the pulse. The synthetic seismogram is then obtained from the Fourier transform:

$$S(t) = \int_{-\infty}^{+\infty} R_o(\omega) G(\omega) e^{i\omega(t + z/v_o)} d\omega \quad (4.4)$$

where $G(\omega)$ is the complex spectrum of the incident pulse and z/v_o is a time delay factor. The Fourier integral was evaluated by the method described in Chapter 3 (or see Appendix 2).

Since it was imperative that an accurate working program be obtained, the initial development of the program centered about a duplication of the results of Berryman and his group. That such a program has been developed is evidenced by figures 4.1 and 4.2. The former is a copy from Berryman et al for one case which they considered; the latter is the result obtained by the author. In similar comparisons between the different cases which Berryman et al considered, the author's results corresponded nearly identically, small

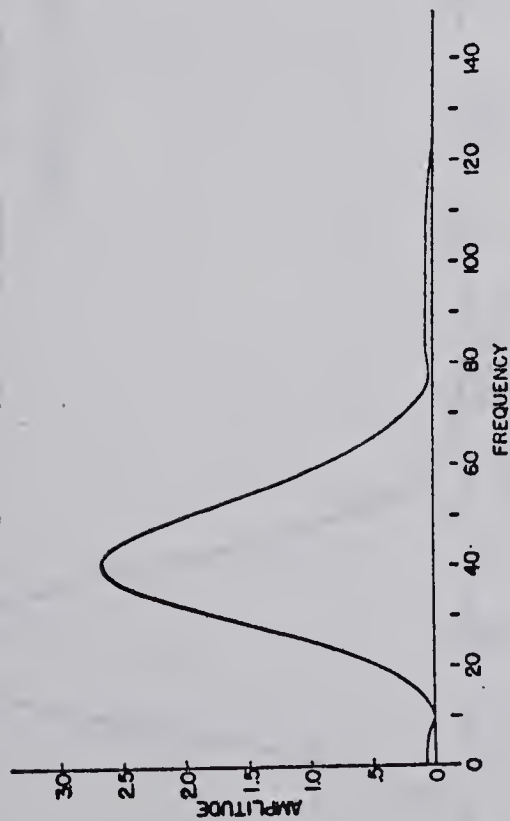


FIG. 4. Amplitude spectrum of incident pulse.

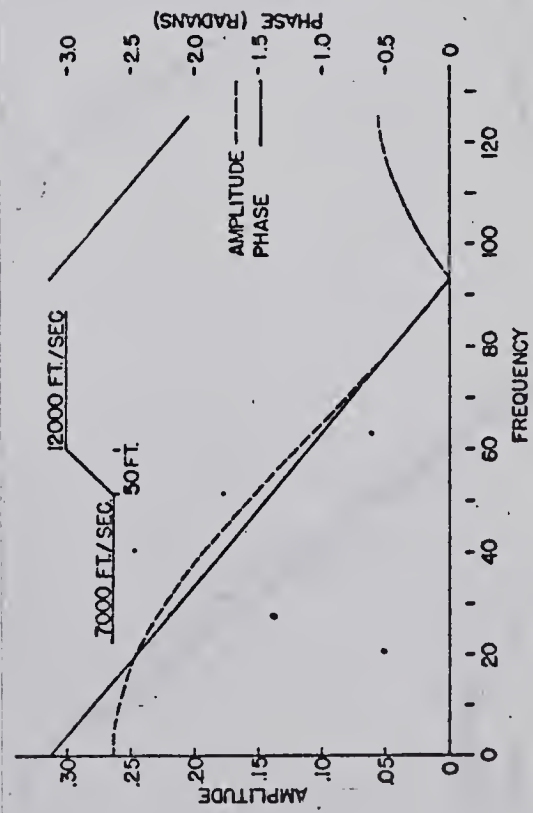


FIG. 5. Amplitude and phase characteristics for single transition layer ($b = 100 \text{ ft/sec/ft}$).

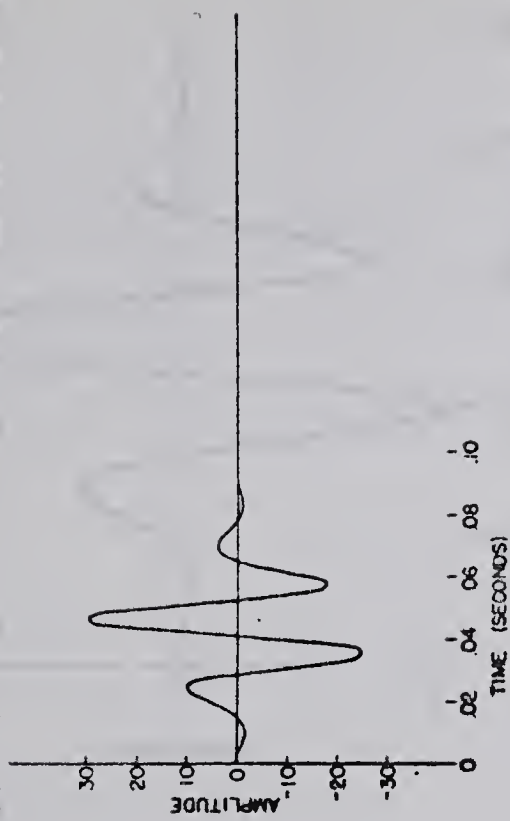


FIG. 3. The incident pulse.

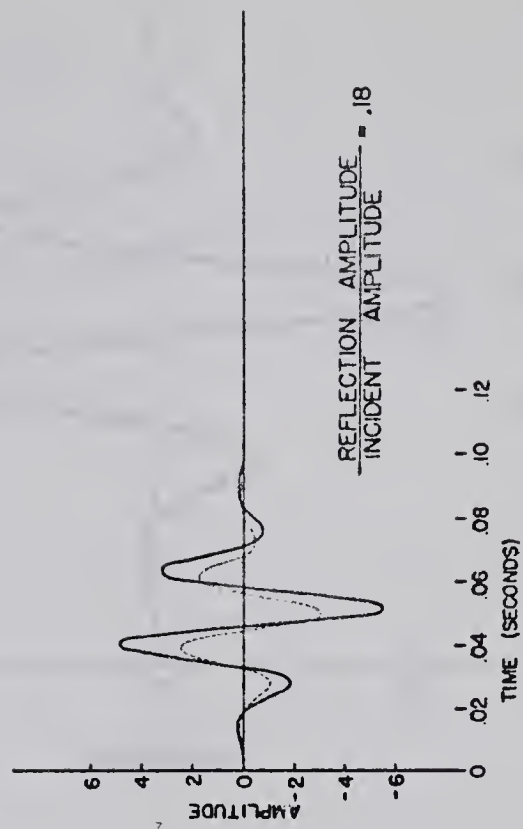


FIG. 6. Reflected pulse from the transition layer ($b = 100 \text{ ft/sec/ft}$).

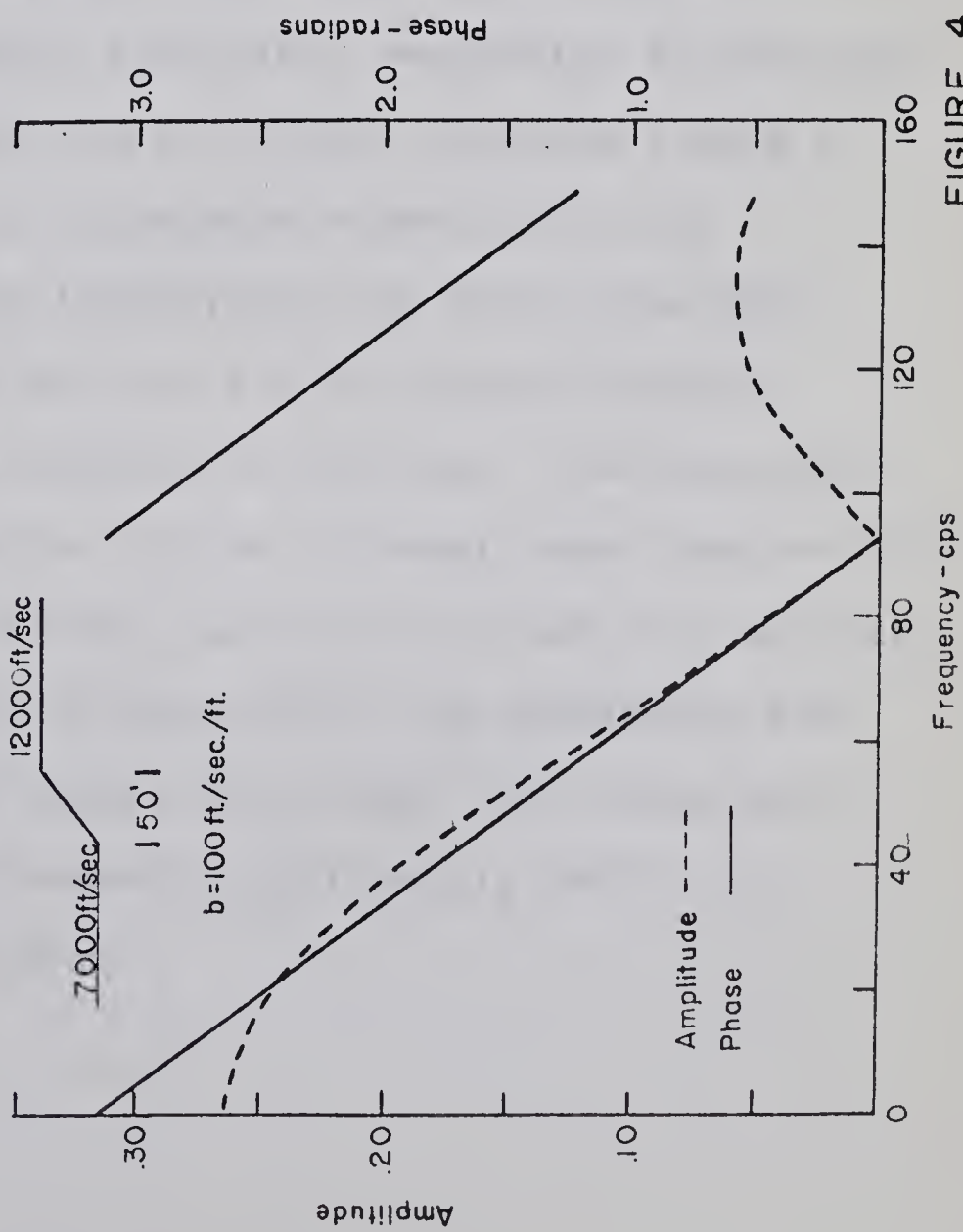
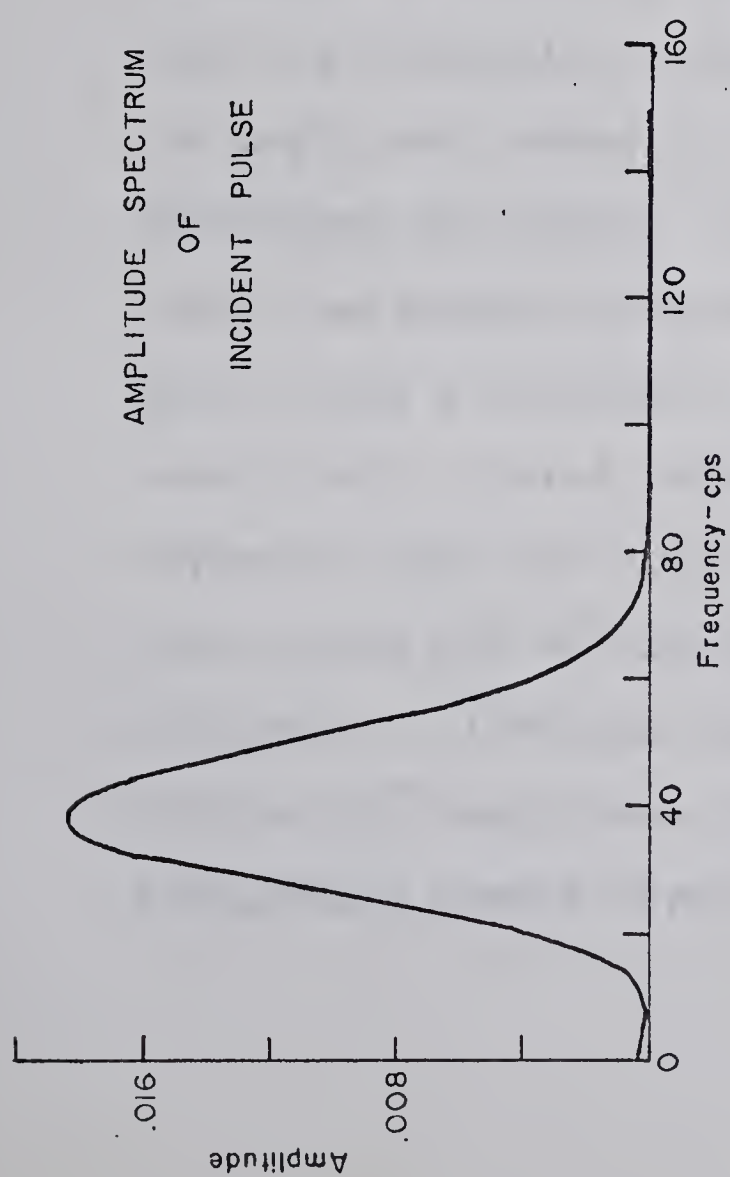
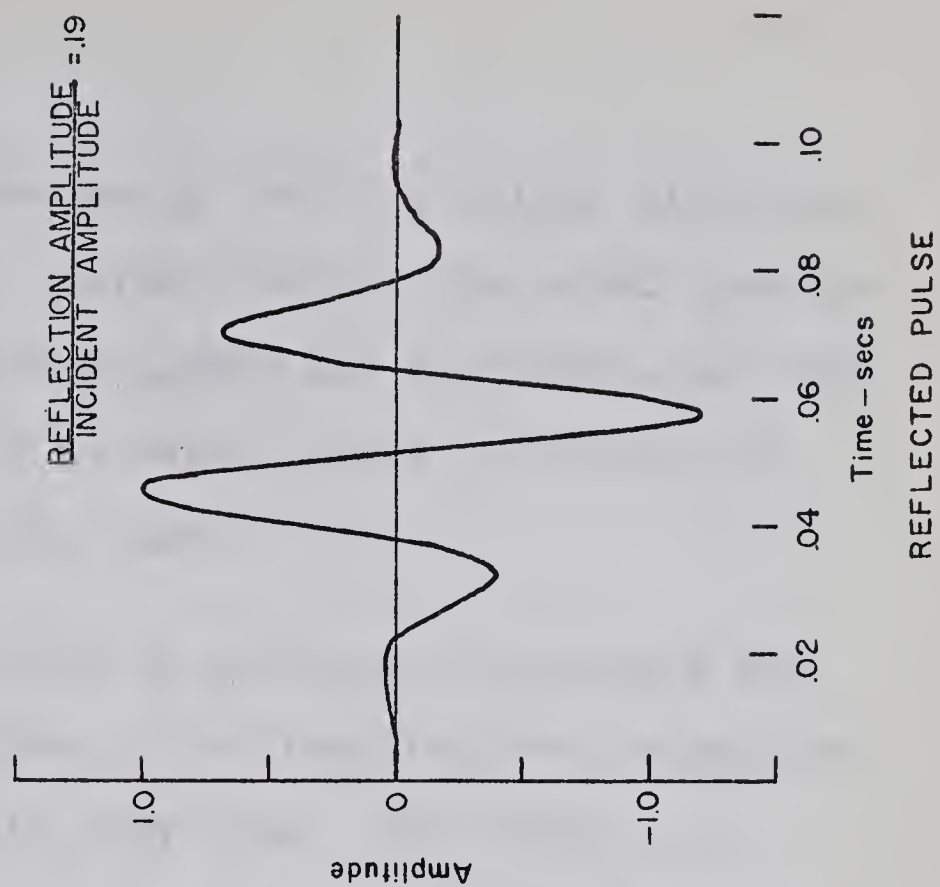
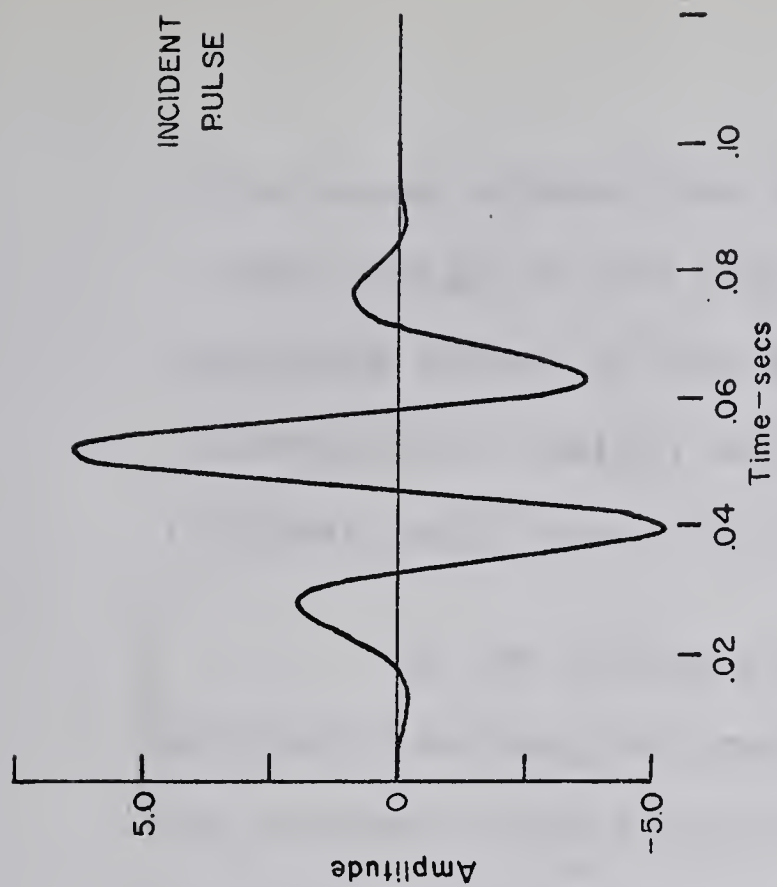


FIGURE 4.2

differences between the two being due to a slight difference in the period of the input pulse. It will be noted that the amplitude scales on the two diagrams are different, but that corresponding ratios, such as peak-to-peak reflection to incident amplitudes, are the same.

A few points should be mentioned concerning the synthetic seismogram program. The time involved to perform the Fourier integrations is very long. For example, a synthetic seismogram 16 seconds long took 7 hours on the IBM 7040 computing system. This large time factor was mainly due to the necessity of using very small increments in frequency in order to obtain sufficient resolution to delineate just the reflecting events and not obtain spurious events of low amplitude caused by an inadequate superposition of amplitudes and phases. To illustrate this point, the synthetic seismogram program was run for an assumed crustal model using a frequency increment of $1/16$ cps. The resultant record had a Conrad reflector but an extremely weak Mohorovičić reflector plus two other events, at about 6.4 and 10.1 seconds, which could not be explained physically. By decreasing the increment to $1/40$ cps the magnitude of both the Conrad and Mohorovičić events was increased significantly and no unexplainable events were found.

The maximum frequency interval which can be used is governed by the length of record section desired. For example, with an interval of 0.5 cps the maximum record length obtainable is 2 seconds because the entire record for the two seconds repeats continuously, as is to be expected when an integral form is reduced to a series. The inverse transform involves the terms " $\cos 2\pi ft$ " and with $f = 0.5$ cps, this term has the same value for $t = 0$ as for $t = 2.0$ since the cosine term is cyclic with a period of 2π radians.

Future plans include a modification of the synthetic seismogram program to include an automatic volume control factor and possibly some function representing the instrument response which is included in a true field record. Of prime concern will be a detailed analysis of the program to see if its operation time can be reduced, as this is a severe limiting factor.

4.2 The Mohorovičić Discontinuity as a Transition Zone

One of the first points investigated was the range over which a velocity discontinuity, represented by a linear gradient from a lower to a higher velocity, could prevail and still give a good reflection. Figure 4.3 includes some results from this study. It will be noted from the diagram

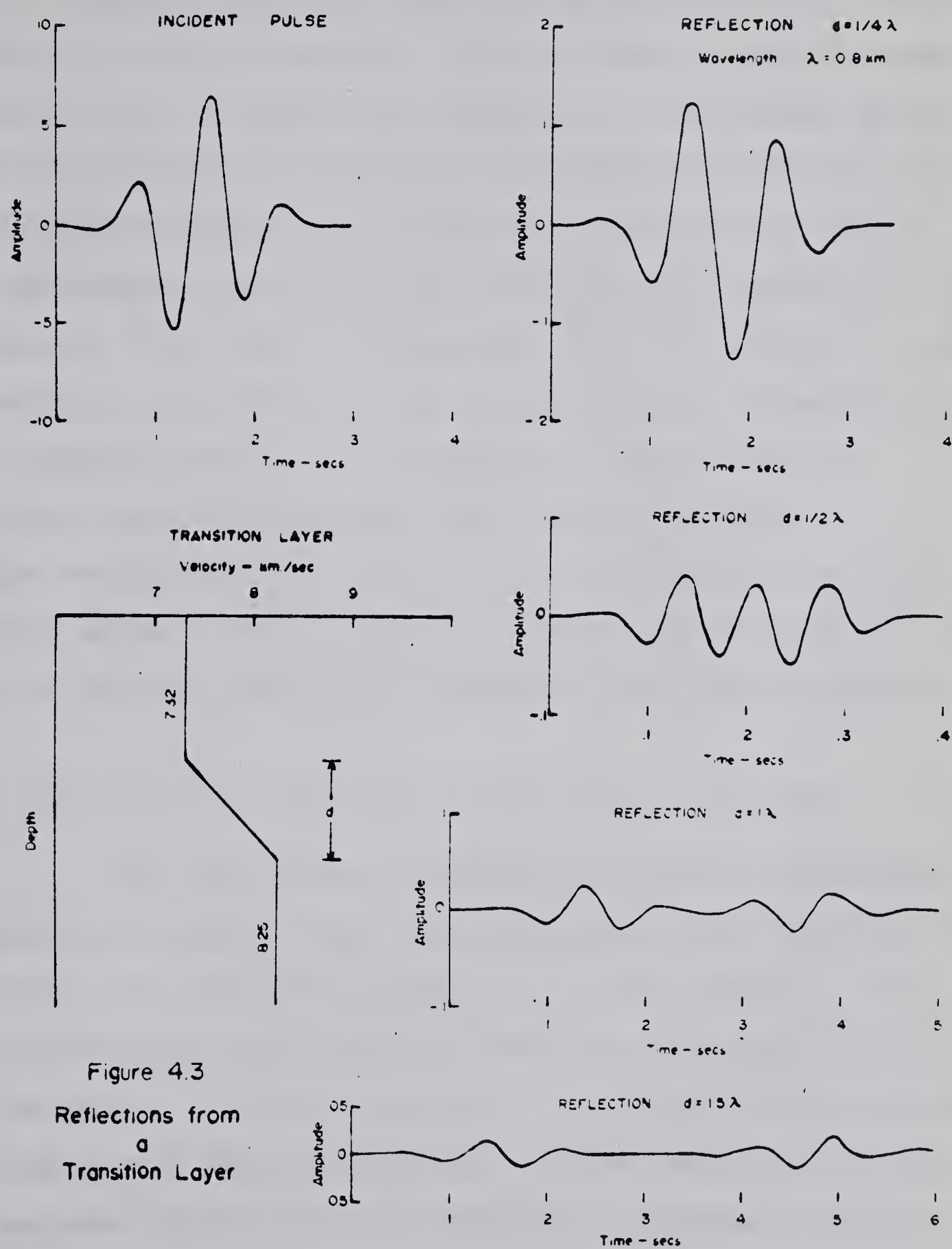


Figure 4.3
Reflections from
a
Transition Layer

that a change in velocity from 7.32 to 8.25 km./sec. (representative of the refraction velocity values at the M discontinuity) over a distance the order of $1/4$ wavelength gives a distinct reflected pulse, but over greater distances such a distinctive pulse is not obtained. The width of such a $1/4$ wavelength transition zone would be $1/5$ kilometer for a frequency of 10 cps or 2 kilometers for a frequency of 1 cps. Therefore, if a reflection is obtained from a transition zone, the transition must be 2 kilometers or less in extent, dependent upon frequency and the velocity contrast. A larger reflection coefficient could be obtained by an interference pattern from a group of closely spaced transition layers, but the general principle illustrated above still applies.

4.3 The Synthetic Seismogram from Acoustic Log Data

For the purpose of making a synthetic seismogram, digitized acoustical logs from two wells at LSD 10-15-18-19 W4M and LSD 10-21-18-21 W4M (figure 2.3) were acquired. The well information was obtained from Petrex Data Agencies, Ltd. on IBM punch cards and consisted of the travel time in microseconds over a one-foot interval. Since velocity and depth values are required for the synthetic seismogram program, this necessitated that a program be written to convert the time data to velocity data. This was done but within the program the velocity values were computed as an average over

a ten-foot interval. Synthetic seismograms characterized by input pulses with dominant frequencies of 20, 28, and 40 cps were generated from the well log data. As would be expected the seismograms with the higher frequency input pulse exhibited much more detail than the corresponding ones with a lower frequency pulse. A reasonable correlation between the synthetic seismograms and field records from the same area, kindly provided by Tenneco Oil and Minerals, Limited, could be made.

The principal reason for generating synthetic seismograms was to obtain some indication of the effects of multiple reflections on deep reflecting events. Some examples of simple multiple reflections which could be produced are illustrated in figure 4.4.

In making the synthetic seismogram, a horizontally layered model of the crust was considered, the information at depth taken from the refraction data. In order to generate multiples between the surface and any strong reflector within the sedimentary strata, a near-surface velocity of 1.22 km./sec. (4000 ft./sec.) was assumed, the velocity increasing over a 3 meter interval to 2.90 km./sec. (9500 ft./sec.), this system then representing a velocity step function. The velocity-depth values from the acoustical log nearest the Lomond profile formed the next part of the model, these representing

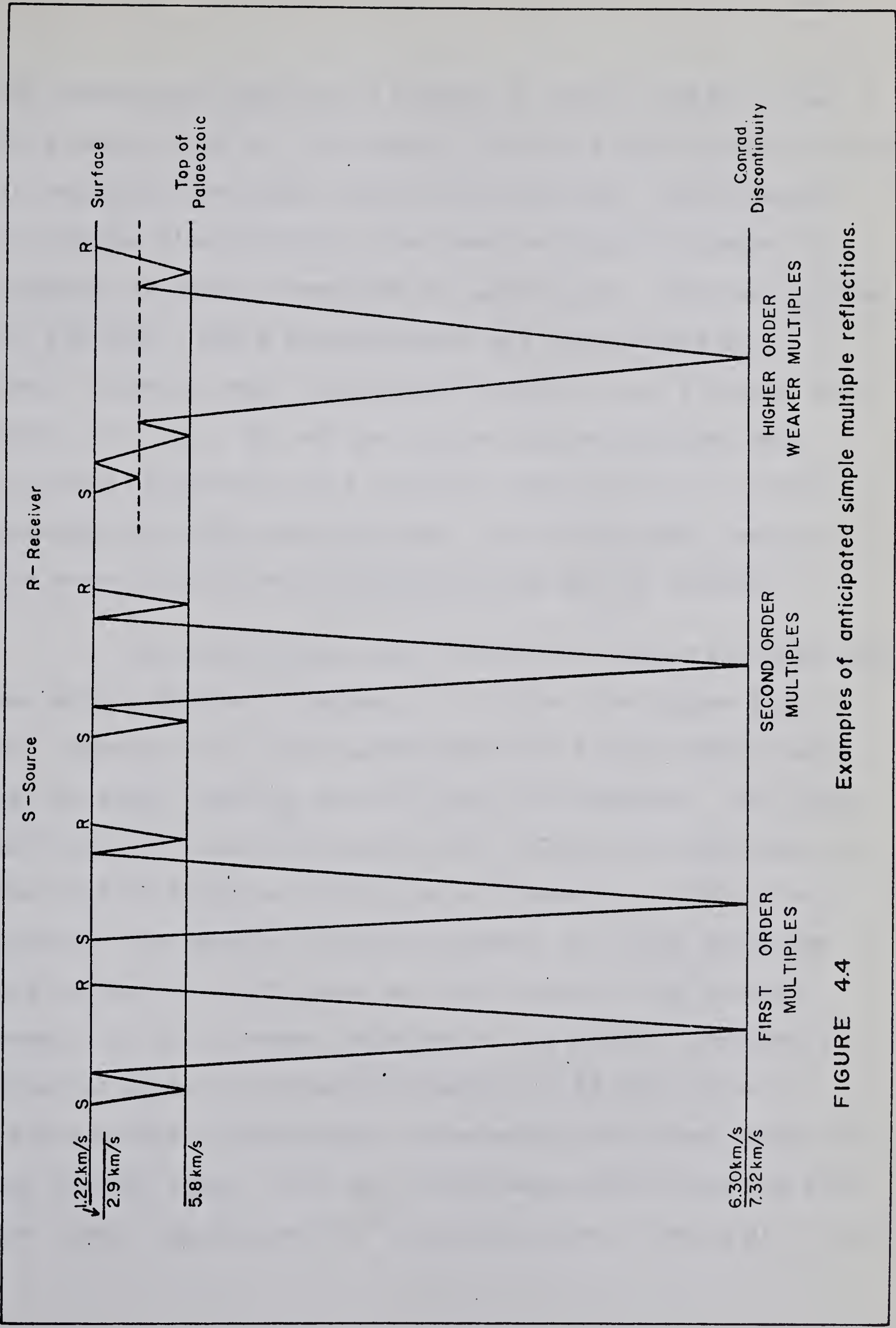


FIGURE 4.4 Examples of anticipated simple multiple reflections.

the sedimentary section to a depth of about 1.67 km. From this depth to 34 km., the model included a slow linear increase in velocity from about 5.90 to 6.30 km./sec. To represent the Conrad discontinuity, there was an abrupt increase in velocity at 34 km. from 6.30 to 7.32 km./sec. over an interval of 3 meters. The M discontinuity was represented by a sharp increase from 7.35 to 8.25 km./sec. over 3 meters at a depth of 47 km. All of the induced discontinuities were included essentially as a velocity step function to obtain maximum reflection coefficients. With this model, nearly the worst case of multiple reflections may be studied.

The input pulse was the same one described previously, but with a dominant frequency of 13 cps. In figure 4.5, the upper half of the diagram shows the Ricker wavelet used as the input together with its Fourier transform. The lower half of the illustration gives the reflection coefficient of the crustal model as a function of frequency. Within the synthetic seismogram computer program, the pulse transform and reflection coefficient are multiplied in the complex domain and the inverse transform of the product computed to give the signal. Plotted in figure 4.6 is the entire 16 second synthetic seismogram representing reflected energy from the crustal model. The two strong deep reflections are from the Conrad and Mohorovičić discontinuities. Events at 1.7 and

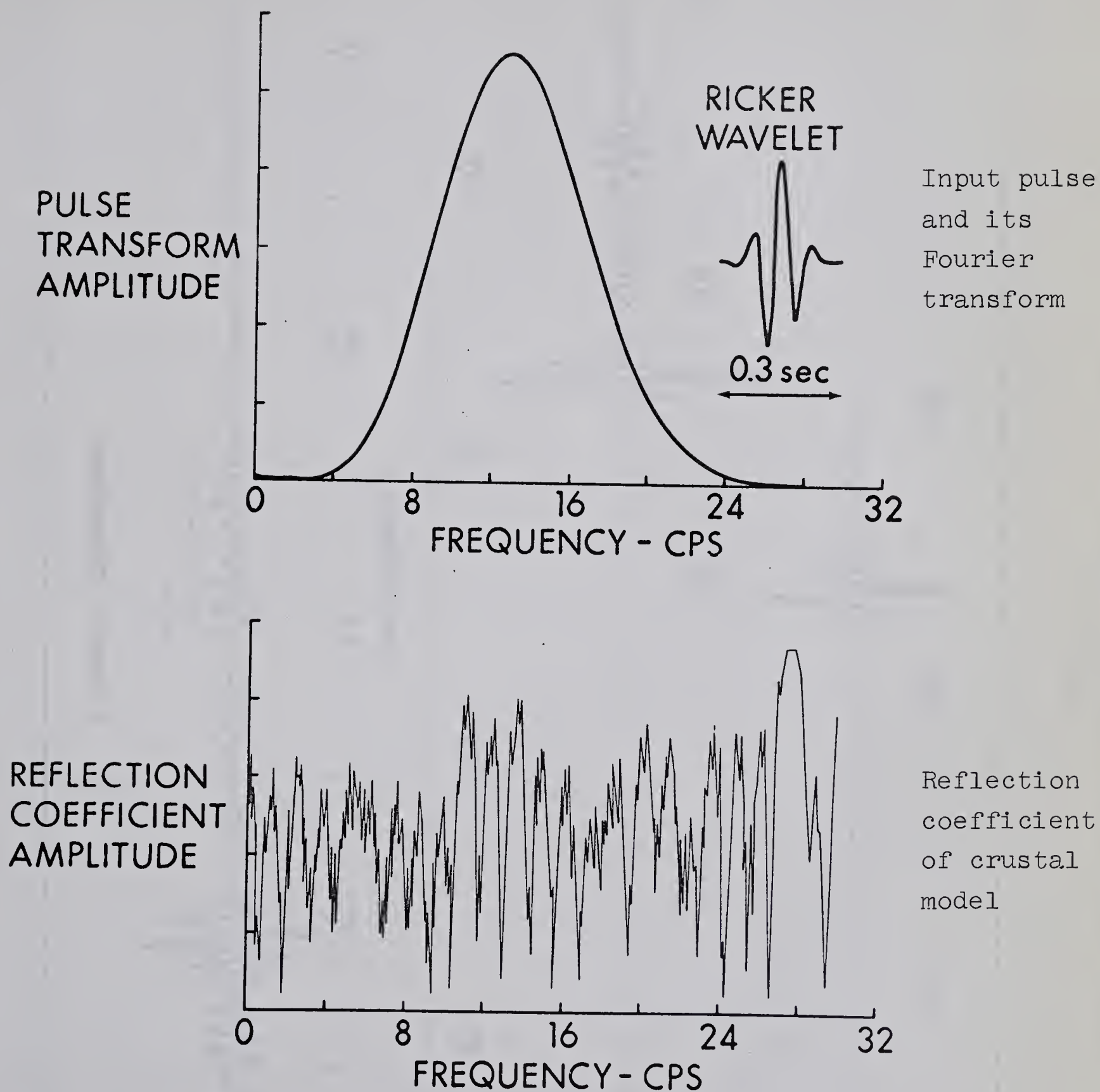


FIGURE 4.5

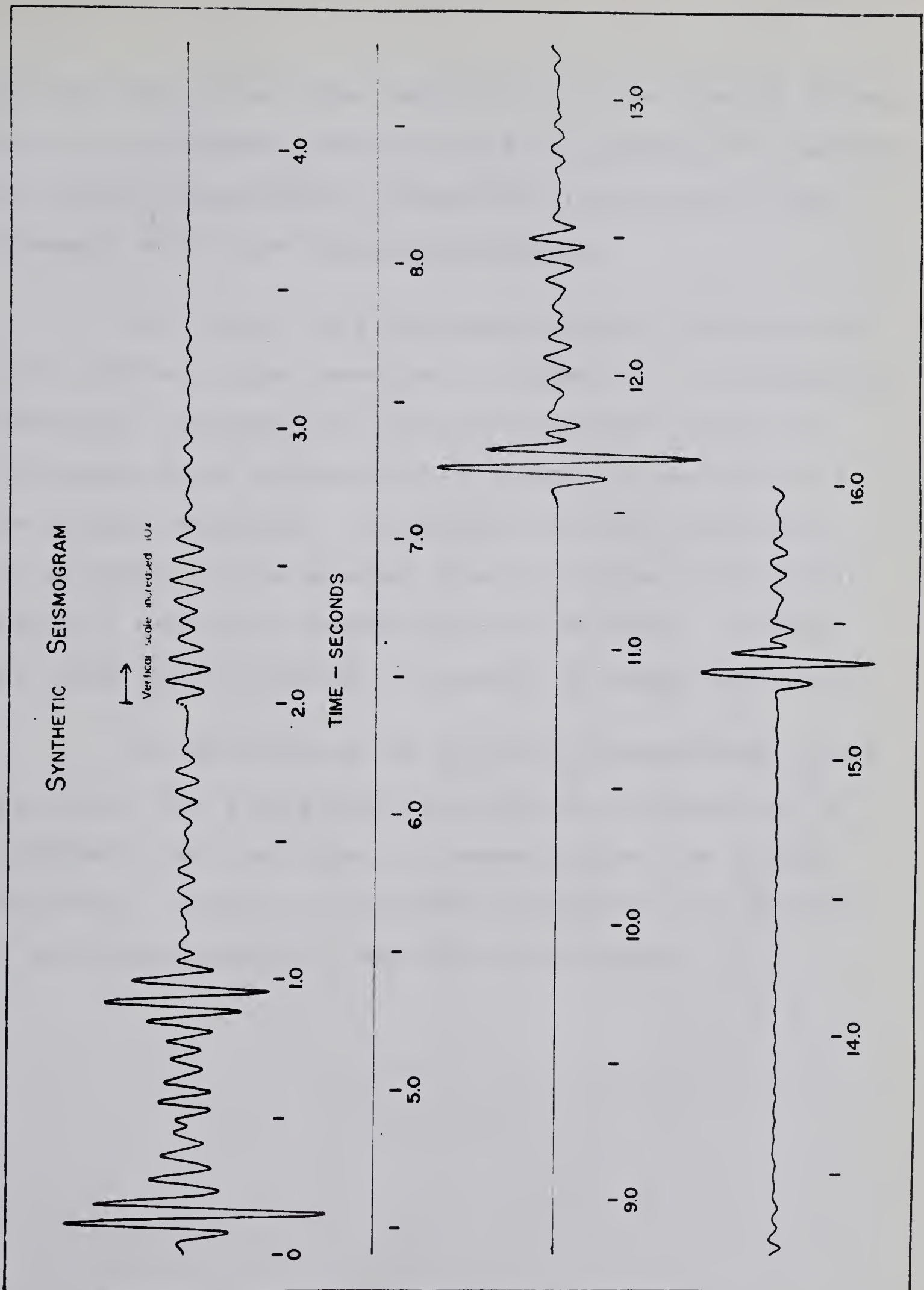


FIGURE 4.6

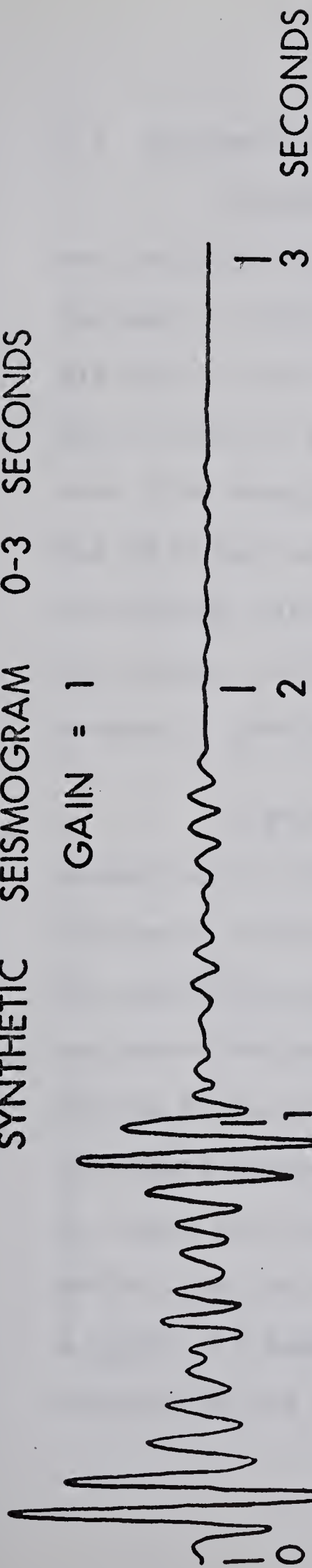
12.5 seconds are multiple reflections of the interval between the initial surface event and the strong phase at 0.9 seconds, the latter representing a reflection from the top of the Paleozoic within the sedimentary section.

An actual field recording together with portions of the synthetic are presented in figure 4.7. The synthetic seismogram indicates that multiply-reflected events are attenuated quite severely within about 1.5 seconds after the primary reflection. Comparing the field record with the synthetic, it is apparent that the signal on the field record at about 12.4 seconds may be a multiple. However, the event at 13.8 seconds is probably a primary reflection.

On the basis of the synthetic seismograms, it has been shown that strong multiple reflections should not be a problem later than about 1.5 seconds after the primary reflection. This is an important conclusion to be applied in the interpretation of any field recordings.

SYNTHETIC SEISMOGRAM 0-3 SECONDS

GAIN = 1



SYNTHETIC SEISMOGRAM 11 SECONDS

GAIN = 10

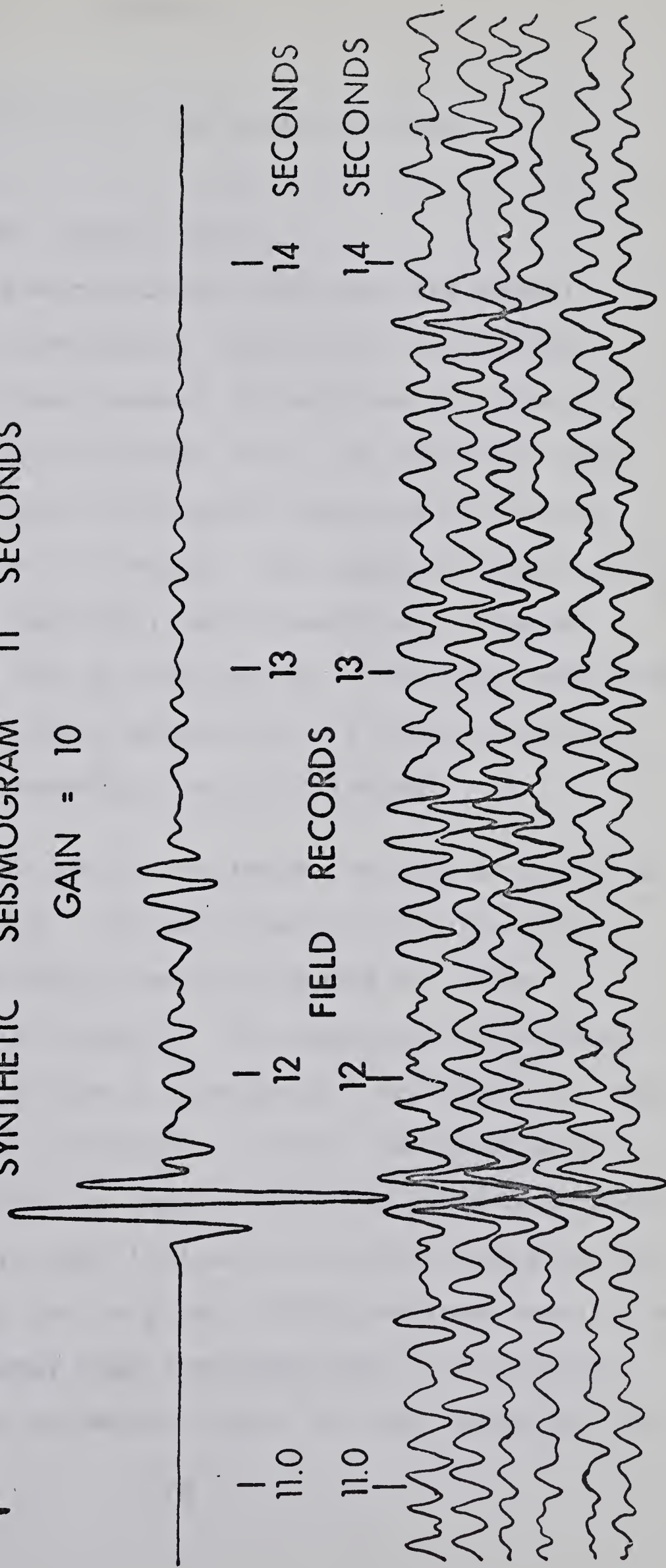


FIGURE 4.7. Field recording and selected portions of the synthetic seismogram.

CHAPTER 5.

INTERPRETATION OF THE ANALOG RECORDS

5.1 Suffield and Lake Newell Data.

Experiments were carried out near Lake Newell and on the Suffield Experimental Station for the primary purpose of obtaining deep crustal reflections at a location different from the initial Lomond site. At Suffield, data were obtained along three 6-kilometer sections of an east-west line nearly 33 km. in length. The signal-to-noise ratio was very low and the data will need considerable digital processing before it can be interpreted. The noise consisted of surface (Stoneley) waves generated in a highly weathered series of low and intermediate velocity lenses.

A portion of one of the better records acquired is presented in figure 5.1. Coherent events which possibly represent reflected energy have been marked on traces recorded through use of arrays. In comparison, the single component seismometers show a considerable amplitude of long period surface waves. Although no attempt has been made to correlate phases across the various Suffield records because of their poor quality, some indication of what layers may be reflecting the energy can be given. With previous results as a guide, it seems likely that the event near 11.6 seconds represents the Conrad reflector, while the last event may be

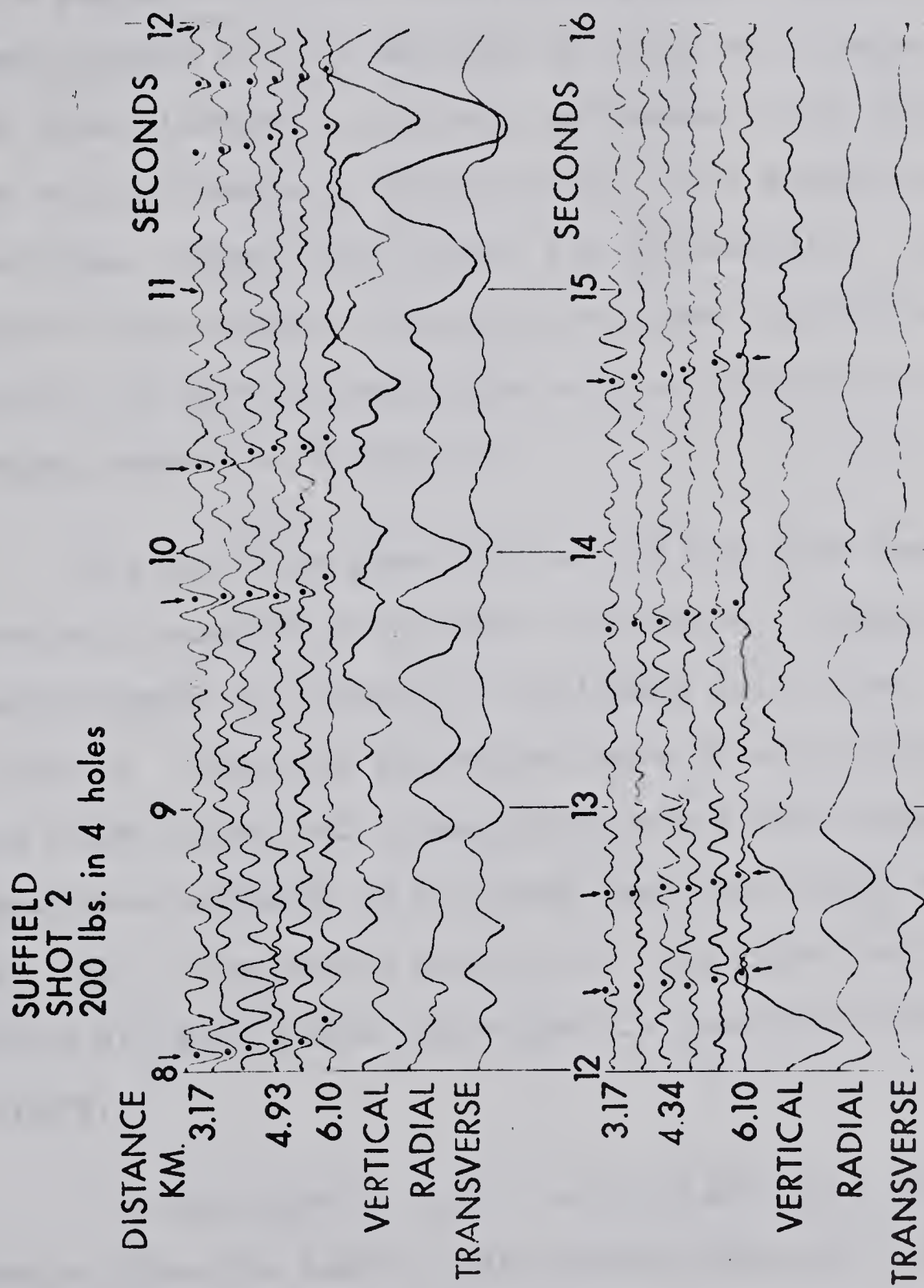


FIGURE 5.1. Field record from the
Suffield profile.

from the M discontinuity. Coherent energy at times prior to 11 seconds could be indicative of the low-velocity layer which is suggested in the refraction summary (figure 2.4). The event marked at 13.8 seconds is found on a number of records from different locations and seems to be characteristic of some velocity-density discontinuity, not mapped by refraction methods, between the Conrad and Mohorovičić. Only when the digital processing techniques have been applied will it be possible to give a definitive meaning to some or all of the phases marked on figure 5.1.

The small program planned for the Lake Newell site was severely hampered by weather conditions, necessitating the postponement of detonation of loaded shot holes by about 2 1/2 months. When the explosives were finally discharged, not all holes fired and consequently the effectiveness of the hole-geophone patterns as a filter was drastically reduced (figure 5.2). The record quality for the third set of traces for which all shot holes discharged is generally better than the others.

The shallowest event, near 10 seconds, could be a reflection from the low-velocity layer inferred from refraction data. A reflection at this time was also noted at Suffield and on a record from the eastern end of the Lomond profile. The event at 11.6 seconds is probably from the

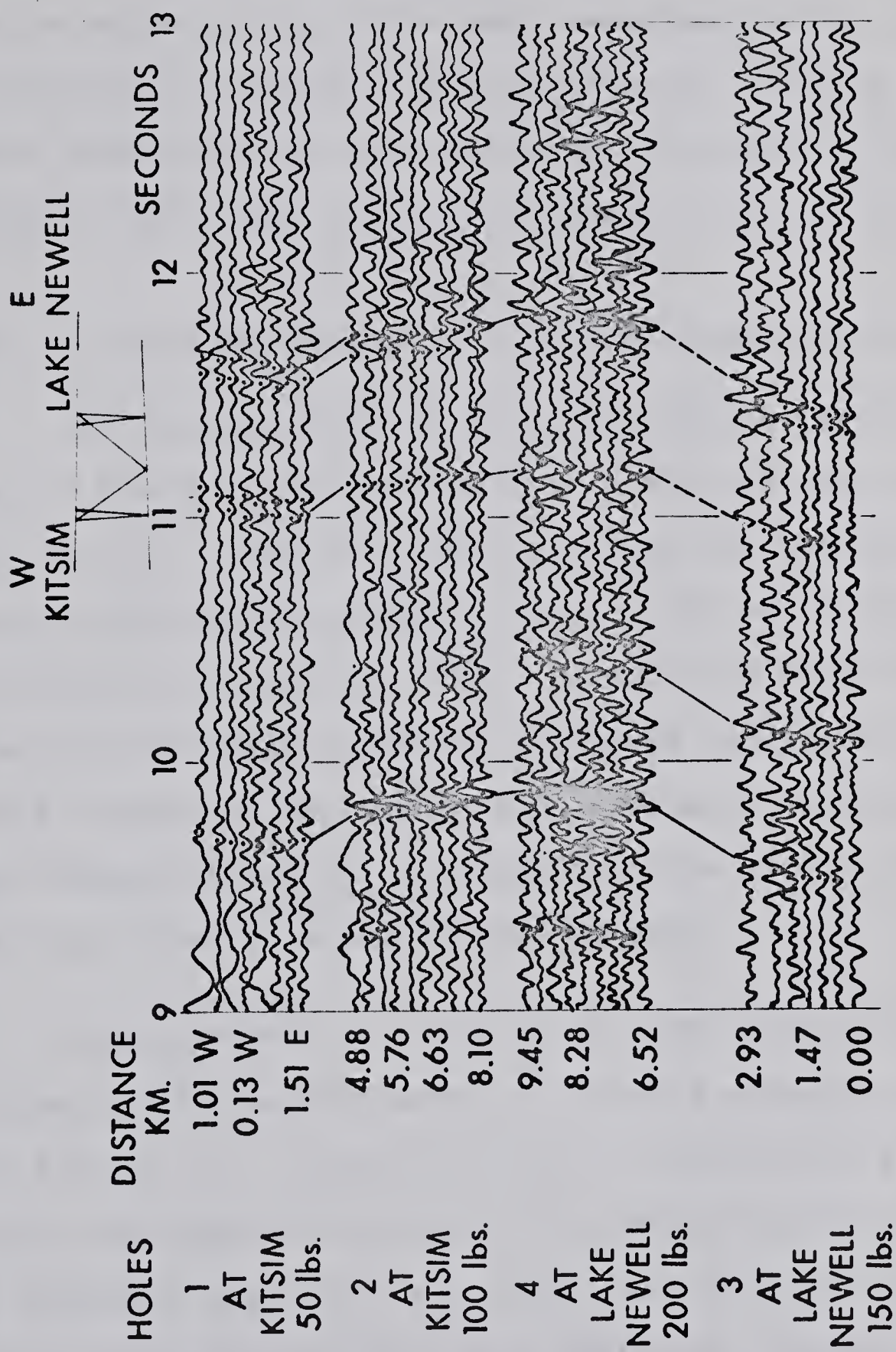


FIGURE 5.2. Field records from the Lake Newell profile.

Conrad discontinuity. If the correlation across the record section is correct, then there must be approximately 1/2 km. of west dip over a distance of 9 kilometers. Such an interpretation agrees with gravity data which indicate a high around Lake Newell and values 10 milligals lower at Kitsim.

5.2 The Velocity Determination along the Lomond Profile

The initial phase of the deep crustal reflection program was begun along the line now referred to as the 'Lomond profile'. Detector group spacings for the data acquired in 1965 were increased from the 293 meter distance used in 1964 to 586 meters. This proved to be an unfortunate decision for the greater detector spacings resulted in large step-outs across any one record and correlation from trace to trace became difficult. In addition, the program for 1965 was curtailed by several weeks of rain.

Approximately half of the data recorded along the Lomond profile during the summer of 1964 is reproduced in figures 5.3 and 5.4. The other half of the data is similar in quality and represents duplicate coverage with a slight offset to permit application of signal enhancement programs. There is a noticeable lack of high amplitude coherent energy from 4 to 11 seconds after the shot instant, although a few weak events may be seen on some traces. The first prominent

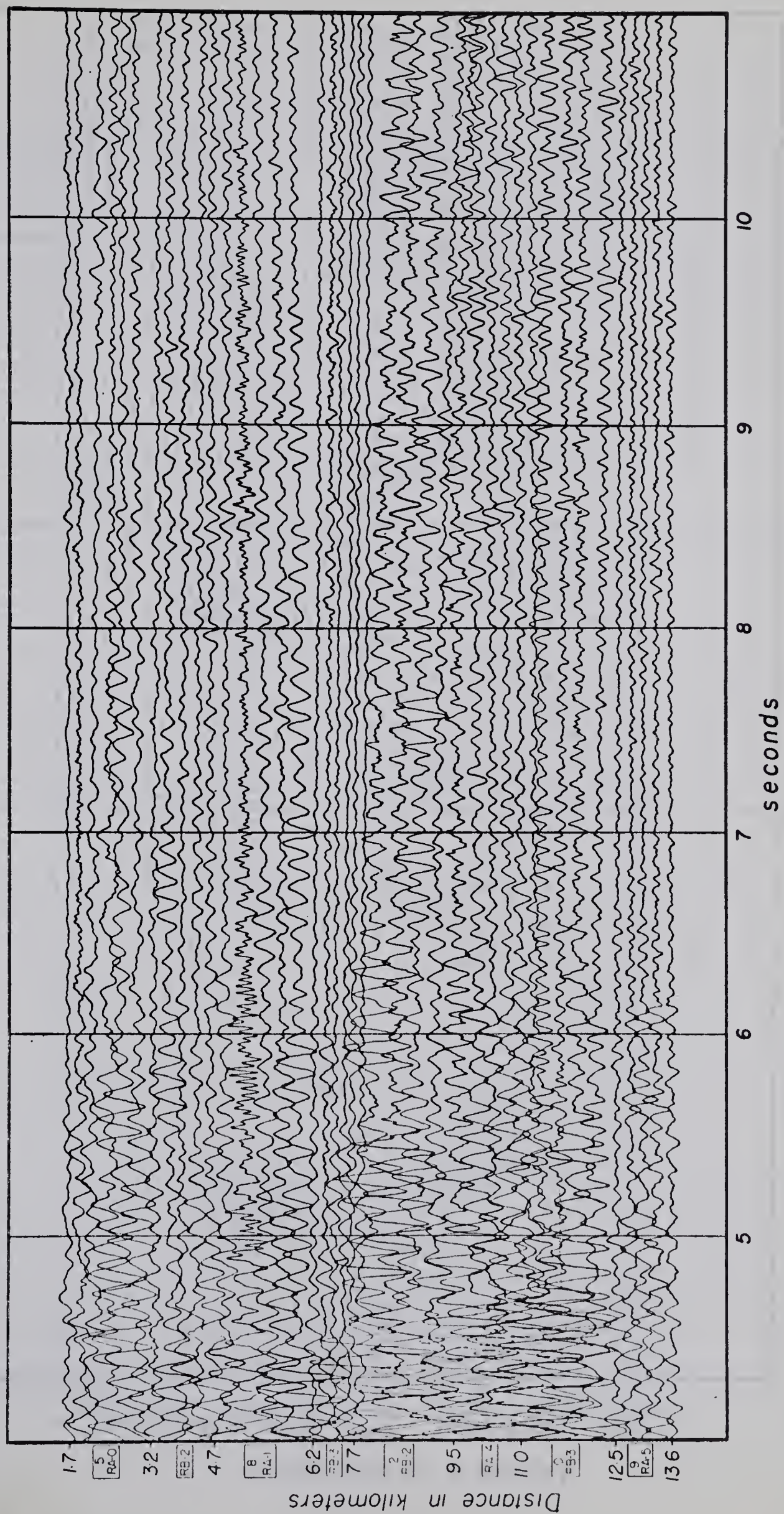


FIGURE 5.3. Lomond profile reflection data (1964) between 4 and 11 seconds after the shot instant.

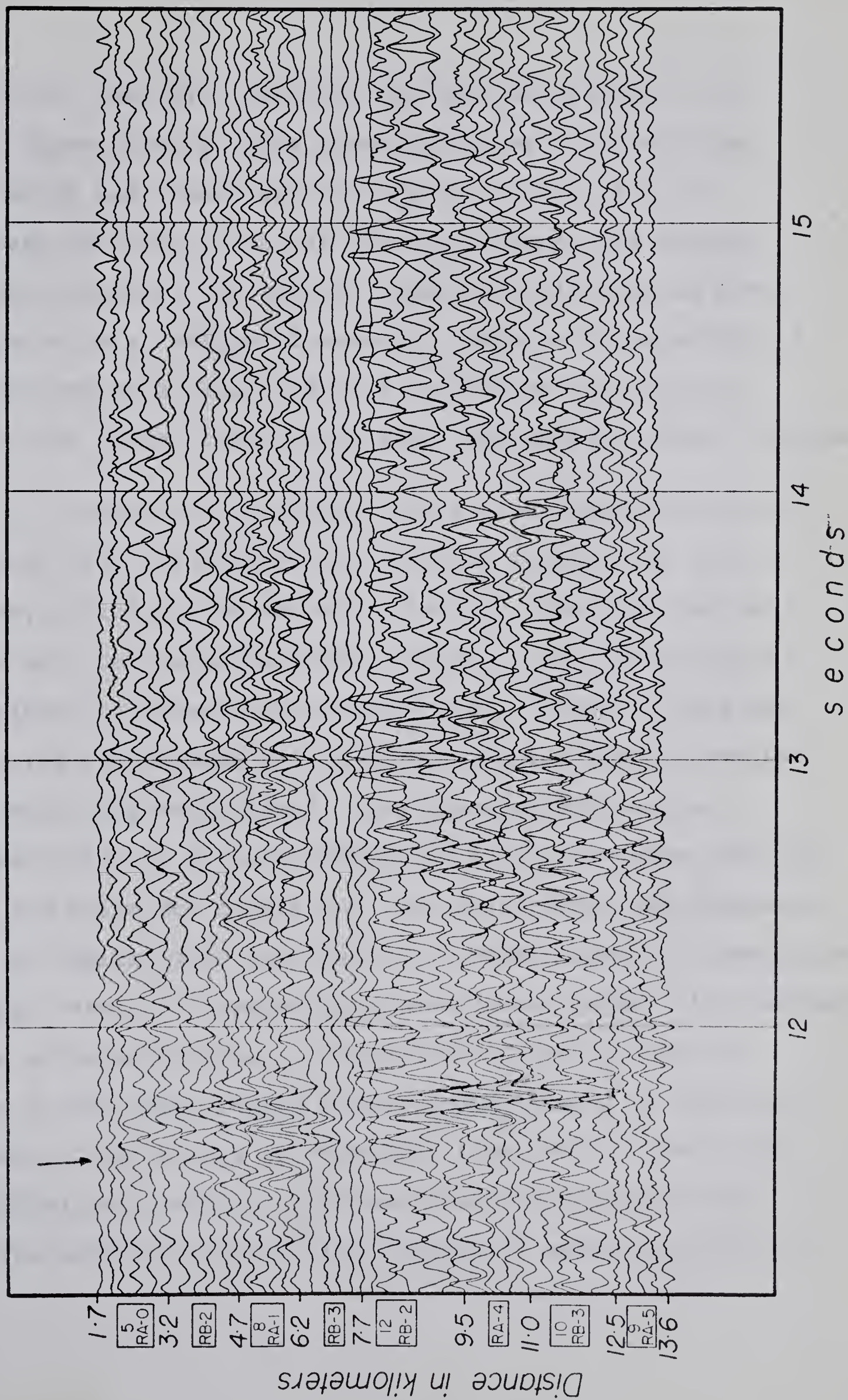


FIGURE 5.4. Lomond profile reflection data (1964) between 11 and 16 seconds after the shot instant.

reflection, near 11.6 seconds, has been attributed to the Conrad discontinuity. The arrow indicates the particular cycle which was chosen as the zero for normalizing the digitized data and which was timed to compute the average vertical velocity. It will be noted that although no event appears to exist before 11 seconds, there is a suggestion of coherent energy at 13.0 and 13.8 seconds on some of the traces, the latter time having also been noted on other records.

Reproduced in figure 5.5 is a photograph of three different field recordings for the time interval 10 to 12.8 seconds, including the Conrad reflector. The final set of traces with no distances marked beside it are the low gain equivalents of those immediately above. One point this set of records illustrates is the widely varying signal-to-noise ratio which was encountered. The upper seismogram is representative of a region where the signal-to-noise ratio is quite low while the middle and lower recordings are characteristic of regions with high ratios. Traces marked 'V' designate a single vertical component geophone; those marked 'A' designate arrays of seismometers. A comparison of the two sets of traces on the upper record gives a good example of the effectiveness of the arrays in rejecting long period noise. To be particularly noted on the lower two recordings is the definite motion of the vertical component seismometer at the

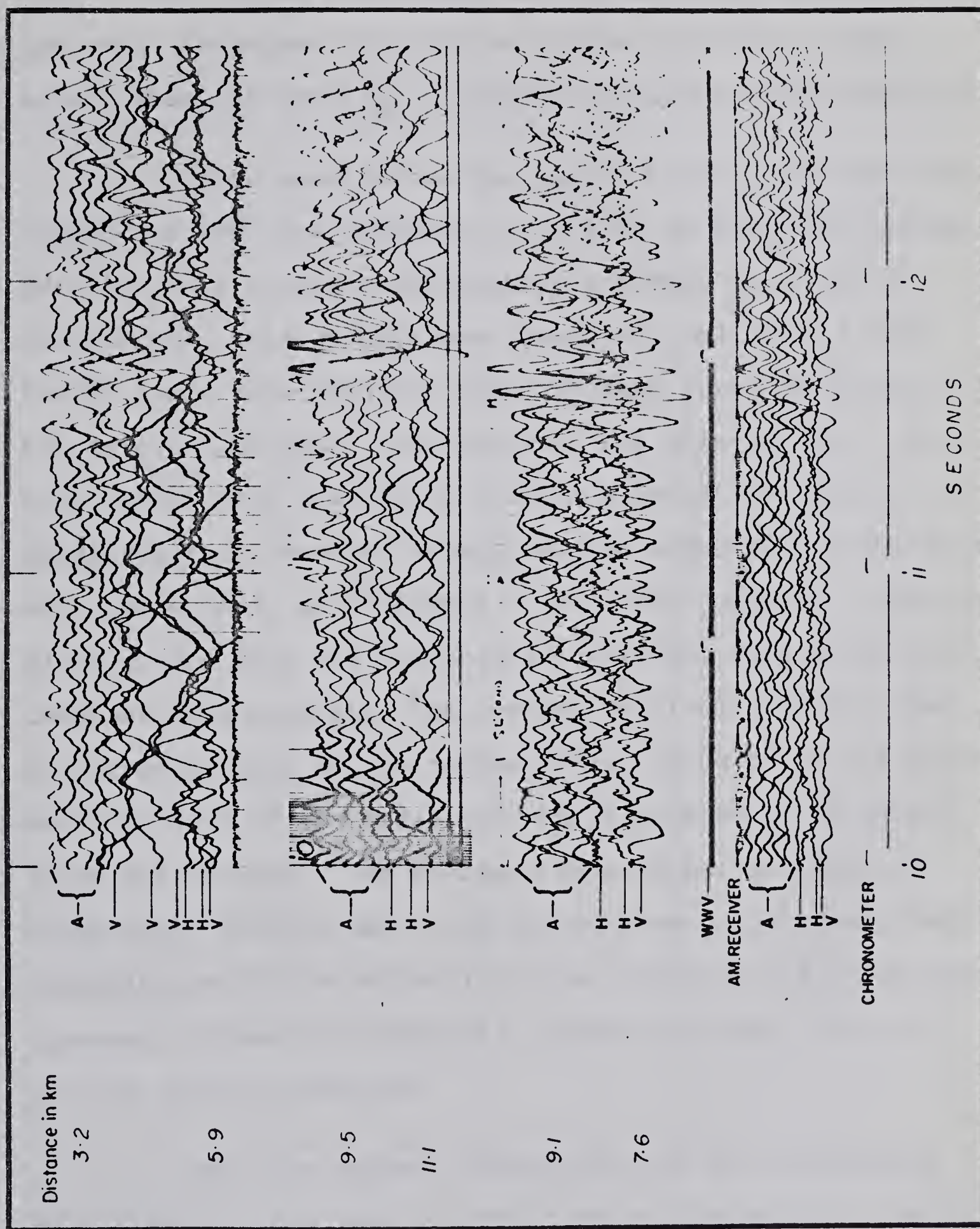


FIGURE 5.5. Lomond profile seismograms (1964) for time interval 10 to 12.8 seconds.

time of the Conrad event while at the same time the horizontal component geophones (H) show no unusual activity. This establishes the vertical incidence character of the reflections.

Prior mention has been given to the fact that the program of 1964 was designed to utilize an expanding spread profile, this having approximately a common depth point. All the available records were examined, and times to the Conrad event were read for each distance from the center of the detector group to the center of the hole pattern. The time values were reduced to a datum plane at the top of the Mississippian system at an approximate depth of 1.7 kilometers. With these data, an X^2 versus T^2 plot was computed. From the slope of the line and its y-axis intercept, determined by a least-squares analysis, the average vertical velocity from the Mississippian to the reflector was found to be 6.4 km./sec. and the depth of the reflector was calculated to be 35 km. below the surface. The standard deviations, assuming no correlation errors, were 1.0% in both the velocity and depth. Comparison with the refraction data of figure 2.4 shows good agreement between the computed values and those indicated for the Conrad refractor.

That the correct correlation on the seismograms from 1964 has been made is evidenced by figure 5.6. The six stacked traces represent 72 of the original recorded traces.

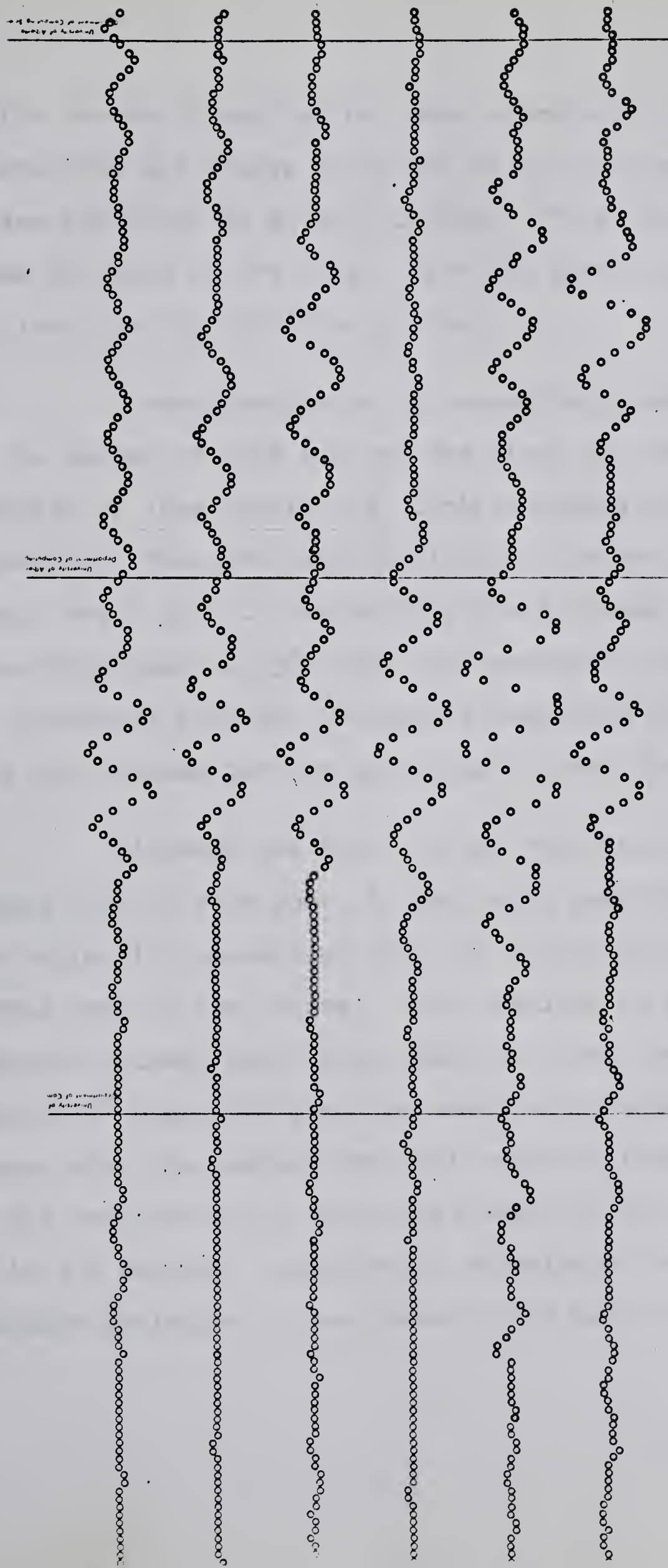


FIGURE 5.6. IBM 1403 line printer output of six 600% composited traces. The circles enclose numbers referring to the trace plotted (1 to 6). The output also includes a listing of the plotted digital values.

If the correct phase had not been correlated, the similarity between the six traces would not be as striking and the pulses would not be so well defined. This illustration also shows the form of the output from the plotting program which utilizes the IBM 1403 line printer.

A continuation of the expanding spread was completed in the summer of 1965 but the Bow River to the east of position +7 (see figure 2.3) limited expansion in that direction. Thus the additional data obtained were not from a common depth point. Compounding the problems already mentioned, recordings made in 1965 were most generally either overshoot or undershot; that is, the gain adjustments of the amplifiers were not optimum for the acquiring of good visual seismograms.

Although the data for the continuation of the Lomond profile were poor, it was found possible to correlate the reflection associated with the Conrad discontinuity across most of the traces. This resulted in additional time-distance values, which were added to those from 1964, and another X^2 versus T^2 plot was computed (figure 5.7). From these data, the average vertical velocity from the Mississippian to the reflector at a calculated depth of 34 km. was found to be 6.2 km./sec. Assuming no correlation errors, the standard deviation of the velocity and depth values was 0.4%.

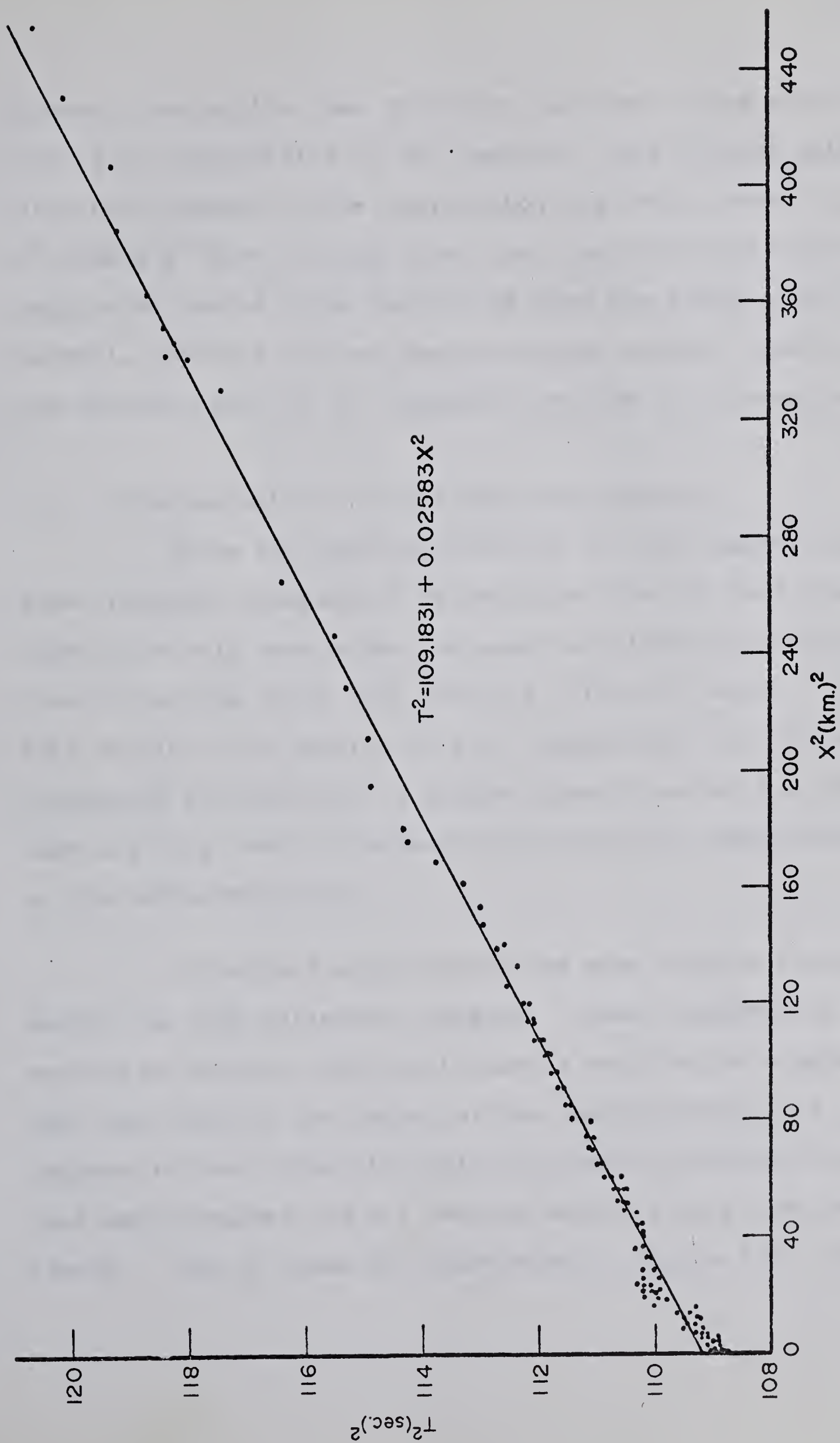


FIGURE 5.7. X^2 versus T^2 diagram of the Conrad reflection for all available data along the Lomond profile.

However, correlation was difficult for some traces and this limits the reliability of the results. By following slightly different phases for the correlation and using these in an x^2 versus T^2 plot, it was found that the depth and velocity magnitudes varied by as much as 3% from the stated quantities. As well, evidence of some deep structure severely restricts the dependability of the expanding profile in this region.

5.3 Interpretation of the Lomond Seismograms.

While the previous sections of this chapter have shown numerous examples of reflections from the deep crust, these have only been noted and some correlated with velocity discontinuities known from previous refraction work. In this section, the results will be consolidated to obtain some structural information. A Bouguer gravity survey has been made and this tends to support the structural implications of the reflected events.

Of notable significance are some results recorded during the 1965 reflection program. These consisted of several records at exactly vertical incidence obtained on a spread 1320 feet long in the center of the Lomond profile. A pattern of four holes with only 10 pounds of explosive per hole was detonated and all records showed strong deep reflecting events. One of these is illustrated in figure 5.8. The

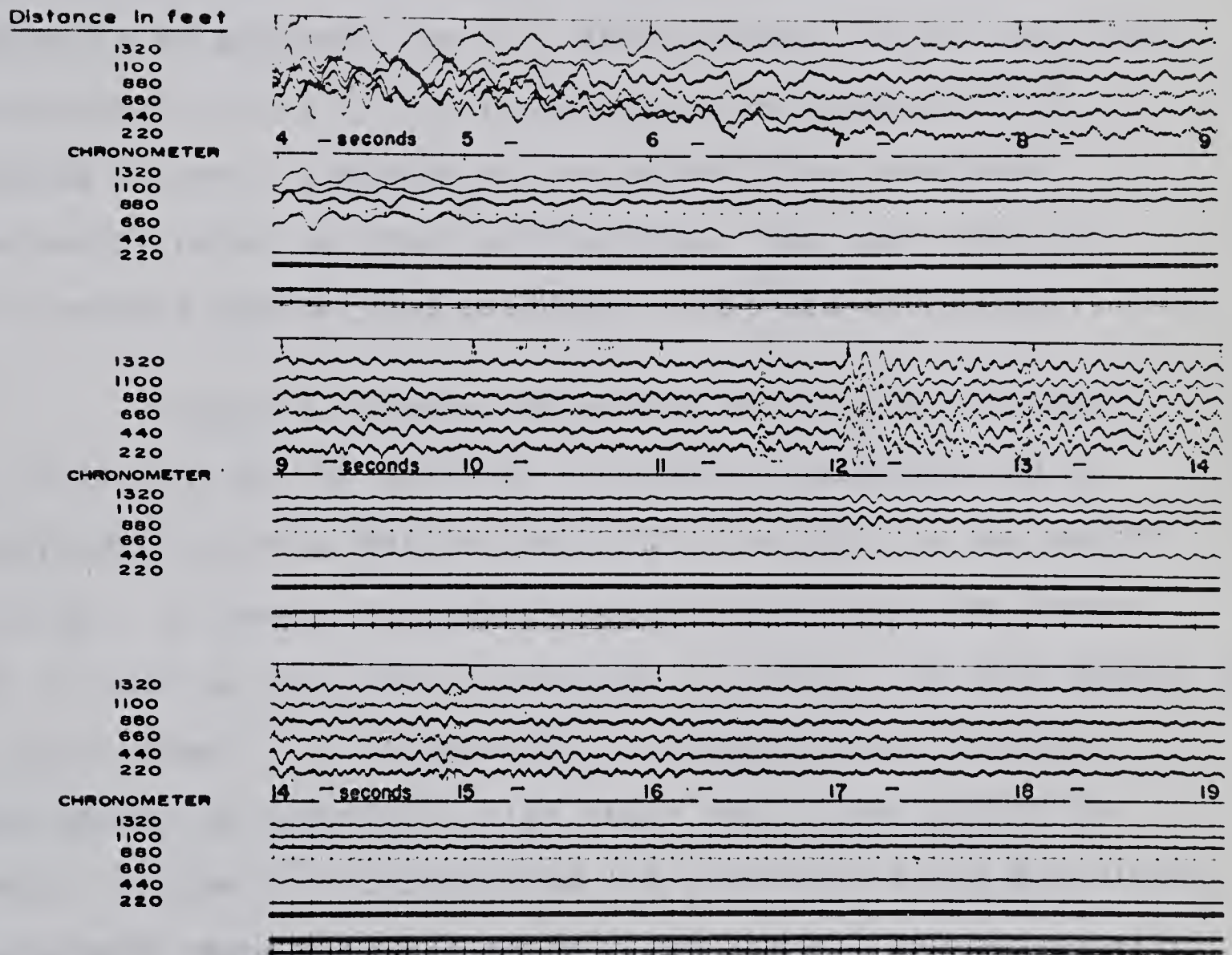


FIGURE 5.8. Seismogram at vertical incidence from position 0 on Lomond profile.

strongest event is undoubtedly that marked just after 12.0 seconds, although weaker arrivals occur at 11.5, 13.0, 13.8 and 14.8 seconds. Utilizing information derived from the synthetic seismogram, the 13.0 second event may be a multiple reflection, but it is not likely that the phase at 13.8 seconds is one. Arrivals at the latter time have been frequently noted on other seismograms. The last event at 14.8 seconds may be from the Mohorovičić discontinuity.

Figure 5.9 shows the strong reflection occurring at 12 seconds on the vertical incidence seismogram and an equivalently strong reflection at 11.6 seconds on two nearby records. It seems reasonable to correlate these two events, but to what is the time discrepancy of nearly one half second to be attributed? It is possible to explain these results very simply by assuming a high angle fault deep within the crust. Figure 5.10 illustrates the geometry of the postulated fault with respect to the seismic ray paths. In the process of faulting, it is likely that any horizon in the vicinity of the fault will be folded: concave up on the deep side, concave down on the shallow side. Because the amplitude of a reflected wave is very sensitive to curvature of the reflecting surface, a focussing effect might be expected to enhance an event from the deep side of the reflector. The weak event at 11.5 seconds may represent diffracted energy from the edge of the fault.

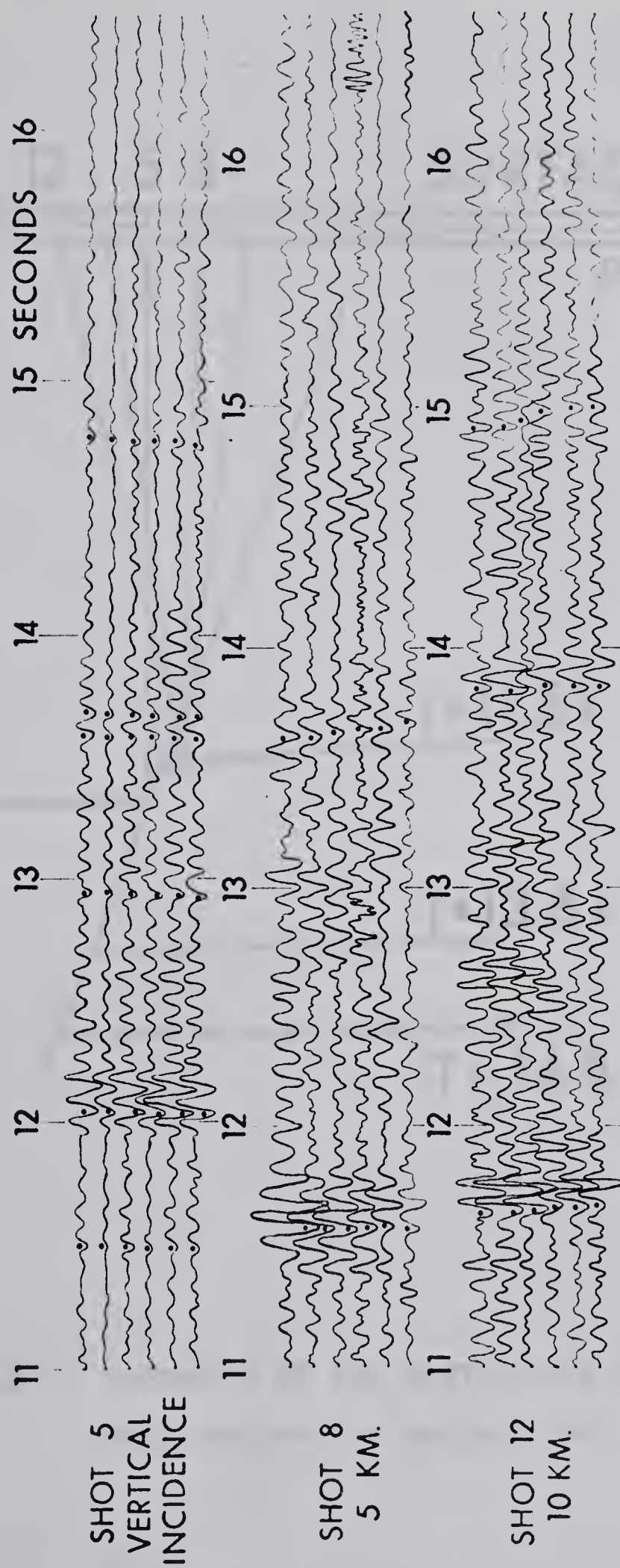


FIGURE 5.9. Record sections from three different shots along the Lomond profile.

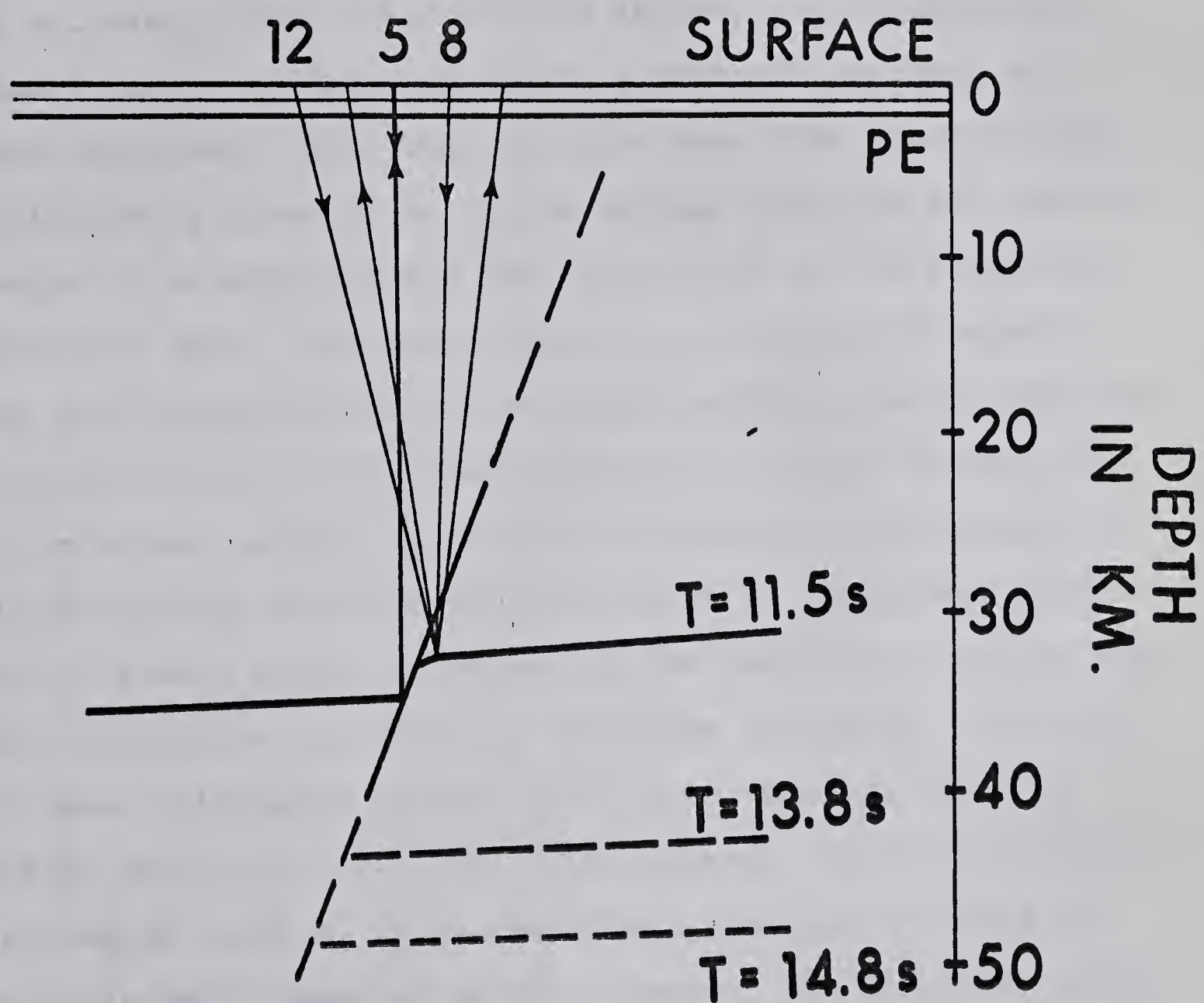
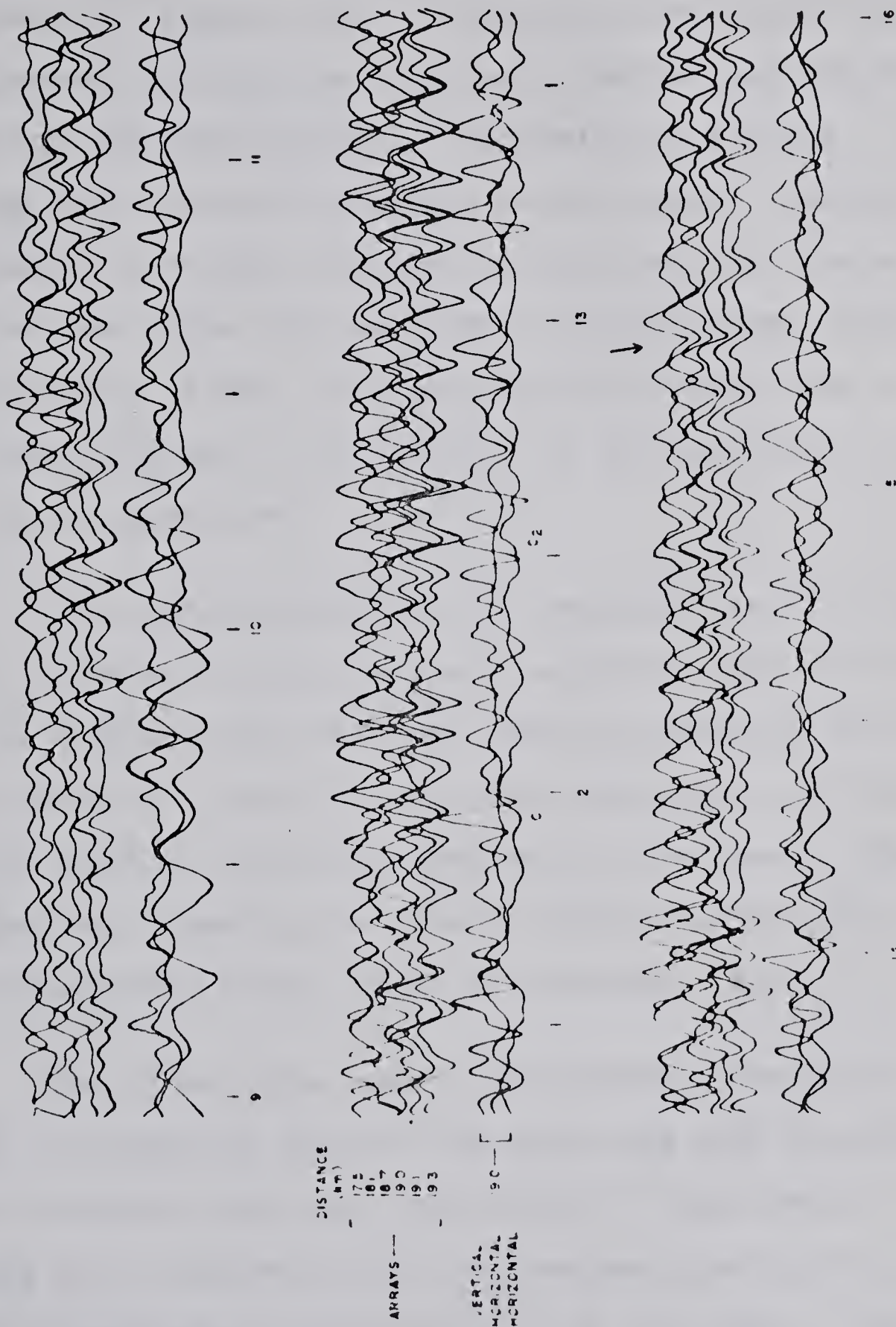


FIGURE 5.10. Geometry of the postulated fault with respect to seismic ray paths.

Tracings of a seismogram, recorded in 1965 about 19 kilometers from the explosion source, are illustrated in figure 5.11. A number of possible reflections exist on this recording. That many of these come from near-vertical incidence is attested to by the strong motion of the vertical component seismometer and the weak motion of the horizontal component ones. The phase marked C_1 , at about 12 seconds, has been correlated with the Conrad reflector on the upthrown side of the fault. However there is an equally strong, if not stronger, event, C_2 , near 12.5 seconds, a time which for the horizontal distance involved would be consistent with the 12 second event, representing the downthrown side of the deep horizon on the vertical incidence recording. The long distance seismogram (figure 5.11) also contains coherent energy near 14.0, 14.5, and 15.3 seconds. From the synthetic seismogram results, it is not likely that any of these are multiple reflections of earlier events. The first two times could be related to reflections from the shallow and deep sides of the 13.8 second horizon recorded on a number of records. The last time value is probably indicative of an event reflecting from the shallow side of the M discontinuity.

LOMOND PROFILE (1965) - FIELD SEISMOGRAM



A Bouguer gravity anomaly map for southern Alberta is presented in figure 5.12. On this map, the closely spaced dots represent 333 gravity stations at which readings were made by the Geophysics group, University of Alberta. The remaining dots represent stations where Bouguer anomalies were obtained from data compiled by the Dominion Observatory. At 15 stations where both university and government data were available, it was found that Bouguer values from the former agreed within a fraction of one milligal with those listed by the government.

For southern Alberta, the regional trend is negative towards the Rocky Mountain system, but this trend is interrupted by a pronounced east-west feature centering on the Lomond reflection profile. The large anomalies are likely to be due to density variations deep within the crust. The large gradient crossing the Lomond profile, marked EAB, may be interpreted simply as an intrabasement fault.

Two dimensional model calculations, assuming a throw of 3 kilometers down to the north and some plausible density contrast, have been carried out. These gravity computations are consistent with the observed gravity field if the fault penetrates a major section of the crust. The postulated fault occurs in rock of the Churchill Geological

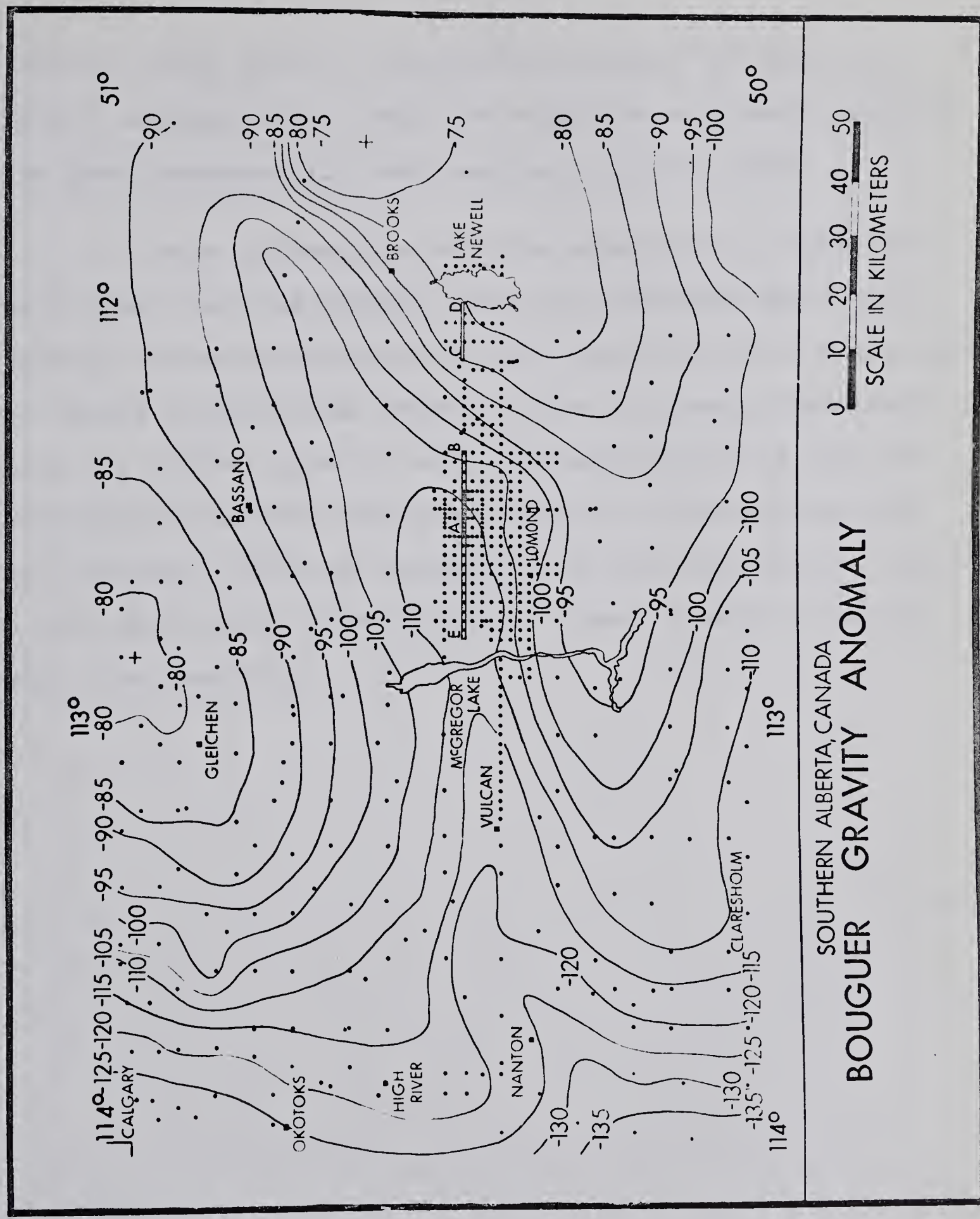


FIGURE 5.12

Province (K-Ar dates of 1800 million years) but does not affect Cambrian rock. Thus the suggested east-west fracture has been preserved for over one half billion years.

More information will be necessary to verify the structural features deduced from the available data. The seismic reflection program for the summer of 1966 is designed to record a continuous profile across the postulated fault. As well, further gravity data, refracted arrivals from the Precambrian basement and ground magnetic observations will be obtained. After an integration of this geophysical data, a more definitive interpretation of deep crustal structure should be possible.

CONCLUSIONS

Seismograms recorded in southern Alberta clearly demonstrate the existence of near-vertical incidence deep reflecting events from within the earth's crust. These reflections have been obtained along three lines over a distance of 150 kilometers. Arrays of geophones and shot holes have been designed to synthesize a filter of long period surface waves. These have effectively increased the signal-to-noise ratios. Establishment of their vertical incidence character has been achieved through the use of vertical- and horizontal-component geophones.

In addition to photographic seismograms, the data were recorded on FM magnetic tape recorders with a wide dynamic range. Digitization of these analog recordings, their subsequent normalization and the compositing of appropriate traces show that such a procedure improves signal-to-noise ratios. The application of more sophisticated data processing techniques, such as optimum filtering, deconvolution and velocity filtering, before stacking should enhance the ratios even more.

Other analytic techniques, such as Fourier transformations and autopower spectral analyses, indicate that the

reflection associated with the Conrad discontinuity has a dominant frequency of about 11 cps. Additional autopower spectra show that the reflection wavelets have the greatest amount of seismic energy in the frequency range from 5 to 15 cps. Therefore, additional band pass filtering in the digital domain would likely improve the general quality of the seismograms.

For theoretical analyses, a synthetic seismogram program has been developed. It is based on elastic wave theory in a layered media in which the velocity is a linear function of depth, and assumes plane waves at normal incidence. Any desired seismic wavelet, in the time or frequency domain, may be used as the signal input. Three important conclusions have been extracted from analyses with the program:

- (1) Multiple reflections, most likely between the surface and the top of the Paleozoic, may be prevalent shortly after any major reflecting event but they are severely attenuated within 1.5 seconds of the start of the primary reflection.

- (2) Any transition zone from within the deep crust must be less than 1 kilometer in extent for a significant reflection to be recorded.

(3) Strong reflections on the synthetic seismogram were from step-function velocity contrasts, these modelling the deep crustal layers. On the field seismograms, strong signals reflecting from the Conrad discontinuity have been found to have a frequency near 11 cps. Together with the transition zone information, these facts indicate that the extent of the transition zone at the Conrad must be small--less than 0.5 kilometer.

A major advance from most previous data is the correlation of one reflection, attributed to the Conrad discontinuity, over a profile 30 kilometers in extent. The expanding spread technique enabled the average vertical velocity and depth to the Conrad to be obtained for the first time and formed an independent check on assumptions made in refraction analyses. The average velocity from the top of the Mississippian to the discontinuity at a calculated depth of 34 km. \pm 3% was computed to be 6.2 km./sec. \pm 3%. The presence of deep structure beneath the region has limited the precision of the velocity calculations.

Reflecting events other than the strong Conrad reflector have been indicated on a number of different seismograms from different locations. One of these is an earlier reflection at about 10 seconds and may be a weak event

from a low velocity layer postulated from refraction data. Two later reflections around times of 13.0 and 13.8 seconds, the latter having larger amplitudes, frequently appear. These imply that additional layering, not resolved by the refraction method, may exist within the deep crust. The latest reflection observable on any of the seismograms is at a time near 15 seconds. This event has been attributed to the Mohorovičić discontinuity, its arrival times agreeing consistently with times to be expected as a result of refraction information. Definitively proving the existence of any of these deep horizons requires more data with correlatable reflecting events.

Evidence for a high angle fault, with a throw of 3 kilometers within the deep crust, has been presented. A Bouguer gravity survey indicates a large anomaly centering on the Lomond profile. Model calculations show that a throw of 3 km. is sufficient to produce the necessary gradient. Dipping of the Conrad reflector to the west as suggested by seismograms near Lake Newell is also accordant with the observed gradient.

This treatise illustrates the wide extent of information which the reflection method, through its superior resolution, can add to knowledge of the deep crust. It is to be hoped that this thesis has contributed to the establishment of the seismic reflection technique as a reliable and powerful means for deep crustal research.

BIBLIOGRAPHY

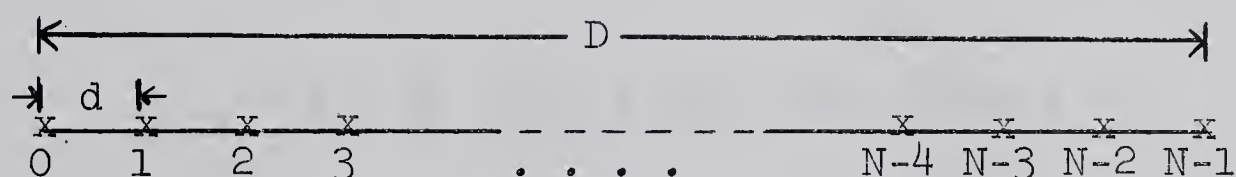
- Bath, M. and E. Tryggvason, Deep seismic reflection experiments at Kiruna, Geofisica Pura E Applicata - Milano, 51: 79-90, 1962.
- Belousov, V. G., B. S. Vol'vovski, I. S. Vol'vovski and V. A. Ryaboi, Experimental investigation of the recording of deep reflected waves, Bulletin Academy of Sciences, USSR, Geophysics Series, English Translation, No. 8: 662-669, 1962.
- Berryman, L. H., P. L. Goupillaud and K. H. Waters, Reflections from multiple transition layers, Part I - theoretical results, Geophysics, 23: 223-243, 1958.
- Blackman, R. B. and J. W. Tukey, The Measurement of Power Spectra, Dover Publications, New York, 1958.
- Cumming, G. L., G. D. Garland and K. Vozoff, Seismological measurements in southern Alberta, Vela Uniform Project 8652, Geophysics Research Directorate, AFCRL, Bedford, Mass., 1962.
- Dix, C. H., Reflection seismic crustal studies, Geophysics, 30: 1068-1084, 1965.
- Dohr, G., Ein Beitrag der Reflexionsseismik zur Erforschung des tieferen Untergrundes, Geologische Rundschau, 46: 17-26, 1957 (Translated by T. Gretener).
- German Research Group for Explosion Seismology, Crustal structure in western Germany, Zeitschrift für Geophysik, 30 (5): 209-234, 1964.
- Green, C. H., Velocity determinations by means of reflection profiles, Geophysics, 3: 295-306, 1938.
- Howe, H. S., Fourier analysis of non-periodic pulses on automatic computers, National Bureau of Standards Report 5018, 1956.

- Jones, H. J. and J. A. Morrison, Cross-correlation filtering, Geophysics, 19: 660-683, 1954.
- Junger, A., Deep basement reflections in Big Horn County, Montana, Geophysics, 16: 499-510, 1951.
- Kanasewich, E. R. and G. L. Cumming, Near-vertical incidence seismic reflections from the 'Conrad' discontinuity, J. Geophys. Res., 70: 3441-3446, 1965.
- Lee, Y. W., Statistical Theory of Communication, John Wiley and Sones, New York, 1960.
- MacDonald, G.J.F. and N. F. Ness, Stability of phase transitions within the earth, J. Geophys. Res., 65: 2173-2190, 1960.
- Maureau, G. T., Crustal structure in western Canada, M.Sc. thesis, University of Alberta, 1964.
- Musgrave, A. W., Applications of the expanding reflection spread, Geophysics, 27: 981-993, 1962.
- Nakamura, Y. and B. F. Howell, Jr., Maine seismic experiment: frequency spectra of refraction arrivals and the nature of the Mohorovičić discontinuity, Bull. Seismol. Soc. Am., 54: 9-18, 1964.
- Narans, H. D., J. W. Berg, Jr., and K. L. Cook, Sub-basement seismic reflections in northern Utah, J. Geophys. Res., 66: 599-603, 1961.
- Ricker, N., Wavelet contraction, wavelet expansion and control of seismic resolution, Geophysics, 18: 769-792, 1953.
- Robertson, G., Intrabasement reflections in southwestern Alberta, Geophysics, 28: 910-955, 1963.
- Savit, C. H., J. T. Brustad and J. Sider, The moveout filter, Geophysics, 23: 1-25, 1958.
- Shor, G. G., Deep reflections from southern California blasts, Trans. Amer. Geophys. Union, 36: 133-138, 1955.
- Steinhart, J. S. and R. P. Meyer, Explosion studies of continental structure, Carnegie Inst. Wash. Publ. 622, 1961.
- Tuve, M. A., H. E. Tatel and P. J. Hart, Crustal structure from seismic exploration, J. Geophys. Res., 59: 415-422, 1954.

APPENDIX 1.

GEOPHONE-HOLE PATTERNS

This section is an extension of derivations presented in an article by Savit et al (1958) entitled "The Moveout Filter". Consider an array of N seismometers spread evenly over a distance D .



Since the form of any wave impinging upon the seismometers will be a function of both time and distance, the input to the geophone group can be expressed by a double Fourier series.

$$y_{in} = \sum_{j=1}^{\infty} \sum_{p=1}^{\infty} A_{j,p} \left[\sin \left(\omega_p t + \frac{2\pi}{\lambda_j} x + \phi_{j,p} \right) \right]$$

where $\omega_p \equiv$ angular frequency

$\lambda_j \equiv$ wavelength

$v_{j,p} = \frac{\omega_p \lambda_j}{2\pi} \equiv$ apparent phase velocity of any Fourier component.

For the following analyses, a single frequency and wavelength is considered as the input to the geophone array.

$$y_{in} = A \sin \left(\omega t + \frac{2\pi}{\lambda} x + \phi \right) \quad (A1.1)$$

The normalized output from the array is the sum of individual outputs:

$$y_{out} = y = \frac{1}{N} \sum_{n=0}^{N-1} A \sin \left(\omega t + \frac{2\pi}{\lambda} nd + \phi \right)$$

It is evident from the diagram that $d = \frac{D}{N-1}$.

$$y = \frac{1}{N} \sum_{n=0}^{N-1} A \sin \left(\omega t + \frac{2n\pi}{N-1} \frac{D}{\lambda} + \phi \right) \quad (A1.2)$$

We utilize Lagrange's trigonometrical identity:

$$\sum_{m=0}^{n-1} \sin (x + my) = \frac{\sin \left(x + \frac{n-1}{2} y \right) \cdot \sin \frac{ny}{2}}{\sin \frac{y}{2}}$$

and A1.2 becomes

$$y = \frac{\sin \left(\frac{N\pi}{N-1} \frac{D}{\lambda} \right)}{N \sin \left(\frac{\pi}{N-1} \frac{D}{\lambda} \right)} \sin \left(\omega t + \frac{\pi D}{\lambda} + \phi \right) \quad (A1.3)$$

Comparing A1.2 with A1.3 we note that the output of the group is equivalent to that of one seismometer placed at $x = D/2$ and having the amplitude

$$A_N = \left| \frac{\sin \left(\frac{N\pi}{N-1} \frac{D}{\lambda} \right)}{N \sin \left(\frac{\pi}{N-1} \frac{D}{\lambda} \right)} \right|$$

We wish to evaluate the effect of the grouping for noise suppression. Evidently the most effective would be an infinite number of seismometers spaced over the distance D . Thus we consider the limit as N approaches infinity of A_N .

$$\lim_{N \rightarrow \infty} A_N = \left| \frac{\sin \frac{\pi D}{\lambda}}{\frac{\pi D}{\lambda}} \right| = A_{\infty} \quad (\text{A1.4})$$

This formula was included in the computer program to give the equivalent response of an infinite number of geophones over a distance D .

Consider a symmetric array of $2n + 1$ detectors of arbitrary sensitivity placed at locations $x = 0, \pm \frac{1}{n} \frac{D}{2}, \pm \frac{2}{n} \frac{D}{2}, \dots, \pm \frac{D}{2}$ with sensitivities given by $a_0, a_1, a_2, \dots, a_n$. We specify that the output of the array be unity for a signal arriving normal to the surface, corresponding to a signal

with infinite phase velocity and thus infinite wavelength.

The input signal is

$$y_{in} = \cos \left(\omega t + \frac{2\pi}{\lambda} x + \phi \right) \quad (A1.5)$$

The output of the group becomes with $d = \frac{1}{n} \frac{D}{2}$

$$y_{out} = \sum_{k=-n}^{k=+n} a_k \cos \left(\omega t + \frac{2\pi}{\lambda} kd + \phi \right) \quad (A1.6)$$

Expand the cosine term within the summation sign of A1.6.

$$\begin{aligned} \cos \left(\omega t + \frac{2\pi}{\lambda} kd + \phi \right) &= \\ &= \cos (\omega t + \phi) \cos \frac{2\pi}{\lambda} kd - \sin (\omega t + \phi) \sin \frac{2\pi}{\lambda} kd \end{aligned}$$

However, the second factor will not contribute to the summation since the a_k are symmetric about $x = 0$ and the sine function is odd. That is

$$\sum_{k=-n}^{k=+n} a_k \sin \frac{2\pi}{\lambda} kd = 0$$

Then using the symmetry of a_k , A1.6 becomes

$$\begin{aligned}
y_{\text{out}} &= a_o \cos(\omega t + \phi) + 2 \sum_{k=1}^n a_k \cos(\omega t + \phi) \cos \frac{2\pi}{\lambda} k d \\
&= \cos(\omega t + \phi) \left[a_o + 2 \sum_{k=1}^n a_k \cos \frac{2\pi}{\lambda} k d \right] \\
&= G_1 \cos(\omega t + \phi)
\end{aligned}$$

where G_1 , the amplitude of the response is

$$G_1 = a_o + 2 \sum_{k=1}^n a_k \cos \frac{2\pi}{\lambda} k d \quad .$$

Normalized to the desired unit response gives the amplitude:

$$G = \frac{a_o + 2 \sum_{k=1}^n a_k \cos \frac{2\pi}{\lambda} k d}{a_o + 2 \sum_{k=1}^n a_k} \quad (\text{A1.7})$$

If we now let $N = 2n + 1$, the number of detectors, then

$$n = \frac{N-1}{2} \text{ so } d = \frac{2}{N-1} \frac{D}{2} = \frac{D}{N-1} \quad .$$

With these substitutions, A1.7 becomes

$$\begin{aligned}
G &= \frac{a_o + 2 \sum_{k=1}^n a_k \cos \left(\frac{2\pi k}{N-1} \right) \frac{D}{\lambda}}{a_o + 2 \sum_{k=1}^{\frac{N-1}{2}} a_k} \quad (\text{A1.8})
\end{aligned}$$

A similar analysis will give for $M = 2m$ seismometers located at $\pm \frac{d}{2}$, $\pm \frac{3d}{2}$, ..., $\pm \frac{(2m-1)d}{2}$ with sensitivities of a_1 , a_2 , ..., a_m , an amplitude response of

$$G = \frac{\sum_{k=1}^{\frac{M}{2}} a_k \cos \pi \frac{2k-1}{M-1} \frac{D}{\lambda}}{\sum_{k=1}^{\frac{M}{2}} a_k} \quad (\text{A1.9})$$

Equation A1.9 is identical to equation 2.1. The effects of a hole pattern can be derived in an identical manner. If we call the amplitude response of the hole pattern H , then the combined effect of the geophone-hole pattern is

$$R = |G| |H|. \quad (\text{A1.10})$$

A computer program was written which evaluated G , H and R for any desired symmetric configuration, at the same time calculating the response of an infinite number of seismometers over the specified distance D . It might be noted that the argument of the cosine term for the geophone pattern and the hole pattern, $\frac{D_G}{\lambda}$ and $\frac{D_H}{\lambda}$, respectively, will in general be different. The evaluation of the combined response must be done for various wavelengths, but the individual terms of G and H must be considered at the same wavelength. For this reason, two parameters

$$Z_G = \frac{D_G}{\lambda} = \frac{(N_G - 1) d_G}{\lambda}$$

$$Z_H = \frac{D_H}{\lambda} = \frac{(N_H - 1) d_H}{\lambda}$$

were used and Z_H was derived as a function of Z_G , specifying λ to be the same. This gave

$$Z_H = \frac{(N_H - 1) d_H}{(N_G - 1) d_G} Z_G \quad (A1.11)$$

where d_H and d_G are the distances between individual holes and detectors, respectively; N_H and N_G are the number of holes and detectors, respectively.

The following graphs show the amplitude responses for the various configurations indicated thereon.

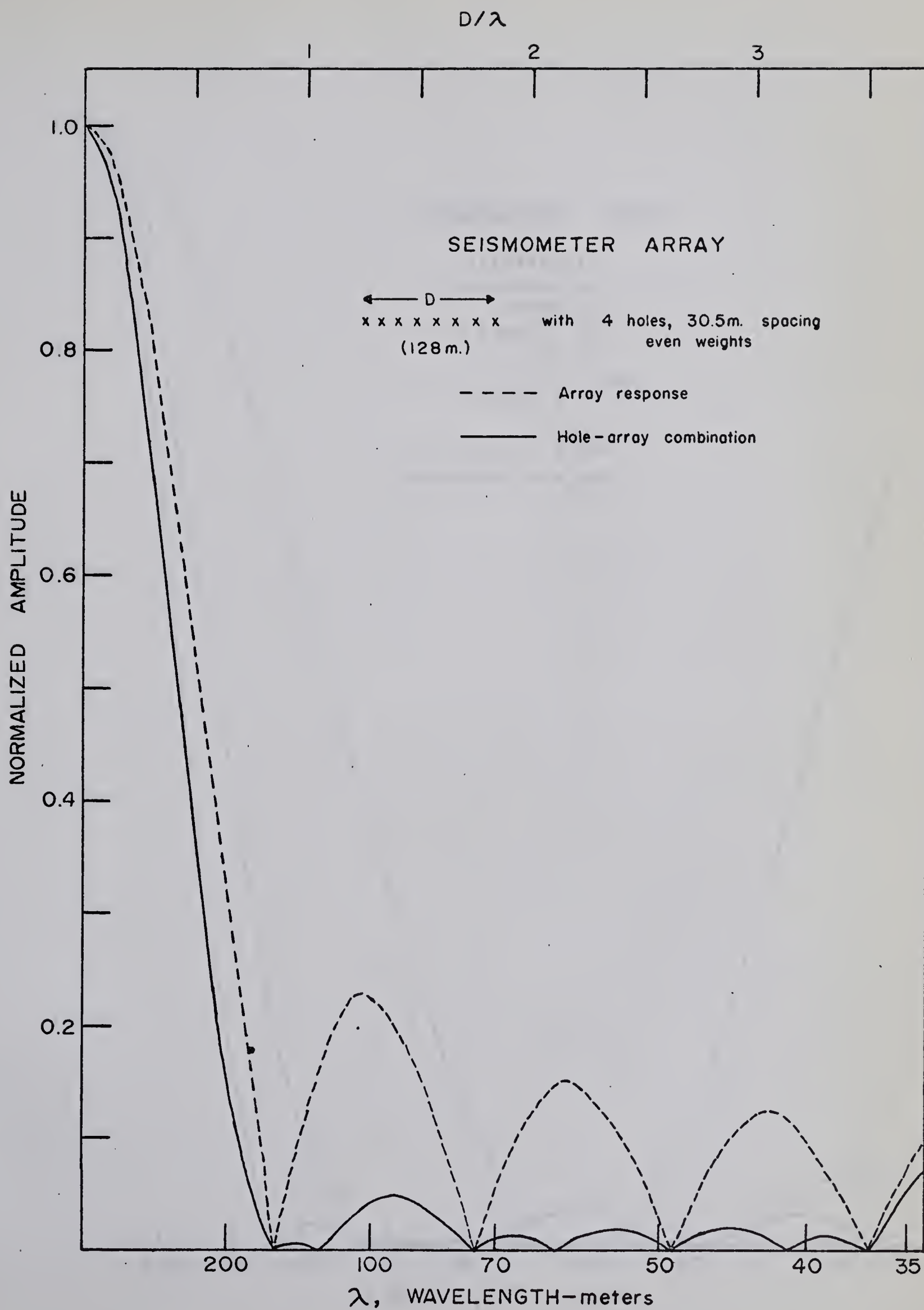


FIGURE A1.1

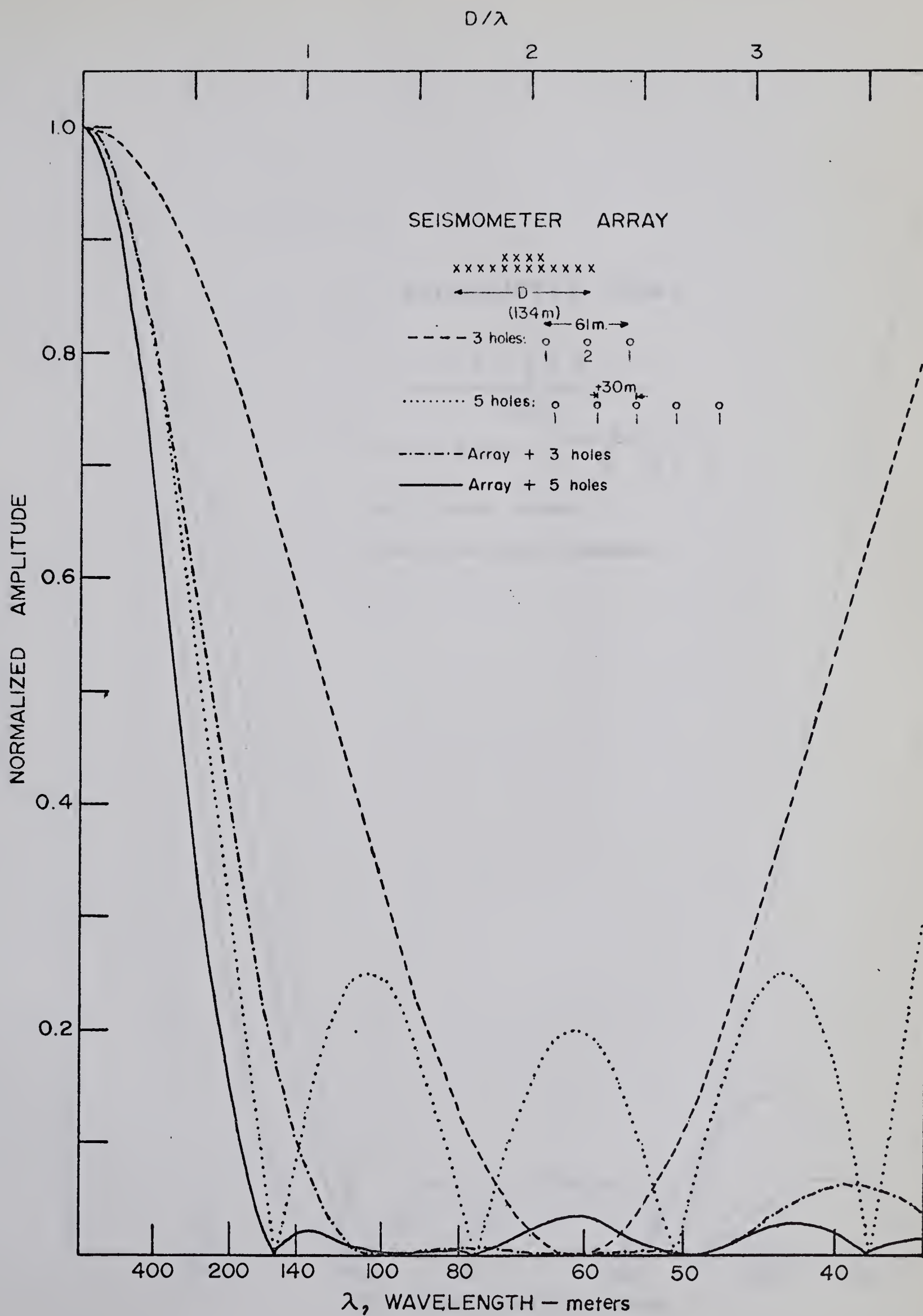


FIGURE A1.2

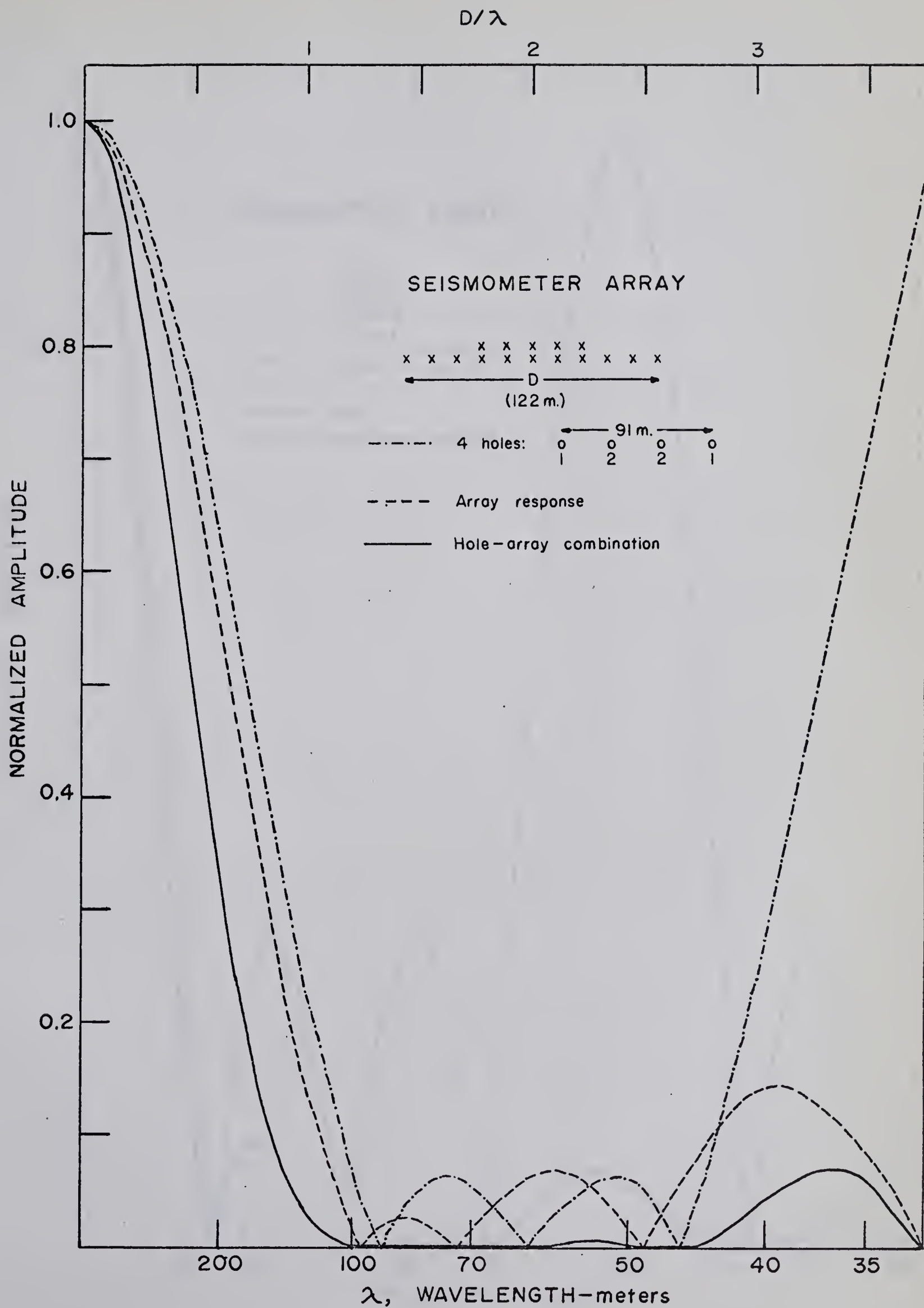


FIGURE A1.3

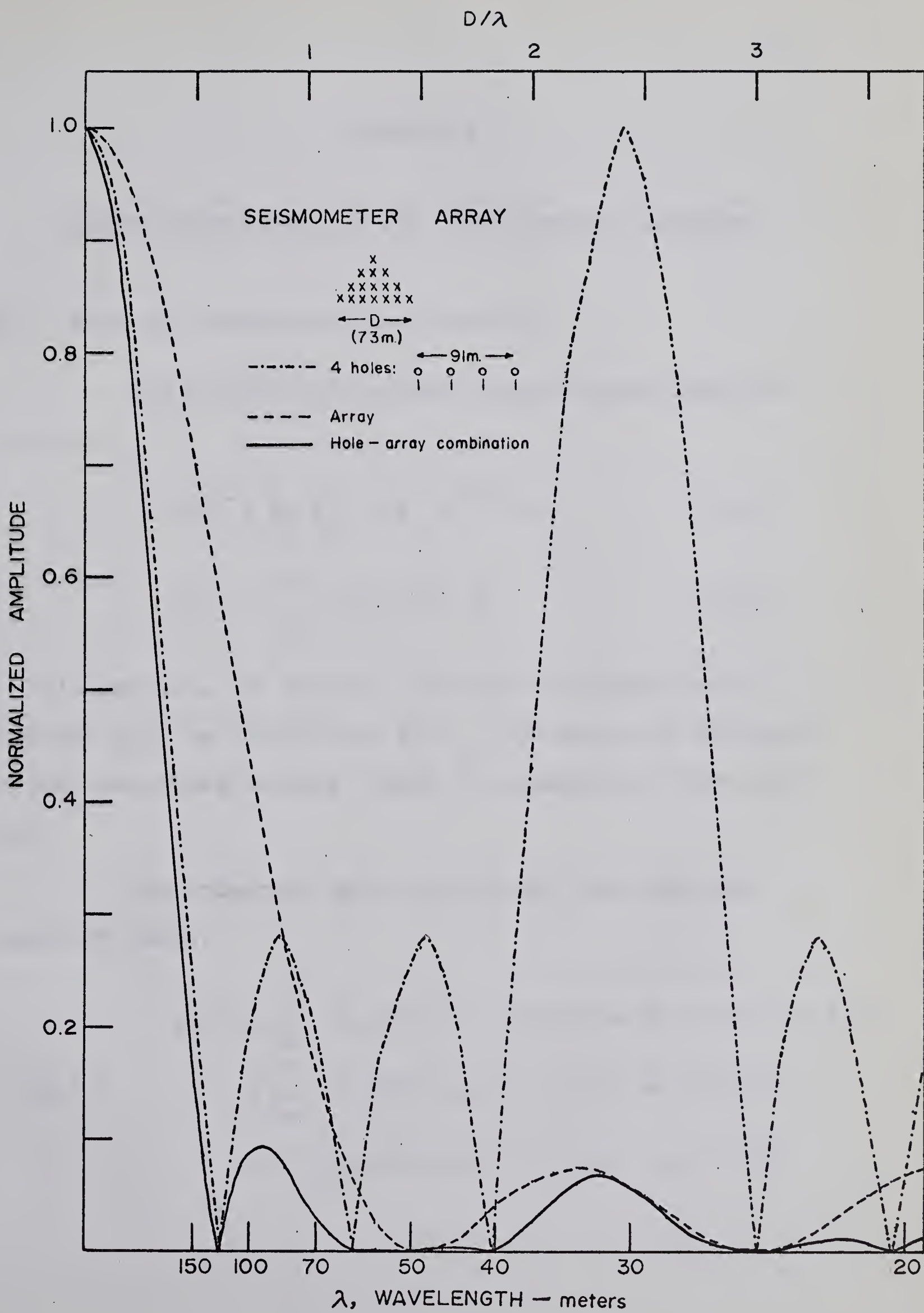


FIGURE A1.4

APPENDIX 2.

FOURIER TRANSFORMATION AND POWER SPECTRA ANALYSES

A2.1 Fourier Integration on a computer

The Fourier and inverse Fourier transforms are given by

$$S(\omega) = \frac{1}{2\pi} \int_{-\infty}^{\infty} s(t) e^{-i\omega t} dt \quad (\text{A2.1})$$

$$s(t) = \int_{-\infty}^{\infty} S(\omega) e^{i\omega t} d\omega \quad (\text{A2.2})$$

In this section, the equation suitable for application on a computer will be derived for A2.2. The method is analogous to that described by Howe (1956) for equations of the type A2.1.

The integral, A2.2, is divided into real and imaginary parts.

$$\begin{aligned} s(t) &= \int_{-\infty}^{\infty} [S_R(\omega) + i S_I(\omega)] [\cos \omega t + i \sin \omega t] d\omega \\ (\text{A2.3}) \quad &= \int_{-\infty}^{\infty} [S_R(\omega) \cos \omega t - S_I(\omega) \sin \omega t] d\omega \\ &+ i \int_{-\infty}^{\infty} [S_R(\omega) \sin \omega t + S_I(\omega) \cos \omega t] d\omega \end{aligned}$$

Empirically, the signal $s(t)$ must be real so the imaginary part of $s(t)$ must vanish. We note this will occur when $S_R(\omega)$ is even and $S_I(\omega)$ is odd. With these conditions A2.3 becomes

$$(A2.4) \quad s(t) = 2 \int_{-\infty}^{\infty} S_R(\omega) \cos \omega t \, d\omega - 2 \int_{-\infty}^{\infty} S_I(\omega) \sin \omega t \, d\omega$$

Empirically, $S_R(\omega)$ and $S_I(\omega)$ are known at discrete intervals of frequency. We approximate a continuous function by assuming each varies linearly between interval points. Thus we first wish to evaluate each of the above integrals when they are integrated between finite limits, assuming linear variations between limits.

Consider first

$$(A2.5) \quad \int_0^{\infty} S_R(\omega) \cos \omega t \, d\omega$$

Let ω_j and ω_{j+1} be the values at the beginning and end of the $(j+1)$ th interval, respectively. The corresponding function values are $S_R(\omega_j)$ and $S_R(\omega_{j+1})$. Then the contribution to A2.5 from this interval, assuming the linear variation, is

$$\begin{aligned}\Delta S_R &= \int_{\omega_j}^{\omega_{j+1}} S_R(\omega) \cos \omega t \, d\omega \\ &= \int_{\omega_j}^{\omega_{j+1}} \cos \omega t \left[S_R(\omega_j) + \frac{S_R(\omega_{j+1}) - S_R(\omega_j)}{(\omega_{j+1} - \omega_j)} (\omega - \omega_j) \right] d\omega\end{aligned}$$

$$\begin{aligned}\Delta S_R &= \int_{\omega_j}^{\omega_{j+1}} \left\{ \cos \omega t [S_R(\omega_j) \omega_{j+1} - S_R(\omega_j) \omega_j + S_R(\omega_{j+1}) \omega \right. \\ &\quad \left. - S_R(\omega_{j+1}) \omega_j - S_R(\omega_j) \omega + S_R(\omega_j) \omega_j] / (\omega_{j+1} - \omega_j) \right\} d\omega\end{aligned}$$

$$\begin{aligned}\Delta S_R &= \frac{S_R(\omega_j) \omega_{j+1} - S_R(\omega_{j+1}) \omega_j}{\omega_{j+1} - \omega_j} \int_{\omega_j}^{\omega_{j+1}} \cos \omega t \, d\omega \\ &\quad + \frac{S_R(\omega_{j+1}) - S_R(\omega_j)}{\omega_{j+1} - \omega_j} \int_{\omega_j}^{\omega_{j+1}} \omega \cos \omega t \, d\omega\end{aligned} \tag{A2.6}$$

Now

$$\int_{\omega_j}^{\omega_{j+1}} \cos \omega t \, d\omega = \frac{1}{t} [\sin(\omega_{j+1} t) - \sin(\omega_j t)] \tag{A2.7}$$

$$\int_{\omega_j}^{\omega_{j+1}} \omega \cos \omega t \, d\omega = \frac{1}{t^2} [\cos(\omega_{j+1} t) - \cos(\omega_j t)] \tag{A2.8}$$

$$+ \frac{1}{t} [\omega_{j+1} \sin(\omega_{j+1} t) - \omega_j \sin(\omega_j t)]$$

Using A2.7 and A2.8 in A2.6 leads to

$$\begin{aligned}
 \Delta S_R = & \frac{S_R(\omega_{j+1}) - S_R(\omega_j)}{(\omega_{j+1} - \omega_j)t^2} [\cos(\omega_{j+1}t) - \cos(\omega_j t)] \\
 & + \left\{ S_R(\omega_{j+1})\omega_{j+1} \sin(\omega_{j+1}t) - S_R(\omega_{j+1})\omega_j \sin(\omega_j t) \right. \\
 & - S_R(\omega_j)\omega_{j+1} \sin(\omega_{j+1}t) + S_R(\omega_j)\omega_j \sin(\omega_j t) \\
 & + S_R(\omega_j)\omega_{j+1} \sin(\omega_{j+1}t) - S_R(\omega_j)\omega_{j+1} \sin(\omega_j t) \\
 & \left. - S_R(\omega_{j+1})\omega_j \sin(\omega_{j+1}t) + S_R(\omega_{j+1})\omega_j \sin(\omega_j t) \right\} \\
 & \bigg/ (\omega_{j+1} - \omega_j)t .
 \end{aligned}$$

Simplifying we obtain

$$\begin{aligned}
 \Delta S_R = & \frac{S_R(\omega_{j+1}) - S_R(\omega_j)}{(\omega_{j+1} - \omega_j)t^2} [\cos(\omega_{j+1}t) - \cos(\omega_j t)] \\
 & + \frac{S_R(\omega_{j+1}) \sin(\omega_{j+1}t) - S_R(\omega_j) \sin(\omega_j t)}{t}
 \end{aligned} \tag{A2.9}$$

Summing consecutive intervals to obtain the total value of the integral A2.5, we notice that $[S_R(\omega_{j+1})\sin(\omega_{j+1}t)]/t$ for the first interval equals $[S_R(\omega_j)\sin(\omega_j t)]/t$ for the second interval; hence these terms cancel. If we sum for all

intervals, all interior points vanish leaving the first and last points. However, at $\omega = 0+$ and at some higher frequency (depending on the maximum frequency content of the signal) the values of S_R approach zero. That is, $S_R(\omega_j)$ is zero for the first interval; $S_R(\omega_{j+1})$ is zero for the last interval. Thus the second term of A2.9 vanishes upon summation over all intervals.

This gives for A2.5

$$\begin{aligned}
 & \int_0^\infty S_R(\omega) \cos \omega t \, d\omega \\
 (A2.10) \quad & = \sum_j \frac{S_R(\omega_{j+1}) - S_R(\omega_j)}{(\omega_{j+1} - \omega_j) t^2} [\cos(\omega_{j+1} t) - \cos(\omega_j t)]
 \end{aligned}$$

where the sum is over all the intervals.

Evidently $\int_0^\infty S_I(\omega) \sin \omega t \, d\omega$ will give a result identical in form

$$\begin{aligned}
 & \int_0^\infty S_I(\omega) \sin \omega t \, d\omega \\
 (A2.11) \quad & = \sum_j \frac{S_I(\omega_{j+1}) - S_I(\omega_j)}{(\omega_{j+1} - \omega_j) t^2} [\sin(\omega_{j+1} t) - \sin(\omega_j t)]
 \end{aligned}$$

Using A2.10 and A2.11 in A2.4 allows $s(t)$ to be calculated. The form of the equation is appropriate for use on a digital computer.

A2.2 Power Spectra Analyses

The theory presented in this appendix is a modification of information presented by Lee (1960) and Blackman and Tukey (1958).

Assume we have recorded a function $f(t)$ generated by a random stationary Gaussian process. The integral of the square of $f(t)$ must be finite. As well, the signal must have no D. C. value:

$$(A2.12) \quad \bar{f} = \lim_{T \rightarrow \infty} \int_{-T/2}^{T/2} f(t) dt = 0$$

The variance is defined as

$$C(0) = \lim_{T \rightarrow \infty} \frac{1}{T} \int_{-T/2}^{T/2} [f(t) - \bar{f}]^2 dt$$

or by A2.12

$$(A2.13) \quad C(0) = \lim_{T \rightarrow \infty} \frac{1}{T} \int_{-T/2}^{T/2} [f(t)]^2 dt$$

The autocovariance of the function $f(t)$ is defined by

$$(A2.14) \quad C(\tau) = \lim_{T \rightarrow \infty} \frac{1}{T} \int_{-T/2}^{T/2} f(t) f^*(t + \tau) dt$$

where the "*" refers to the complex conjugate and τ is the lag.

In this study, we will consider real signals.

The autocovariance is often called the autocorrelation coefficient although strictly speaking the latter term should refer to the normalized function

$$\phi(\tau) = C(\tau) / C(0) \quad .$$

The signal $f(t)$ in the autocorrelation coefficient extends over the range $-T/2$ to $+T/2$ but $f(t + \tau)$ extends from $(-T/2 + \tau)$ to $(T/2 + \tau)$. To avoid complications, we require that $f(t) = 0$ if t exceeds the range $|t| > T/2$.

The Fourier transform of $f(t)$ is

$$(A2.15) \quad F(\omega) = \frac{1}{2\pi} \int_{-\infty}^{+\infty} f(t) e^{-i\omega t} dt$$

while the inverse transform is given by

$$(A2.16) \quad f(t) = \int_{-\infty}^{+\infty} F(\omega) e^{i\omega t} d\omega$$

Substituting for $f(t + \tau)$ in A2.14 gives for the autocorrelation coefficient

$$C(\tau) = \lim_{T \rightarrow \infty} \frac{1}{T} \int_{-T/2}^{T/2} f(t) \int_{-\infty}^{+\infty} F(\omega) e^{i\omega(t + \tau)} d\omega dt$$

or changing the order of integration

$$C(\tau) = \lim_{T \rightarrow \infty} \frac{1}{T} \int_{-T/2}^{T/2} F(\omega) e^{i\omega\tau} \int_{-\infty}^{+\infty} f(t) e^{i\omega t} dt d\omega$$

From A2.15 with $\omega = -\omega$

$$(A2.17) \quad C(\tau) = \lim_{T \rightarrow \infty} \frac{2\pi}{T} \int_{-T/2}^{T/2} F(\omega) e^{i\omega\tau} F(-\omega) d\omega$$

We now define

$$P(\omega) = \lim_{T \rightarrow \infty} \frac{2\pi}{T} [F(\omega) \cdot F(-\omega)]$$

or

$$(A2.18) \quad P(\omega) = \lim_{T \rightarrow \infty} \frac{2\pi}{T} |F(\omega)|^2$$

Equation A2.17 becomes

$$(A2.19) \quad C(\tau) = \int_{-\infty}^{+\infty} P(\omega) e^{i\omega\tau} d\omega$$

$P(\omega)$ is the power spectrum and is given by the inverse Fourier transform

$$(A2.20) \quad P(\omega) = \frac{1}{2\pi} \int_{-\infty}^{+\infty} C(\tau) e^{-i\omega\tau} d\tau$$

Since the autocorrelation function is even this can be rewritten as a one-sided Fourier cosine transform

$$(A2.21) \quad P(\omega) = \frac{1}{\pi} \int_0^{\infty} C(\tau) \cos \omega\tau \, d\tau$$

It should be noted that the autocorrelation function and the power spectrum of a random function are related to each other by a Fourier cosine transformation.

In reality, the records we examine are finite in extent. For such cases we cannot estimate $C(\tau)$, the autocorrelation function for arbitrarily long lags. Thus we define an apparent autocorrelation function

$$(A2.22) \quad C_a(\tau) = \frac{1}{T_r - |\tau|} \int_{-\frac{1}{2}(T_r - |\tau|)}^{\frac{1}{2}(T_r - |\tau|)} f(t - \frac{1}{2}\tau) f(t + \frac{1}{2}\tau) \, dt$$

with $|\tau| \leq \tau_m < T_r$ where τ_m is the maximum desired lag value and T_r is the record length. The autocorrelation function, A2.22, may be rewritten as

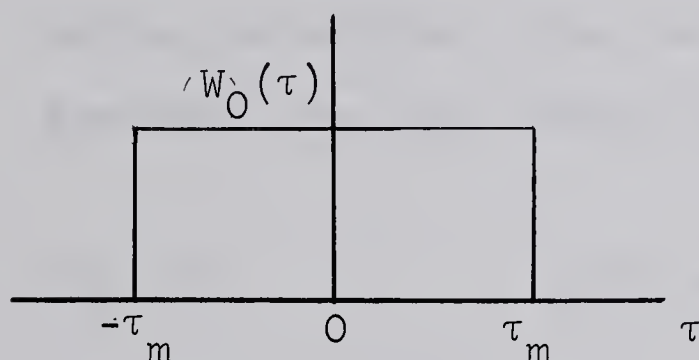
$$(A2.23) \quad C_a(\tau) = \frac{1}{T_r - \tau} \int_{-\frac{T_r}{2}}^{\frac{T_r}{2} - \tau} f(t) f(t + \tau) \, dt$$

The similarity between this equation and the computational formula, equation 3.4, is evident.

$$(3.4) \quad C(L) = \frac{1}{N-L} \sum_{i=1}^{N-L} G_i G_{i+L}$$

$$L = 0, 1, 2, \dots, (N-1) .$$

The inability to use infinitely long lags means that we are effectively multiplying the true autocorrelation (with infinite lag) by a time lag window, depicted below.

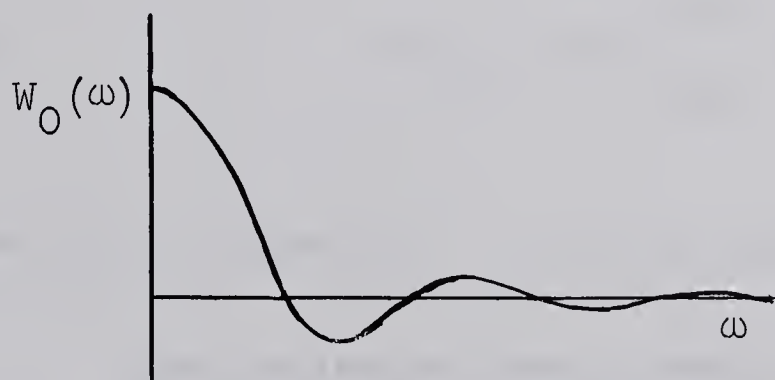


$$W_O(\tau) = 1, \quad |\tau| < \tau_m$$

$$W_O(\tau) = \frac{1}{2}, \quad |\tau| = \tau_m$$

$$W_O(\tau) = 0, \quad |\tau| > \tau_m$$

Taking the Fourier transform of this function gives the spectral window.



$$W_O(\omega) = 2 \tau_m \frac{\sin \omega \tau_m}{\omega \tau_m}$$

In computing the power spectrum, the result is thus multiplied by the square of the function, $W_O(\omega)$. This obviously introduces objectionable side bands of frequencies into the computed power spectrum, as the first side band has an amplitude 20% of that of the main lobe.

To partially overcome this difficulty, special lag windows which give less weight to the long lags have been constructed. These are treated as weighting functions for C_a , producing a modified apparent autocorrelation function.

$$(A2.24) \quad C_{ma}(\tau) = W(\tau) C_a(\tau)$$

Having determined this, we calculate the estimated power spectrum from the cosine transform A2.21.

$$(A2.25) \quad P_e(\omega) = \frac{1}{\pi} \int_0^{\infty} C_{ma}(\tau) \cos \omega\tau \, d\tau$$

The similarity between this function and equation 3.5, the computational formula is also evident:

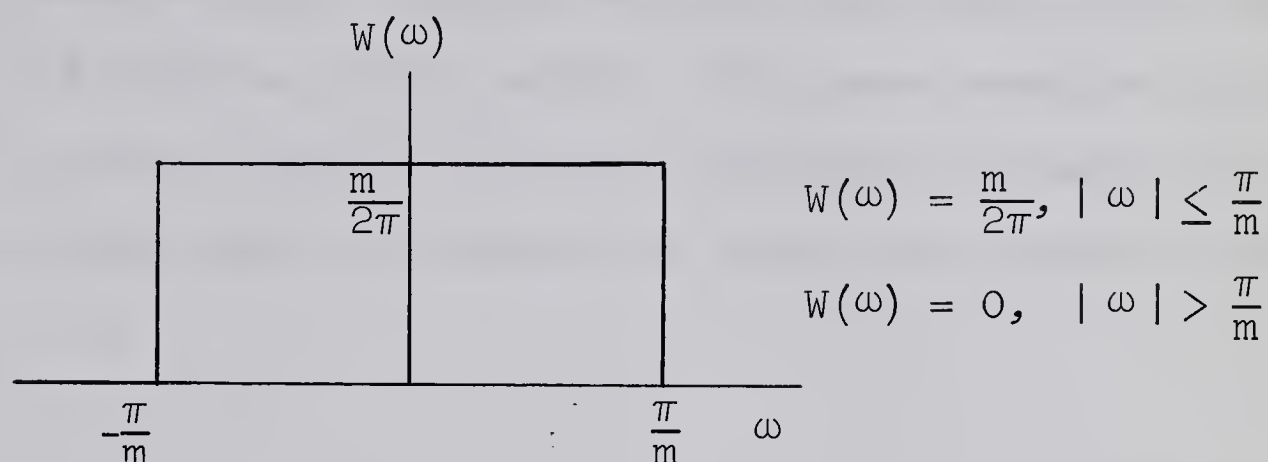
$$(3.5) \quad P(J) = 2\tau \sum_{L=0}^{N-1} W(L) C(L) \cos \frac{\pi LJ}{M}$$

where in the equation τ is the digitizing interval.

The estimated power spectrum gives a weighted average of power density over a range of frequencies and not the local power density. As the maximum lag, τ_m , becomes greater the approximation between the two becomes better.

A2.3 The Daniell Window

The ideal window would be one whose frequency response was square-shaped:



The Daniell window, used in the power spectral calculations in this thesis, approaches this ideal as closely as the data allow. To calculate its time lag window, we calculate the inverse Fourier transform of $W(\omega)$, above, by A2.16.

$$\begin{aligned}
 \omega(\tau) &= \frac{m}{2\pi} \int_{-\pi/m}^{\pi/m} 1 \cdot e^{i\omega\tau} d\omega \\
 &= \frac{m}{2\pi i\tau} \left[e^{i\omega\tau} \right]_{-\pi/m}^{\pi/m} \\
 &= [e^{i\pi\tau/m} - e^{-i\pi\tau/m}] / 2i \left(\frac{\pi\tau}{m} \right) \\
 \omega(\tau) &= \frac{\sin \frac{\pi\tau}{m}}{\frac{\pi\tau}{m}} .
 \end{aligned}$$

The lag, τ , can have values between 0 and $\pm T_r$, the record length, so that the square window can only be approximated. Use of this Daniell window requires more computer time because the autocorrelation function must be computed for all lags up to the maximum record length. The power spectra computed with the Daniell window represent smoothed averages over a controllable range of frequencies about any required frequency.

APPENDIX 3. LISTINGS OF COMPUTER PROGRAMS

This appendix documents the Fortran IV listings of the principal computer programs which have been developed and used in this thesis.

A3.1 The On-line Printer Plotting Program

This program gives a quick method of plotting (six traces per run) on the on-line IBM 1403 printer. Input data should be on tape with the reel mounted on drive number 4. The control cards required for its use are listed below.

1. 123456X --- beginning in column 1. Columns 8 to 10 inclusive give "RUNS", the number of graphs to be plotted, including those that are skipped.
2. Blank card.
3. Blank card.
- 4, 5, ... 1 card for each run. The data are in (4I5) format and gives the following parameters:
TOTAL REJECT CARDS SKIP where
TOTAL is the total number of cards in the run
REJECT is the number of cards to be rejected before the plotting begins
CARDS is the number of cards to be plotted
SKIP is the frequency of plotted points; e.g. a "2" means every second value after the first is plotted.


```

WRITE(6,98)
CLASS=50
MARK(1)=11
MARK(2)=31
MARK(3)=51
MARK(4)=71
MARK(5)=91
MARK(6)=111
C   SETS CENTERS OF GRAPH
    INCR=CARDS-SKIP-1
    DO 12 I4=1,INCR,SKIP
    DO 13 I5=1,6
13  Istor2(I5)=IDIGIT(I5)
C   STOR2 HAS THE CONFIGURATIONS
    DO 14 I6=1,6
    S=-1
    IF(N(I6,I4).GE.0)S=1
    IF(N(I6,I4).LT.0)N(I6,I4)=-N(I6,I4)
    Istor1(I6)=N(I6,I4)/50
    IF(Istor1(I6).GT.9)Istor2(I6)=IDIGIT(7)
    IF(Istor1(I6).GE.9)Istor1(I6)=9
14  Istor1(I6)=S *Istor1(I6)+MARK(I6)
    K1=Istor1(1)
    K2=Istor1(2)
    K3=Istor1(3)
    K4=Istor1(4)
    K5=Istor1(5)
    K6=Istor1(6)
    IA(K1)=Istor2(1)
    IA(K2)=Istor2(2)
    IA(K3)=Istor2(3)
    IA(K4)=Istor2(4)
    IA(K5)=Istor2(5)
    IA(K6)=Istor2(6)
    WRITE(6,15)(IA(J5),J5=1,120)
    DO 16 I8=1,120
16  IA(I8)=IA2(I8)
12  CONTINUE
    GO TO 5
55  CARDS=TOTAL*6
    DO 56 IIBB=1,CARDS
56  READ (4,8)
5   CONTINUE
    STOP
    END

```

\$ENTRY PLOT

A3.2 The Normalization Program

This program normalizes all traces to a chosen standard trace. It allows for input traces of unequal length but the output traces are all of one length. A formula representing the normalization process is given in Chapter 3 as

$$(3.1) \quad N_i = (G_i - \bar{G}) \frac{\sum_j |G_j^{\text{std}} - \bar{G}^{\text{std}}|}{\sum_j |G_j - \bar{G}|}$$

The control cards required for use of the program are listed below (symbols are defined on comment cards).

1. IB, STMC in (2I5) format.
2. TESTHH, STNO8, STNO9, CENTST, PTSST, STCH, SKIP1, NCARD, MC1, MC2, MCN in (3(4X,A1), 10I5) format.
3. NRUN, TESTH, ZERO, ONE, TWO, ... , NINE in (1X, I4, 11A1) format.
4. The following cards are required for each run, giving a total for part 4 of 7 cards.
 - a. SKIP, RECORD, NOPTS, MC, MCC, MN in (7I5) format.
 - b. CHAN, CENPT in (2I5) format is required for each of 6 channels.


```

$JOB          735027
$IE JOB RMC8
$IBFTC NORM   NODECK
  DIMENSION VECT1(5500),VECT2(5500),NORM(6),TITL(5),M(6)
  REAL VECT2,NORM,MEAN,M
  INTEGER SKIP,VECT1,RECORD,TOTAL
  INTEGER R3333,STMC
  INTEGER ADJUST,CENPT,CHAN,SERIAL
  INTEGER IMAG(79)
  INTEGER ONE,TWO,THREE,FOUR,FIVE,SIX,SEVEN,EIGHT,NINE,ZERO,TESTH
  REWIND 4
  REWIND 2
  DATA CH12/6HENDCAR/
  READ (5,119) IB,STMC
C   IB..... 0 IF IT IS THE FIRST RUN
C               1 IF PART OF OUTPUT TAPE HAS BEEN OBTAINED
C   STMC .. STANDARD NO. OF POINTS TO THE LEFT OF CENTER TO BE USED
119  FORMAT (15I5)
101  FORMAT(A6)
     IF (IB.EQ.0) GO TO 100
103  READ(2,101)CHARAC
     IF (CHARAC.LQ.CH12) GO TO 102
     GO TO 103
102  BACKSPACE 2
100  CONTINUE
     INTEGER CENTST,ADJ,PTSST,STCH,SKIP1,STNO8,STNO9,TESTHH,TOT
     INTEGER CHEC,REC1
     DIMENSION CHEC(80),REC1(5500),REC2(5500)
     READ (5,110) TESTHH,STNO8,STNO9,CENTST,PTSST,STCH,SKIP1,NCARD,MC1,
110  1MC2,MCN
110  FORMAT (3(4X,A1),15I5)
C   TESTHH .. AN H
C   STNO8 ... THE TENS DIGIT OF THE STANDARD RECORD NUMBER
C   STNO9 ... THE UNITS DIGIT OF THE STANDARD RECORD NUMBER
C   CENTST .. CENTER OF THE STANDARD CHANNEL
C   PTSST ... NUMBER OF POINTS IN THE STANDARD CHANNEL
C   STCH .... NUMBER OF THE STANDARD CHANNEL
C   SKIP1 ... THE NUMBER OF RECORDS THAT MUST BE PASSED BY TO GET TO
C               THE CORRECT STANDARD RECORD NUMBER
C   NCARD ... THE NUMBER OF CARDS IN THE STANDARD RECORD
C   MC1 .. NO. OF POINTS TO LEFT OF CENTER TO BE NORMALIZED
C   MC2 .. NO. OF POINTS TO RIGHT OF CENTER TO BE NORMALIZED
C   MCN .. NO. OF POINTS TO EITHER SIDE OF CENTER TO BE USED IN
C               OBTAINING THE NORMALIZING CONSTANT
     DO 70 KZ=1,999999
     READ (4,52) (CHEC(J),J=1,80)
52  FORMAT (80A1)
     IF (CHEC(2).EQ.TESTHH) SKIP1=SKIP1-1
     IF (SKIP1.LT.0) GOTO 71
70  CONTINUE
71  IF (CHEC(8).NE.STNO8) WRITE (6,998) CHEC(8)
998  FORMAT (1X,14HCHEC(8) READS ,A1)
     IF (CHEC(9).NE.STNO9) WRITE (6,997) CHEC(9)
997  FORMAT (1X,14HCHEC(9) READS ,A1)
     IF (CHEC(8).NE.STNO8) GO TO 69

```



```

      IF (CHEC(9).NE.3TNO9) GO TO 69
      IF (STCH.EQ.1) GO TO 59
      N3=NCARD*(STCH-1)
      DO 58 KW = 1,N3
58      READ (4,53)
      53      FORMAT (1H1)
59      READ (4,60) (REC1(J),J=1,PTSST)
60      FORMAT (18I4)
      ADJ=CENTST-1-MC1
      TOT=MC1+MC2+1
      DO 61 KV=1,TOT
      IND=ADJ+KV
61      REC2(KV)=REC1(IND)
      ADD=J.
      MCNN=2*MCN+1
      IS1=MC1+1-MCN
      IS2=IS1+MCNN-1
      DO 62 KU=IS1,IS2
62      ADD=ADD+REC2(KU)
      REAL NORMAL,MEANY
      MEANY=ADD/FLOAT(MCNN)
      NORMAL=C.
      DO 63 KT=IS1,IS2
63      NORMAL=NORMAL+ABS(REC2(KT)-MEANY)
      REWIND 4
      READ(5,1)NRUN,TESTH,ZERO,ONE,TWO,THREE,FOUR,FIVE,SIX,SEVEN,EIGHT,NINE
1      LINE
      1      FORMAT(1X,I4,11A1)
C      NRUN ..... THE NUMBER OF RUNS
C      TESTH ... AN H
C      ZERO...NINE ARE NUMBERS 0-9 INCL. WITH NO SPACES
      SERIAL=0
      DO 2 KA=1,NRUN
      REWIND 3
      READ(5,3)SKIP,RECORD,NOPTS,MC,MCC,MN
      3      FORMAT(7I5)
C      SKIP ..... NO. OF RECORDS TO BE SKIPPED AFTER PREVIOUS RECORD DONE
C      RECORD .. THE RECORD NUMBER DESIRED EX. RECORD 3 IS 30
C      NOPTS ... THE NUMBER OF POINTS IN THIS RECORD
C      MC ..... NO. OF POINTS TO THE LEFT OF CENTER TO BE NORMALIZED
C      MCC .. NO. OF POINTS TO RIGHT OF CENTER TO BE NORMALIZED
C      MN ... NO. OF PTS. TO EITHER SIDE OF CENTER TO OBTAIN CHAN. NORM
      DO 4 KB=1,999999
      READ(4,5)(IMAG(J),J=1,79)
      5      FORMAT(1X,79A1)
      IF(IMAG(1).EQ.TESTH)SKIP=SKIP-1
      IF(SKIP.LT.0)GO TO 7
      4      CONTINUE
      7      CALL HELP(ZERO,ONE,TWO,THREE,FOUR,FIVE,SIX,SEVEN,EIGHT,NINE,RECORD,
1,IMAG)
      6      IF(RECORD.GT.SERIAL)GO TO 8
      14     WRITE(6,9)RECORD
      9      FORMAT(1X,10HRECORD NO.,I4,15HIS OUT OF ORDER)
      25     GO TO 11
      8      SERIAL=RECORD

```



```

DO 13 KL=1,6
RECORD=RECORD+1
READ(5,3)CHAN,CENPT
C   CHAN ... CHANNEL NO. --MUST BE WRITTEN WITH RECORD NO. IN FRONT
C   CENPT ... THE CENTER POINT OF THE CHANNELL
IF(RECORD.NE.CHAN)GO TO 14
READ(4,16)(VECT1(KM),KM=1,NOPTS)
IF (MC.EQ.STMC) GO TO 45
LL=STMC-MC
DO 46 JJ=1,LL
46  VECT2(JJ)=0.
ADJUST=CENPT-1-MC
TOTAL=MC+MCC+1+LL
LJ=LL+1
DO 47 JK=LJ,TOTAL
JL=JK-LJ+1
INDEX=ADJUST+JL
47  VECT2(JK)=VECT1(INDEX)
GO TO 48
45  ADJUST=CENPT-1-MC
16  FORMAT(18I4)
TOTAL=MC+MCC+1
DO 17 KF=1,TOTAL
INDEX=ADJUST+KF
17  VECT2(KF)=VECT1(INDEX)
C   VECT2 IS FLOATING POINT VECTOR  VECT1 IS INTEGER VARIABLE VECTOR
48  SUM=0.
MNN=2*MN+1
ISTAR=MC+1-MN
ISTAR2=ISTAR+MNN-1
DO 18 KG=ISTAR,ISTAR2
18  SUM=SUM+VECT2(KG)
MEAN=SUM/FLOAT(MNN)
SUM=0
DO 19 KH=ISTAR,ISTAR2
19  SUM=SUM+ABS(VECT2(KH)-MEAN)
M(KE)=MEAN
NORM(KE)=SUM
WRITE(3,12)(IMAG(KI),KI=1,4),RECORD,(IMAG(KI),KI=10,79)
12  FORMAT(1X,4A1,I5,70A1)
WRITE(3,20)(VECT2(KJ),KJ=1,TOTAL)
20  FORMAT(1X,5E14.7)
13  CONTINUE
REWIND 3
DO 21 KK=1,6
READ(3,31)ALPHA,RECORD,(TITLE(KI),KI=1,5)
31  FORMAT(A5,I5,5A6,40H
READ(3,20)(VECT2(KJ),KJ=1,TOTAL)
COR=NORMAL/NORM(KK)
IF(MC.EQ.STMC) GO TO 701
LM=STMC-MC
DO 702 JJJ=1,LM
702 VECT1(JJJ)=0
LN=LM+1

```



```

DO 703 JJL=LN,TOTAL
VECT1(JJL)=(VECT2(JJL)-A(KK))*COR
703 IF(IABS(VECT1(JJL)).GT.999) VECT1(JJL)=999*(VECT1(JJL)/IABS(VECT1(
1JJL)))
GO TO 24
701 DO 22 KL=1,TOTAL
VECT1(KL)=(VECT2(KL)-A(KK))*COR
22 IF(IABS(VECT1(KL)).GT.999) VECT1(KL)=999*(VECT1(KL)/IABS(VECT1(KL)
1))
24 WRITE(6,31)ALPHA,RECORD,(TITLE(KI),KI=1,5)
R3333=RECORD-1
IF(KK.EQ.1)WRITE(2,31)ALPHA,R3333,(TITLE(KI),KI=1,5)
WRITE(2,16)(VECT1(KE),KE=1,TOTAL)
21 WRITE(6,99)(VECT1(KE),KE=1,TOTAL)
99 FORMAT(1X,18I4)
2 CONTINUE
WRITE(2,101)CH12
GO TO 25
11 REWIND 4
REWIND 2
REWIND 3
69 STOP
END

```

```

$IBFTC SUB DECK
SUBROUTINE HELP(ZERO,ONE,TWO,THREE,FOUR,FIVE,SIX,SEVEN,EIGHT,NINE,
1RECORD,IMAG)
INTEGER AD,RECORD
INTEGER ONE,TWO,THREE,FOUR,FIVE,SIX,SEVEN,EIGHT,NINE,ZERO
DIMENSION IMAG(79),N(5)
RECORD=0
N(1)=10000
N(2)=1000
N(3)=100
N(4)=10
N(5)=1
DO 1 J=1,5
K=4+J
IF(IMAG(K).EQ.ONE)AD=1
IF(IMAG(K).EQ.TWO)AD=2
IF(IMAG(K).EQ.THREE)AD=3
IF(IMAG(K).EQ.FOUR)AD=4
IF(IMAG(K).EQ.FIVE)AD=5
IF(IMAG(K).EQ.SIX)AD=6
IF(IMAG(K).EQ.SEVEN)AD=7
IF(IMAG(K).EQ.EIGHT)AD=8
IF(IMAG(K).EQ.NINE)AD=9
IF(IMAG(K).EQ.ZERO)AD=0
1 RECORD=RECORD+AD*N(J)
RETURN
END
$ENTRY NORM

```


A3.3 The Autopower Spectra Program

This program calculates autocorrelation coefficients and autopower density spectra of input data with variable format. It includes a choice of three types of lag windows: Hanning, Hamming or Daniell. The relevant formulae are given in Chapter 3. For the autocorrelation coefficient,

$$(3.4) \quad C(L) = \frac{1}{N-L} \sum_{i=1}^{N-L} G_i G_{i+L}$$

where $L = 0, 1, 2, \dots, (N-1)$. The formula for computation of the autopower spectra is

$$(3.5) \quad P(J) = 2\pi \sum_{L=0}^{N-1} W(L) C(L) \cos \frac{\pi LJ}{M}$$

where $J = 0, 1, 2, \dots, M$

M is the specified maximum J value.

Control cards required for the use of this program are listed below (symbols are defined on comment cards).

1. INPUT, NPOWER in (5X, 10I5) format.
2. (FMT(J), J=1,12) in (1X, 12A6) format.
3. RECOR1, RECOR2, NOPTS, MLAG, C1, MTYPE, MR in (5X, 10I5) format.
4. DELT in (5X, F10.5) format.


```

$JOB          735059
$IBJOB CROSS
$IBFTC ERK1
C      THIS PROGRAM CALCULATES AUTO POWER DENSITY SPECTRA AND AUTO
C      CORRELATION OF INPUT DATA WITH VARIABLE FORMATS
COMMON/DAT/A(3000),B(3000),C(6000),D(6000)
COMMON/CONST/RECOR1,RECOR2,NOPTS,MLAG,INPUT,CENT1,END1,C2,C1,MTYPE
DIMENSION FMT(12)
INTEGER A,B
INTEGER RECOR1,RECOR2,NOPTS,MLAG,CENT1,END1,C2,C1
C      DELT *** THE DIGITIZING INTERVAL IN SECONDS OR MILES
C      NOPTS *** THE NUMBER OF POINTS
C      MLAG *** THE MAXIMUM FREQUENCY INCREMENT
C      END1 *** THE END POSITION OF THE CORRELATION VECTOR
C      CENT1 *** THE CENTRE POSITION OF THE CORRELATION VECTOR
C      INPUT *** UNIT FROM WHICH DATA IS TO BE READ
C      FMT DEFINES FORMAT OF INPUT DATA (1X,1814,7X)
C      RECOR1 = 1, RECOR2 = 0 FOR AUTO CORRELATION
C      RECOR1 = 1, RECOR2 = 2 FOR CROSS CORRELATION
C      C2 *** 1 AUTO CORRELATIONS WANTED
C      *** 0 CROSS CORRELATIONS WANTED
C      C1 *** 1 AUTO POWER DENSITY SPECTRA WANTED
C      *** 3 CROSS POWER DENSITY SPECTRA WANTED
C      MTYPE *** 1 FOR HANNING WINDOW. (MLAG SHOULD EQUAL NOPTS/10)
C      *** 2 FOR HAMMING WINDOW. (MLAG SHOULD EQUAL NOPTS/10)
C      *** 3 FOR DANIEL WINDOW. (MLAG SHOULD EQUAL NOPTS)
C      RATIO NOPTS/MR SPECIFIES THE TYPE OF DANIEL WINDOW (RECOMMEND 10)
C      FOR HANNING AND HAMMING WINDOWS MLAG SHOULD EQUAL MR
C      NPOWER .. NO. OF DATA SETS FOR CALCULATION OF AUTOPOWER SPECTRA
1      FORMAT(5X,10I5)
8      FORMAT (1X,12A6)
9      FORMAT (5X,F10.5)
      READ (5,1) INPUT, NPOWER
      READ(5,8)(FMT(J),J=1,12)
      READ (5,1) RECOR1,RECOR2,NOPTS,MLAG,C1,MTYPE,MR
      READ (5,9) DELT
      CENT1=MLAG+1
      END1=MLAG+CENT1
      DO 50 IK=1,NPOWER
      WRITE (6,51) IK
51      FORMAT (1H1,4HSET ,12,14H OF INPUT DATA)
      READ(INPUT,FMT)(A(J),J=1,NOPTS)
      WRITE (6,FMT)(A(J),J=1,NOPTS)
      C2=0
      IF(RECOR2.NE.0)GO TO 5
      DO 6 J=1,NOPTS
6      B(J)=A(J)
      C2=1
      GO TO 7
5      READ(INPUT,FMT)(B(J),J=1,NOPTS)
      WRITE (6,FMT) (B(J),J=1,NOPTS)
7      CALL CROSS(CENT1,NOPTS,C2,MLAG,MTYPE)
      IF(C2.EQ.0)CALL OUTPUT(MLAG,END1,RECOR1,RECOR2,0)
      IF(C2.EQ.1)CALL OUTPUT(MLAG,END1,RECOR1,RECOR2,MLAG)

```



```

DO 20 JA=1,MLAG
JB = CENT1+JA-1
20 WRITE (3,21) JA,C(JB)
21 FORMAT (1X,I5,2X,E14.7)
WRITE (3,22)
22 FORMAT (6H END )
FN= 1./(2.*DELT)
WRITE (6,10) DELT,FN
10 FORMAT(1X,5HDELT=,F8.3,1X,18HNYQUIST FREQUENCY=,F8.3)
WRITE (6,12) NOPTS,MLAG,MR
12 FORMAT(1X,6HNOPTS=,I5,1X,5HMLAG=,I5,1X,3HMR=,I5)
CALL POWER(MLAG,DELT,CENT1,MTYPE,MR)
DO 11 J=1,END1
11 C(J)=D(J)
IF(C1.EQ.1)CALL OUTPUT(MLAG,END1,MTYPE,C1,MLAG)
DO 23 JA=1,MLAG
JB = CENT1+JA-1
23 WRITE (3,21) JA,C(JB)
WRITE (3,22)
50 CONTINUE
STOP
END

```

\$IBFTC SUB10

```

SUBROUTINE CROSS(CENT1,NOPTS,C2,MLAG,MTYPE)
COMMON/DAT/A(3000),B(3000),C(6000),D(6000)
INTEGER A,B
INTEGER CENT1,NOPTS,C2,MLAG
KX = 0
KY = 0
DO 3 J=1,NOPTS
KX = KX + A(J)
3 KY = KY + B(J)
KX = KX/NOPTS
KY = KY/NOPTS
DO 4 J=1,NOPTS
A(J) = A(J) - KX
4 B(J) = B(J) - KY
WRITE (6,6)
6 FORMAT (1HL,38HINPUT VALUES WITH AVERAGE D.C. REMOVED)
WRITE (6,5) (A(J), J=1,NOPTS)
5 FORMAT (1X,18I4,7X)
CALL DOT(NOPTS,0,C(CENT1),1,MTYPE)
DO 1 J=1,MLAG
K1=CENT1+J
CALL DOT(NOPTS,J,C(K1),2,MTYPE)
IF(C2.NE.0)GO TO 1
K2=CENT1-J
CALL DOT(NOPTS,J,C(K2),3,MTYPE)
1 CONTINUE
RETURN
END

```


\$IBFTC SUB11

```

SUBROUTINE DOT(N,NS,ANS,MODE,MTYPE)
COMMON/DAT/A(3000),B(3000),C(6000),D(6000)
INTEGER A,B
FNUM=0.
L=N-NS
DO 1 J=1,L
K=J+NS
1 FNUM = FNUM + FLOAT(A(J))*FLOAT(B(K))
IF(MTYPE.EQ.3)GO TO 2
ANS=FNUM/(FLOAT(L))
GO TO 3
2 ANS = FNUM/(FLOAT(N))
3 RETURN
END

```

\$IBFTC SUB14

```

SUBROUTINE POWER(MLAG,DELT,CENT1,MTYPE,MR)
COMMON/DAT/A(3000),B(3000),C(6000),D(6000)
INTEGER A,B
INTEGER CENT1,END1
DO 1 L=1,MLAG
L1=CENT1+L
CALL WINDOW(MR,L,W,MTYPE)
1 C(L1)=C(L1)*W
END1 = MLAG + CENT1
CALL OUTPUT(MLAG,END1,1,0,MLAG)
DC=0.
DO 2 L=1,MLAG
L1=CENT1+L
2 DC = DC + C(L1)
D(CENT1) = DELT*C(CENT1) + 2.*DELT*DC
DO 3 J=1,MLAG
AC=0.
DO 4 L=1,MLAG
L1 = CENT1 + L
CARG1 = 3.14159*(FLOAT(J))*(FLOAT(L))/(FLOAT(MLAG))
4 AC = AC + C(L1)*COS(CARG1)
J1 = CENT1 + J
3 D(J1) = DELT*C(CENT1) + 2.*DELT*AC
RETURN
END

```

\$IEFTC SUB15

```

SUBROUTINE WINDOW(MR,L,W,MTYPE)
CARG = 3.14159*(FLOAT(L))/(FLOAT(MR))
GO TO (5,6,7),MTYPE
5 W = 0.5 + 0.5*COS(CARG)
GO TO 8
6 W = 0.54 + 0.46*COS(CARG)
GO TO 8
7 W = (SIN(CARG))/CARG
8 RETURN
END

```



```

$IBFTC SUB12
      SUBROUTINE OUTPUT(MLAG,END1,RECOR1,RECOR2,IAD)
      COMMON/DAT/A(3000),B(3000),C(6000),D(6000)
      INTEGER SKIP,END1,RECOR1,RECOR2
4     FORMAT(6(1X,I6,1X,1H*E10.3,1X,2H  ))
5     FORMAT(6(8X,1H*11X,2H  ))
      CALL PAGE(L7,SKIP,RECOR1,RECOR2)
      IR=-MLAG+IAD
      K1=IR-6
      K2=IR-5
      K3=IR-4
      K4=IR-3
      K5=IR-2
      K6=IR-1
      J=1+IAD
12    K1=K1+6
      K2=K2+6
      K3=K3+6
      K4=K4+6
      K5=K5+6
      K6=K6+6
      L=J
      L1=J+1
      L2=J+2
      L3=J+3
      L4=J+4
      L5=J+5
      J=J+6
      IF(J.GT.END1) GO TO 11
      WRITE(6,4) K1,C(L),K2,C(L1),K3,C(L2),K4,C(L3),K5,C(L4),K6,C(L5)
      SKIP=SKIP+1
      L7=L7+1
      IF (L7.EQ.45) CALL PAGE(L7,SKIP,RECOR1,RECOR2)
      IF (SKIP.EQ.5) WRITE(6,5)
1     IF (SKIP.EQ.5) SKIP=0
      GO TO 12
11    IR=MOD(END1+1-L,6)
      IF (IR.EQ.0) WRITE(6,4) K1,C(L),K2,C(L1),K3,C(L2),K4,C(L3),K5,
1 C(L4),K6,C(L5)
      IF (IR.EQ.0) RETURN
      GO TO (6,7,8,9,10),IR
10    WRITE(6,4) K1,C(L),K2,C(L1),K3,C(L2),K4,C(L3),K5,C(L4)
      RETURN
9     WRITE(6,4) K1,C(L),K2,C(L1),K3,C(L2),K4,C(L3)
      RETURN
8     WRITE(6,4) K1,C(L),K2,C(L1),K3,C(L2)
      RETURN
7     WRITE(6,4) K1,C(L),K2,C(L1)
      RETURN
6     WRITE(6,4) K1,C(L)
      RETURN
      END

```



```

$IBFTC SUB13
  SUBROUTINE PAGE(L1,SKIP,RECOR1,RECOR2)
  INTEGER RECOR1,RECOR2
  ISKIP=0
  L1=0
  IF (RECOR2.EQ.0) WRITE(6,1)RECOR1,RECOR1
  IF (RECOR2.EQ.2) WRITE(6,1)RECOR1,RECOR2
1  FORMAT(1H1,29X,28HCROSS CORRELATIONS OF RECORD,1X,15,1X,11HWITH RE
1CORD,1X,15)
  IF (RECOR2.EQ.1) WRITE(6,4)
  IF (RECOR2.EQ.3) WRITE(6,5)
4  FORMAT(1H1,29X,26HAUTO POWER DENSITY SPECTRA)
5  FORMAT(1H1,29X,27HCROSS POWER DENSITY SPECTRA)
  IF(RECOR2.LQ.0)GO TO 6
  IF(RECOR2.EQ.2)GO TO 6
  IF (RECOR1.EQ.1)WRITE(6,7)
  IF (RECOR1.EQ.2) WRITE (6,8)
  IF (RECOR1.EQ.3) WRITE (6,9)
7  FORMAT(30X,19HWITH HANNING WINDOW)
8  FORMAT(30X,19HWITH HAMMING WUNDOW)
9  FORMAT(30X,18HWITH DANIEL WINDOW)
  WRITE(6,2)
2  FORMAT(30X,53H*****
1  /))
  WRITE(6,10)
10 FORMAT(6(6X,1HJ,8X,4HP(J),3X))
  GO TO 11
6  WRITE(6,2)
  WRITE(6,3)
3  FORMAT(6(6X,1HL,8X,4HC(L),3X))
11 RETURN
  END
$ENTRY          ERK1

```


A3.4 The General Stacking Program

This program enables the compositing of a maximum of 8 traces per stack with variable weighting factors. The sub-routine "SUB2", called "CODER", is useful as it enables two numbers in I4 format to be stored as one number, thereby doubling core storage for the input data. Control cards required for its use are listed below (symbols are defined on comment cards).

1. NCARDS, NPTS, NRUNS, NSKIP, INDEX, INPUT, IPTST, IPTEND, JOUT in (5X, 15I5) format.
2. The next control cards depend on the parameter INDEX.
 - a. INDEX = 1. For each run three cards are required.
 - i. NST in (5X, 15I5) format.
 - ii. IRWD, (NTRACE(I), I=1,NST) in (5X, 15I5) format.
 - iii. (WT(I), I=1, NST) in (5X,10F6.5) format.
 - b. INDEX = 2. Two cards are required.
 - i. NST, NSTART in (5X, 15I5) format.
 - ii. (WT(I),I=1,NST) in (5X,10F6.5) format.


```

      IF (IRWD.EQ.10) NREAD=0
C     IRWD = 10  TAPE MUST BE REWOUND BEFORE ANY MORE STACKING CAN OCCUR
      NPTS2 = NPTS/2
      DO 16 I=1,NST
      KA=NTRACE(I)-NREAD-1
      IF (KA.EQ.0) GO TO 13
      DO 15 IA=1,KA
      DO 14 IB=1,NCARDS
14     READ (INPUT,3)
      NREAD = NREAD + 1
      IF (MOD(NREAD,6).EQ.0) READ (INPUT,3)
15     CONTINUE
13     CALL FINDER (I,NCARDS,NPTS,INPUT)
      NREAD = NREAD + 1
      IF (MOD(NREAD,6).EQ.0) READ (INPUT,3)
16     CONTINUE
C     THE @NST@ SETS OF DATA ARE NOW STORED IN MATRIX A
      DO 18 J=1,NPTS2
      JA=2*J-1
      JB=2*J
      RES1 = 0.
      RES2 = 0.
      DO 17 I=1,NST
      CALL CODER (A(I,J),TEMP(1,I),TEMP(2,I),1)
      TEMPOR(1,I) = WT(I)*FLOAT(TEMP(1,I))
      TEMPOR(2,I) = WT(I)*FLOAT(TEMP(2,I))
      RES1 = RES1 + TEMPOR(1,I)
17     RES2 = RES2 + TEMPOR(2,I)
      RESULT(JA) = INT(RES1)
      RESULT(JB) = INT(RES2)
18     CONTINUE
C     THE VECTOR @RESULT@ NOW CONTAINS THE STACKING OF NST CHANNELS
      NF = 2*NPTS2
      WRITE (6,99) NR,NST
      WRITE (6,4) (RESULT(I),I=1,NF)
      GO TO (24,25),JOUT
24     WRITE (3,9) (I,RESULT(I),I=1,NF)
      WRITE (3,6)
      GO TO 29
25     WRITE (2,4) (RESULT(I),I=1,NF)
      NWRIT = NWRIT + 1
      IF (MOD(NWRIT,6).EQ.0) WRITE (2,96)
29     CONTINUE
      NZERO = 6 - MOD(NRUNS,6)
      IF (NZERO.EQ. 6) GO TO 28
      DO 27 I=1,NZERO
      DO 26 II=1,NCARDS
26     WRITE (2,95)
27     CONTINUE
28     GO TO 80
50     READ (5,1) NST,NSTART
C     NSTART          THE NUMBER TO START STACKING FROM AFTER SKIPPING
C                     @NSKIPO@ RECORDS
      READ(5,2) (WT(I),I=1,NST)
      NPTS2=NPTS/2
      NST2=NST/2 + 1

```



```

DO 49 NR = 1,NRUNS
IF ((NR.EQ.1).AND.(NST2.EQ.NSTART)) GO TO 34
IF (NR.GT.1) GO TO 36
DO 31 I=1,NST
IF ((I.GT.1).AND.(I.LE.NST2)) GO TO 32
CALL FINDER (I,NCARDS,NPTS,INPUT)
NREAD = NREAD + 1
IF (MOD(NREAD,6).EQ.0) READ (INPUT,3)
GO TO 31
32 DO 33 IA=1,NPTS2
33 A(I,IA) = A(1,IA)
31 CONTINUE
GO TO 40
34 DO 35 I=1,NST
CALL FINDER (I,NCARDS,NPTS,INPUT)
NREAD = NREAD + 1
IF (MOD(NREAD,6).EQ.0) READ (INPUT,3)
35 CONTINUE
GO TO 40
36 NSTL1 = NST-1
DO 38 I=1,NSTL1
DO 37 IA=1,NPTS2
II=I+1
37 A(I,IA) = A(II,IA)
38 CONTINUE
IF ((NRUNS-NR).LT.(NST2-1)) GO TO 39
CALL FINDER (NST,NCARDS,NPTS,INPUT)
NREAD = NREAD + 1
IF (MOD(NREAD,6).EQ.0) READ (INPUT,3)
GO TO 40
39 DO 43 IA=1,NPTS2
43 A(NST,IA) = A(NSTL1,IA)
C THE DATA IS NOW IN CORE FOR 1 RUN
40 DO 41 J=1,NPTS2
JB=2*J-1
JC=2*J
POINT1=0.
POINT2=0.
DO 42 JA=1,NST
CALL CODER (A(JA,J),TEMP(1,JA),TEMP(2,JA),1)
TEMPOR(1,JA) = FLOAT(TEMP(1,JA))*WT(JA)
TEMPOR(2,JA) = FLOAT(TEMP(2,JA))*WT(JA)
POINT1 = POINT1 + TEMPOR(1,JA)
42 POINT2 = POINT2 + TEMPOR(2,JA)
IPT1 = INT(POINT1)
IPT2 = INT(POINT2)
IM = MOD(NR,3) + 1
GO TO (44,45,46),IM
44 CALL CODER (A(8,J),IPT1,IPT2,2)
GO TO 41
45 CALL CODER (B(1,J),IPT1,IPT2,2)
GO TO 41
46 CALL CODER (B(2,J),IPT1,IPT2,2)
41 CONTINUE
C AFTER ANY 3 RUNS THERE WILL BE 3 SETS OF STACKED DATA STORED IN
C A(8, ),B(1, ),B(2, ).

```



```

      IF (MOD(NR,3).NE.0) GO TO 49
      GO TO (51,52),JOUT
51  N2=NR-2
      N1=NR-1
      WRITE (6,98) N2,N1,NR
      WRITE (6,97)
      DO 47 J=1,NPTS2
      JB=2*J-1
      JC=2*J
      CALL CODER (B(1,J),GRAPH(1),GRAPH(4),1)
      CALL CODER (B(2,J),GRAPH(2),GRAPH(5),1)
      CALL CODER (A(8,J),GRAPH(3),GRAPH(6),1)
      WRITE (6,7) JB,GRAPH(1),GRAPH(2),GRAPH(3)
      WRITE (3,8) JB,GRAPH(1),GRAPH(2),GRAPH(3)
      WRITE (6,7) JC,GRAPH(4),GRAPH(5),GRAPH(6)
      WRITE (3,8) JC,GRAPH(4),GRAPH(5),GRAPH(6)
47  CONTINUE
      WRITE (3,6)
      GO TO 49
52  DO 55 K=1,2
      DO 54 J=1,NPTS2
      CALL CODER (B(K,J),GRAPH(1),GRAPH(2),1)
      MAK = MOD(J,9)
      IF (MAK.EQ.0) MAK=9
      JB = 2*MAK - 1
      JC = 2*MAK
      HOLD(JB) = GRAPH(1)
      HOLD(JC) = GRAPH(2)
      IF (((NPTS2-J).LT.9).AND.(JC.NE.18)) GO TO 59
      IF (JC.NE.18) GO TO 54
      GO TO 61
59  IF (J.NE.NPTS2) GO TO 54
61  WRITE (6,4) (HOLD(JM),JM=1,JC)
      WRITE (2,4) (HOLD(JM),JM=1,JC)
54  CONTINUE
      NWRIT = NWRIT + 1
      IF (MOD(NWRIT,6).EQ.0) WRITE (2,96)
      WRITE (6,97)
55  CONTINUE
      DO 56 J=1,NPTS2
      CALL CODER (A(8,J),GRAPH(1),GRAPH(2),1)
      MAK = MOD(J,9)
      IF (MAK.EQ.0) MAK=9
      JB = 2*MAK - 1
      JC = 2*MAK
      HOLD(JB) = GRAPH(1)
      HOLD(JC) = GRAPH(2)
      IF (((NPTS2-J).LT.9).AND.(JC.NE.18)) GO TO 60
      IF (JC.NE.18) GO TO 56
      GO TO 62
60  IF (J.NE.NPTS2) GO TO 56
62  WRITE (6,4) (HOLD(JM),JM=1,JC)
      WRITE (2,4) (HOLD(JM),JM=1,JC)
56  CONTINUE
      NWRIT = NWRIT + 1
      IF (MOD(NWRIT,6).EQ.0) WRITE (2,96)

```



```

      WRITE (6,97)
49   CONTINUE
      IF (MOD(NWRIT,6).EQ.0) GO TO 80
      KA = 6 - MOD(NWRIT,6)
      DO 58 I=1,KA
      DO 57 II=1,NCARDS
57   WRITE (2,95)
58   CONTINUE
80   STOP
      END

```

\$IEFTC SUB1

```

      SUBROUTINE FINDER (I,NCARDS,NPTS,INPUT)
      COMMON A(8,2000)
      INTEGER A
4     FORMAT (1X,18I4,7X)
      DO 20 IA=1,NCARDS
      KB = 18*IA - 9*(IA-1)
      KA = KB - 17
      IF (IA.NE.NCARDS) GO TO 11
      KB = KB - (18*NCARDS-NPTS)
11    READ (INPUT,4) (A(I,IB),IB=KA,KB)
      IF (IA.EQ.NCARDS) GO TO 13
      KG = 9*IA-8
      KH = 9*IA
      DO 12 IC=KG,KH
      KC = 2*IC - KG
      KD = KC + 1
12    CALL CODER(A(I,IC),A(I,KC),A(I,KD),2)
      GO TO 20
13    KE = 9*NCARDS-8
      KF = NPTS/2
      DO 14 IC=KE,KF
      KC = 2*IC - KE
      KD = KC + 1
14    CALL CODER (A(I,IC),A(I,KC),A(I,KD),2)
20    CONTINUE
      RETURN
      END

```

\$IBFTC SUB2

```

      SUBROUTINE CODER(IN,OUT1,OUT2,OP)
      INTEGER IN,OUT1,OUT2,OP
C     OP = 1   DECOMPRESS...  IN.....OUT1 AND OUT2
C     OP = 2   COMPRESS....   OUT1 AND OUT2 .....IN
      IF (OP.EQ.2) GO TO 1
      OUT2 = IN - IN/10000*10000
      IF (OUT2.GE.9000) OUT2 = 9000-OUT2
      OUT1 = IN/10000
      IF (OUT1.GE.9000) OUT1 = 9000-OUT1
      GO TO 2
1     IF(OUT2.LT.0) OUT2 = -OUT2 + 9000
      IF (OUT1.LT.0) OUT1 = -OUT1 + 9000
      IN = OUT2 + OUT1*10000
2     RETURN
      END

```

\$ENTRY

GENSTK

A3.5 The Synthetic Seismogram Program

This program generates a synthetic seismogram given depth, $Z(J)$, and velocity, $V(J)$, values for a layered earth and some form of an input pulse. For the input pulse, this program either calculates the Ricker wavelet given by

$$(4.2) \quad G(x) = - [\phi^5(x) + \phi^6(x)]$$

with $x = t/T$ or time values of any other pulse may be read in as data. The reflection coefficient R_0 is computed by an iterative procedure from

$$(4.1) \quad R_{j-1}(\omega) = \frac{b_{j-1}\beta_{j-1} + (b_j - b_{j-1}) - b_j\beta_j \left(\frac{1-R_j}{1+R_j}\right)}{b_{j-1}\beta_{j-1} - (b_j - b_{j-1}) + b_j\beta_j \left(\frac{1-R_j}{1+R_j}\right)} e^{-\beta_{j-1} \ln \frac{v_j}{v_{j-1}}}$$

and the synthetic seismogram is then generated from the Fourier integral

$$(4.4) \quad S(t) = \int_{-\infty}^{+\infty} R_0(\omega) G(\omega) e^{i\omega(t+z/v_0)} d\omega$$

Control cards required for use in this program are listed below (symbols are defined on comment cards).

1. NTSETS, TINT, MFREQ, INTF, INDEX in
(5X, 15I5) format.
2. (TE(I), I=1,NTSETS) in (5X, 15I5) format.
3. (TST(I), I=1, NTSETS) in (5X, 15I5) format.
4. (AMP(I), I=1, NTSETS) in (5(1X,F14.5)) format.
5. DELAY in (1X,F14.5) format.

Cards 6 and 7 refer to SUB1, subroutine COEFF.

6. N is (10I5) format.
7. (V(J), Z(J)) in (1X, E14.7, 1X, E14.7) format;
one card is required for each set of values.

The next cards are required for SUB2, subroutine PULSE.

If INDEX = 1:

8. (FMT(J), J=1,12) in (1X,12A6) format.
9. NSAMP in (5X, 15I5) format.
10. G(J), the pulse amplitudes in the time domain
in format FMT(J).
11. ITINT in (5X, 15I5) format.

If INDEX = 2:

8. ITEND, ITINT in (5X, 15I5) format.
9. PERIOD, PULMID in (2(1X, F9.5)) format.


```

$JOB          735055
$IDJOB RMC10
$II FTC SYNTH  NODECK
      DIMENSION FWR(1700),FWI(1700), TIME(1500), S(1500), AMP(10)
      COMPLEX RZ(1700),FW(1700)
      COMMON RZ,FW,OMEGA(1700)
      INTEGER TINT, TEND,TSTART,TE(10),TST(10)
1  FORMAT (5X,15I5)
3  FORMAT (1HL,4(8X,4HTIME,11X,6HSIGNAL,3X))
5  FORMAT (6H END )
6  FORMAT (5(1X,F14.5))
7  FORMAT (2(1X,E14.7))
3  FORMAT (1X,4(2X,E14.7,2X,L14.7))
9  FORMAT (1H1,34HAMPLITUDE MODIFIED BY A FACTOR OF ,F14.5,13H AT TIM
1E T = ,F9.5)
C      TINT IS (TIME INTERVAL)*1000 FOR CALCULATING S VALUES
C      TST(I) ARE THE TIMES AT WHICH DIFFERENT TIME SECTIONS BEGIN
C      AMP(I) ARE AMPLITUDE MODIFYING FACTORS INSTITUTED AT TIME TST(I)
C      TE(I) ARE THE TIMES AT WHICH SECTION I OF PLOT ENDS
C      MFREQ .. MAX. FREQ. DESIRED FOR CALCULATIONS OF FREQUENCY SPECTRA
C      INTF .. FREQUENCY INTERVAL FOR WHICH WE WISH TO CALCULATE SPECTRA
C      INDEX = 1 READ IN PULSE VALUES (TIME DOMAIN)
C      INDEX = 2 CALCULATE GRAM-CHARLIER PULSE
C      NTSETS .. NUMBER OF TIME SECTIONS LOG DIVIDED INTO
C      DELAY***DELAY TIME TO GIVE PROPER START FOR AUTO PLOT OUTPUT
      READ (5,1) NTSETS, TINT, MFREQ, INTF, INDEX
      READ (5,1) (TE(I),I=1,NTSETS)
      READ (5,1) (TST(I),I=1,NTSETS)
      READ (5,6) (AMP(I),I=1,NTSETS)
      READ (5,6) DELAY
      NTOT = MFREQ*INTF
      CALL COEFF(MFREQ,INTF,NTOT)
      CALL PULSE(MFREQ,INTF,NTOT,INDEX)
      DO 11 J=1,NTOT
      FW(J) = RZ(J)*FW(J)
      FWR(J) = REAL(FW(J))
11  FWI(J) = AIMAG(FW(J))
      NF = NTOT-1
      DO 30 IA=1,NTSETS
      TSTART = TST(IA)
      AMPMOD = AMP(IA)
      TEND = TE(IA)
      TMOD = FLOAT (TSTART)*0.001
      WRITE (6,9) AMPMOD,TMOD
      WRITE (6,3)
      DO 24 I=TSTART,TEND,TINT
      T = FLOAT(I)*0.001
      KB = (I - TSTART)/TINT + 1
      IF (TSTART.EQ.1) TIME(KB) = T+DELAY
      IF (TSTART.NE.1) TIME(KB) = T
      A = 0.
      B = 0.
      DO 25 J=1,NF
      DFR = FWR(J+1) - FWR(J)
      DFI = FWI(J+1) - FWI(J)
      WT1 = OMEGA(J)*T
      WT2 = OMEGA(J+1)*T

```



```

      DELTC = COS(WT2) - COS(WT1)
      DELTS = SIN(WT2) - SIN(WT1)
      A = A + DFR*DELTC
25    B = B + DFI*DELTS
      DELTW = OMEGA(2) - OMEGA(1)
      DEN = DELTW*T**2
      A = A/DEN
      B = B/DEN
      S(KB) = (A-B)*AMPMOD*2.
24    WRITE (3,7) TIME(KB), S(KB)
      IM = (TEND - TSTART)/TINT + 1
      IF (MOD(IM,4).EQ.0) IM4 = IM/4
      IF (MOD(IM,4).NE.0) IM4 = IM/4 + 1
      DO 29 M=1,IM4
      M2 = M + IM4
      M3 = M + 2*IM4
      M4 = M + 3*IM4
29    WRITE (6,8) TIME(M),S(M),TIME(M2),S(M2),TIME(M3),S(M3),TIME(M4),
1S(M4)
30    CONTINUE
      WRITE (3,5)
      CALL EXIT
      END

$IBFTC SUB1      NODECK
      SUBROUTINE COEFF(MFREQ,INTF,NTOT)
      COMPLEX RZ(1700),FW(1700)
      COMMON RZ,FW,OMEGA(1700)
      REAL V(600), Z(600), S(600), W, VEL(600)
      COMPLEX B(600), R, D, F, RZERO
      READ (5,100) N
100    FORMAT (10I5)
C      N ..... THE NUMBER OF SETS OF VELOCITY AND DEPTH VALUES
      WRITE (6,400)
400    FORMAT (1H1,4X,9HFREQUENCY,8X,22HREFLECTION COEFFICIENT,8X,10HPHAS
1E OF R,4X,14HAMPLITUDE OF R)
      KK = N+1
      READ (5,200) (V(J),Z(J),J=2,KK)
200    FORMAT (1X,E14.7,1X,E14.7)
C      V(J), Z(J) THE VELOCITY AND DEPTH VALUES
      V(1) = V(2)
      Z(1) = 0.
      S(1) = 0.001
      S(KK) = 0.001
      DO 2 I=2,N
      S(I) = (V(I+1)-V(I)) / (Z(I+1)-Z(I))
      IF (ABS(S(I)).LT.0.001) S(I) = 0.001
2    CONTINUE
      DO 10 M=1,N
      J=N-M+1
      IF (V(J+1).EQ.V(J)) GO TO 10
      VEL(M) = ALOG(V(J+1)/V(J))
10    CONTINUE
      DO 3 I=1,NTOT
      FREQ = FLOAT(I-1)/FLOAT(INTF)
      W = 6.2831854*FREQ
      IF (FREQ.EQ.0.) GO TO 7
      DO 4 J=1,KK

```



```

+ B(J) = CSQRT(CMPLX(1.-4.*(W/S(J))**2,0.))
R = (0.,0.)
DO 5 M=1,N
J=N-M+1
D=S(J)*B(J)
E=S(J+1) - S(J)
F= S(J+1)*B(J+1)*(1.-R)/(1.+R)
IF (V(J+1).EQ.V(J)) GO TO 6
R = ((D+E-F)/(D-E+F))*CEXP(-B(J)*VEL(M))
GO TO 5
6 R = (D+E-F)/(D-E+F)
5 CONTINUE
RZERO = -R
GO TO 8
7 RZERO = (V(1)-V(KK))/(V(KK)+V(1))
8 RZ(1) = RZERO
AMPL = CABS(RZERO)
RR = REAL(RZERO)
RI = AIMAG(RZERO)
PHASE = ATAN2(RI,RR)
WRITE (3,200) FREQ,AMPL
3 WRITE (6,300) FREQ,RZERO,PHASE,AMPL
200 FORMAT (1X,5E16.7)
WRITE (3,201)
201 FORMAT (6H END )
RETURN
END

```

SIBFTC SUB2

```

SUBROUTINE PULSE(MFREQ,INTF,NTOT,INDEX)
COMPLEX RZ(1700),FW(1700)
COMMON RZ,FW,OMEGA(1700)
DIMENSION G(500), FMT(12)
1 FORMAT (5X,15I5)
2 FORMAT (2(1X,F9.5))
3 FORMAT (6H END )
4 FORMAT (1X,18F4.3,7X)
5 FORMAT (1H1,4X,9HREAL S(W),8X,9HIMAG S(W),8X,9HAMPLITUDE,10X,5HPHA
1SE,11X,9HFREQUENCY)
6 FORMAT (6(2X,E14.7))
7 FORMAT (2(1X,E14.7))
450 FORMAT (1H1,7X,4HTIME,7X,12HINPUT SIGNAL)
451 FORMAT(2X,F7.3)
452 FORMAT (1X,12A6)
GO TO (10,11),INDEX
10 READ (5,452) (FMT(J),J=1,12)
READ (5,1) NSAMP
READ (5,FMT) (G(J),J=1,NSAMP)
READ (5,1) ITINT
C NSAMP ... THE NUMBER OF AMPLITUDE VALUES, G(J), FOR THE PULSE
C ITINT ... THE DIGITIZING INTERVAL IN MSEC. FOR INPUT PULSE
WRITE (6,450)
DO 16 J=1,NSAMP
TIM = FLOAT(J*ITINT)*0.001
WRITE (6,7) TIM,G(J)
16 WRITE (3,7) TIM,G(J)
WRITE (3,3)
GO TO 12

```



```

11  A=(1./SQRT(3.1415927*2.))
    WRITE (6,450)
    READ (5,1) ITEND,ITINT
    READ (5,2) PERIOD,PULMID
C   ITEND .. LENGTH OF TIME FOR WHICH INPUT PULSE IS TO BE CALCULATED
C   PERIOD .. PARAMETER CHARACTERISTIC OF PERIOD OF PULSE
C   PULMID .. PARAMETER FOR PULSE CALCULATION PULMID/PERIOD = 5
    DO 49 I=1,ITEND,ITINT
    TTT = FLOAT(I-1)/1000.
    X = (TTT-PULMID)/PERIOD
    FX=(EXP(-X*X/2.))*((((((-X+1.)*X+15.)*X-10.)*X-45.)*X+15.)*X+15.)*X
1A
    G(I) = FX
    WRITE (6,7) TTT,FX
49  WRITE (3,7) TTT,FX
    WRITE (3,3)
    NSAMP = ITEND
12  SCALE1 = 0.001
    NL1 = NSAMP-ITINT
    WRITE (6,5)
    DO 20 IF=1,NTOT
    FREQ = FLOAT(IF-1)/FLOAT(INTF)
    W = 6.2831854*FREQ
    SR = 0.
    SI = 0.
    IF (FREQ.EQ.0.) GO TO 13
    DO 19 I=1,NL1,ITINT
    IM = I + ITINT
    DELTG = G(IM) - G(I)
    WT1 = W*FLOAT(I)*SCALE1
    WT2 = W*FLOAT(I+ITINT)*SCALE1
    DELTC = COS(WT2) - COS(WT1)
    DELTS = SIN(WT2) - SIN(WT1)
    SR = SR + DELTG*DELTG
19  SI = SI + DELTG*DELTS
    GO TO 15
13  DO 14 I=1,NL1,ITINT
    IM = I + ITINT
    DELTG = G(IM) - G(I)
    TADD = (FLOAT(I+ITINT) + FLOAT(I))*SCALE1
14  SR = SR + DELTG*TADD
    SI = SI/6.2831854
    SR = SR/6.2831854
    FW(IF) = CMPLX(SR,SI)
    GO TO 21
15  DELTT = SCALE1*FLOAT(ITINT)
    SR = SR/(DELTT*W**2*6.2831854)
    SI = -SI/(DELTT*W**2*6.2831854)
    FW(IF) = CMPLX(SR,SI)
21  OMEGA(IF) = W
    AMP = CABS(FW(IF))
    PHASE = ATAN2(SI,SR)
    WRITE (3,7) FREQ,AMP
20  WRITE (6,6) FW(IF),AMP,PHASE,FREQ
    WRITE (3,3)
    RETURN
    END

```


B29852